International Journal of Medical & Clinical Imaging
IJMCI, 5(3): 231-314
www.scitcentral.com
ISSN: 2573-1084
Original Research Article: Open Access

Classification and Identification of Human Peripheral Nerve Fibers by Conduction Velocity, Nerve Fiber Diameter and Natural Firing Patterns with Consequences for CNS Repair and Covid-19 Infection Treatment

Giselher Schalow*

Non-Government-Organized Research (NGOR), Switzerland.

Received May 24, 2020; Accepted June 17, 2020; Published October 08, 2020

SUMMARY

Currently, research in human neurophysiology and clinical repair physiology is aimed at developing an effective treatment for patients with CNS injury to improve micturition, defecation, locomotion, and higher mental functions (writing, reading, speaking, thinking, social behaviour) in particular. Through 37 years of basic human research, the goal to repair the human CNS following injury, degeneration or malformation has been achieved. The spinal cord injury patient Nefeli relearned walking (**Figure 1A and 1B**) and urinary bladder functions were repaired.

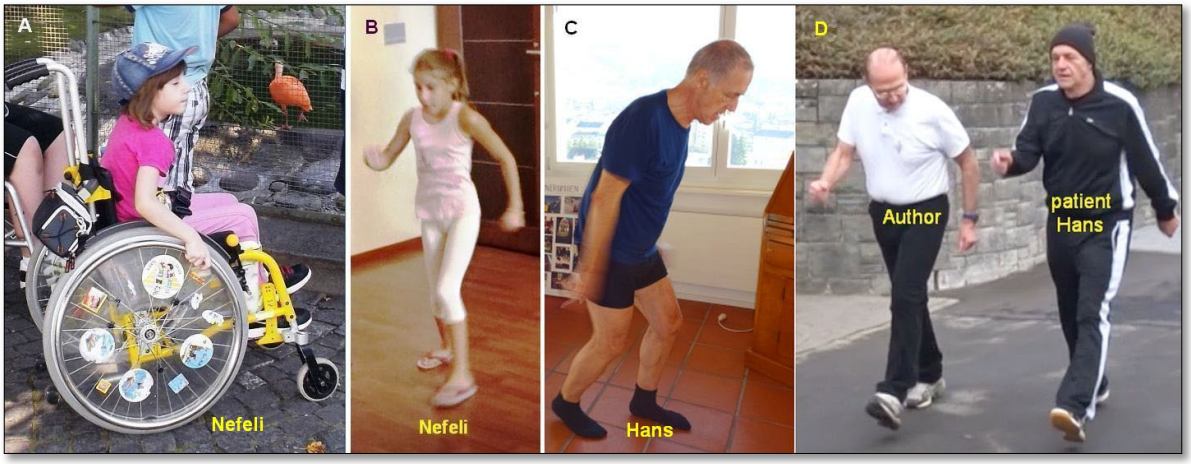

Figure 1. The spinal cord injury patient Nefeli relearned walking and got the urinary bladder repaired through Coordination Dynamics Therapy (CDT). A. Nefeli at the age of 6 after suffering a spinal cord injury by medical malpractice. B. Nefeli at the age of 13, following 4 years of CDT. C. Brain-cancer patient Hans after the removal of the cancer. Note, arms and legs are not coordinated during walking and his face looks quite depressive/exhausted. D. Patient Hans during walking in interpersonal coordination with the Author after 4 months of CDT, 6 months after the operation. Note, he walks physiologically, and he does not look depressive anymore.

The 72-year-old patient Hans, with an anaplastic oligodendroglioma WHO III, re-learned walking **(Figure 1C and 1D)**, running and cycling following the cancer operation. His cognitive functions improved through Coordination Dynamics Therapy (CDT) to have a meaningful life back again **(Figure 1C and 1D)**. This classification scheme is even a basis to inhibit cancer growth and to reduce Covid-19 infection rates through

Corresponding author: Giselher Schalow, Untere Kirchmatte 6, CH-6207 Nottwil, Switzerland, E-mail: g_schalow@hotmail.com

Citation: Schalow G. (2020) Classification and Identification of Human Peripheral Nerve Fibers by Conduction Velocity, Nerve Fiber Diameter and Natural Firing Patterns with Consequences for CNS Repair and Covid-19 Infection Treatment. Int J Med Clin Imaging, 5(3): 231-314.

optimizing the breath depth and the immunology functions of the surfactant of the pulmonary epithelia.

This new development started from scratch by clarifying first the principal aspects of anatomy and developing then a new basic electrophysiological recording technique suitable for use in humans, the simultaneous recording of single afferent and efferent nerve fiber extracellular action potentials (APs) with two pairs of wire electrodes from undissected sacral nerve roots. This technique can be used for intra-operative diagnosis and research. Further developments in morphometry of nerve roots (classification of fiber diameters into four ranges of myelin sheath thickness **(Figure 16)**) made it possible to simultaneously characterize nerve fiber groups by group conduction velocities and group nerve fiber diameters **(Figures 2 and 3)**.

In this way, an exact classification scheme could be constructed for the human peripheral nervous system (**Figure 3)**. The group conduction velocities and group nerve fibre diameters had the following pair-values at 35.5 °C: Spindle afferents: SP1(65 ms^{-1}/13.1 µm), SP2(51/12.1); touch afferents: T1(47/11.1), T2(39/10.1),

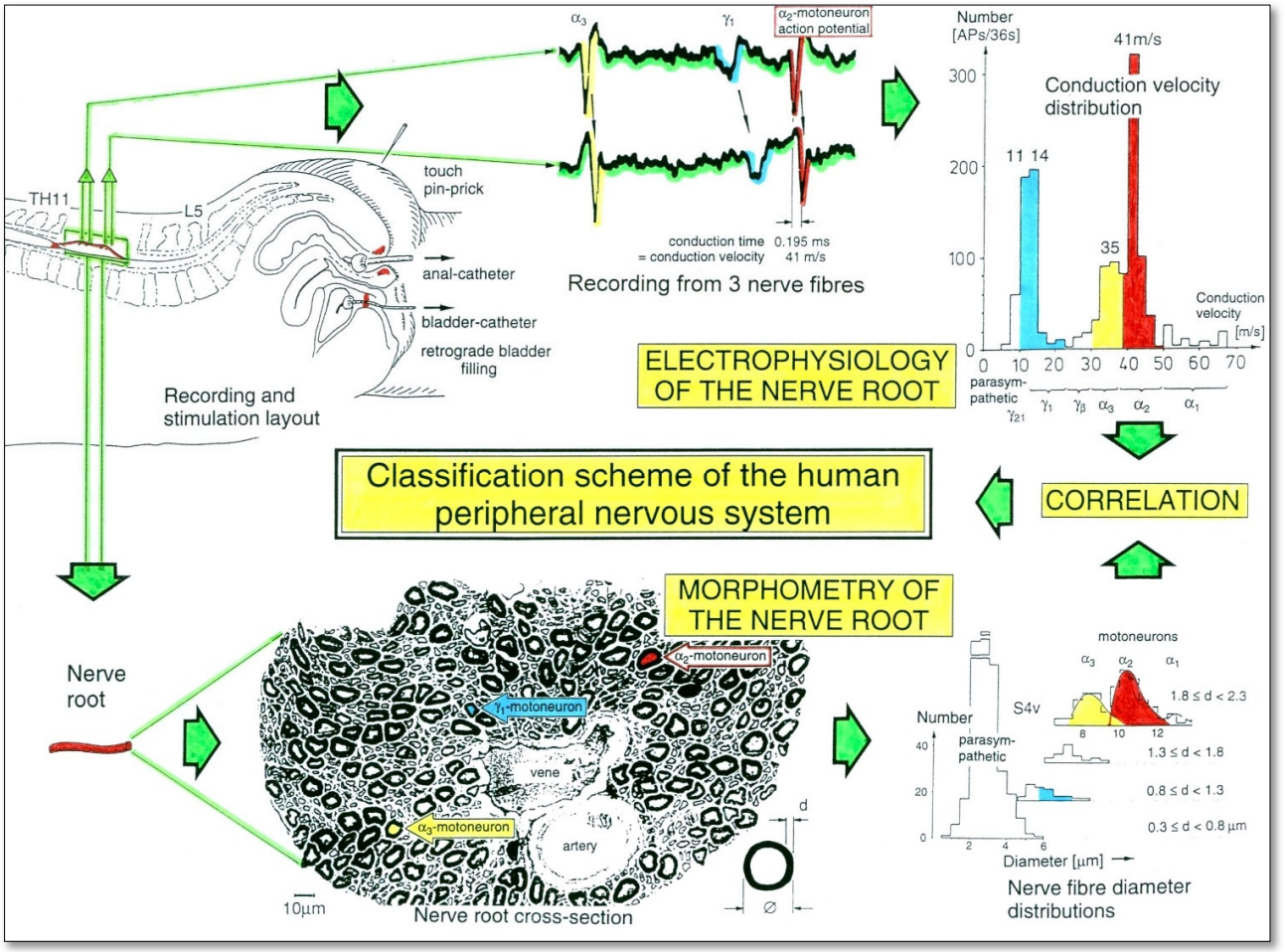

Figure 2. Schematic layout of the classification scheme for the human peripheral nervous system. By recording with two pairs of platinum wire electrodes from a nerve root containing approx. 500 myelinated nerve fibers, a recording is obtained in which three action potentials (APs) from three motoneurons (main AP phase downwards) can be seen. By measuring the conduction times and with the known electrode pair distance (10 mm), a conduction velocity distribution histogram is constructed in which the nerve fiber groups are characterized by ranges of conduction velocity values and peaks in asymmetrical distributions. After recording, the root was removed, fixated, embedded and stained, light microscope cross sections were prepared and used to measure the mean diameter and the myelin sheath thickness (d). Distributions of nerve fiber diameters were constructed for four different ranges of myelin sheath thickness. Nerve fiber groups were characterized by the peak values of asymmetrical distributions. By correlating the peak values of the velocity distributions with those of the diameter distributions obtained from the same root, a classification scheme was constructed of the human peripheral nervous system. Brain-dead human HT6.

T3(27/9.1), T4(19/8.1); urinary bladder afferents: S1(41 ms^{-1}/-), ST(35/-); α-motoneurons: α_{13} (-/14.4), α_{12} (65 ms^{-1}/13.1 µm), α_{11} (60?/12.1)[FF], α_2 (51/10.3)[FR], α_3 (41/8.2)[S]; γ-motoneurons: γ_β(27/7.1), γ_1(21/6.6), γ_{21}(16/5.8), γ_{22}(14/5.1); preganglionic parasympathetic motoneurons: (10 ms^{-1}/3.7 µm).

With respect to electrical stimulation, it was found that the primary spindle afferents likely have the lowest threshold upon electrical nerve root stimulation, followed by α_1-motoneurons (FF), secondary muscle spindle afferents, α_2-motoneurons (FR), α_3-motoneurons (S), γ_β, γ_1 (dynamic), γ_{21} (static), γ_{22} (static) and parasympathetic motoneurons.

This classification and identification scheme represents a solid basis for classifying and identifying nerve fiber groups in the human peripheral nervous system (PNS) and analyzing central nervous system (CNS) functions under physiologic and pathophysiologic conditions at the single-neuron level, even though it is incomplete and holds so far only for nerve fiber diameters larger than approximately 3.5 µm. Anatomical and electrophysiological details are given in the article.

Since it is possible to distinguish APs from afferent and efferent nerve fibers and to extract from the summed activity of a fiber bunch the discharge patterns of single fibers, it is possible to analyze receptor properties of skin afferents, primary and secondary muscle spindle afferents and urinary bladder afferents and analyze parasympathetic and somatic functions of the human CNS for continence and movements. An insight into CNS functions can be obtained from studying simultaneous impulse patterns of single afferent and efferent fibers and the phase relations between the impulses, following natural stimulation. Since human continence functions are mainly located in S3 and S4 segments and segmental functions seem to overlap in their representation in the roots, as indicated by the dermatome overlap, especially continence functions can ideally be analyzed.

With the discovery of three kinds of human premotor spinal oscillators, CNS functions can be investigated based on the behavior of these spinal oscillators, because the spinal oscillators serve as a reference base for identifying neurons and neural network organizations. Since rhythmic activity is recorded from motoneuron axons, it seems that the motoneurons are a part of the rhythm generating sub networks.

In man, there are mainly three organization patterns of somatic neuronal networks in the lower sacral spinal cord, which drive three kinds of striated muscle fibers. **Figure 4** summarizes what has been known so far about these premotor spinal oscillators, which, under physiologic conditions, fire rhythmically with impulse trains. α_1 (FF), α_2 (FR) and α_3-motoneurons (S), characterized by group conduction velocity and group nerve fiber diameter, are integrated in their own neuronal network to fire oscillatory for high activation by their respective afferent input and drive their own respective muscle fiber type.

The α_2-motoneurons of the caudal sacral spinal cord, which sub-serve continence functions, are especially of interest. They are integrated in neuronal network organizations and are firing at 6 to 9 Hz. They innervate fast fatigue-resistant muscle fibers (FR) of histochemical type IIA, which are fast oxidative glycolytic (FOG). The α_2-motoneurons innervating the external (striated) bladder and anal sphincters are mainly specifically driven by oscillators that fire with one to two APs every 110 ms (8.7 Hz) and with three APs every 160 ms (6.25 Hz), respectively **(Figure 4)**. The neuronal network, driving the external anal sphincter, is channeled to fire oscillatory by the activity of secondary muscle spindle afferent fibers (probably innervating the spindles of the anal sphincter) and skin and mucosal afferents innervating the anal canal. The oscillation period (T) of the premotor spinal oscillators is roughly related to the number of APs per impulse train (n_{AP}), and this relationship can be expressed as $T = 70\ ms + 30\ ms \bullet n_{AP}$. So far, preganglionic parasympathetic neurons could not be observed to fire oscillatory. Fusimotors seemed not to fire oscillatory under physiologic conditions but seemed to fire oscillatory following spinal cord injury (SCI).

The author successfully recorded single-nerve fiber action potentials with the same equipment from frog, rat, cat, dog and human nerves (low quality) and nerve roots (high quality). By replacing the wire electrodes by EMG surface electrodes, also electromyographic activity can be recorded with the same equipment and single-motor unit activity compared with single-motoneuron firing patterns. Even though the structure and the function of the neural networks of the human CNS are far from being even partly understood, progress in the understanding of CNS disorder is achieved by making use of the premotor spinal oscillator firing patterns. The spinal oscillators are functional units that organize themselves in preformatted neuronal subnetworks of the CNS by natural adequate impulse patterns of particular afferents and supraspinal centers (brain stem, motor and sensory cortex, cerebellum). In the isolated spinal cord (complete SCI), only the afferent input from the periphery can induce the self-organization of the oscillators. These oscillators are characterized by their rhythm of firing, namely by the

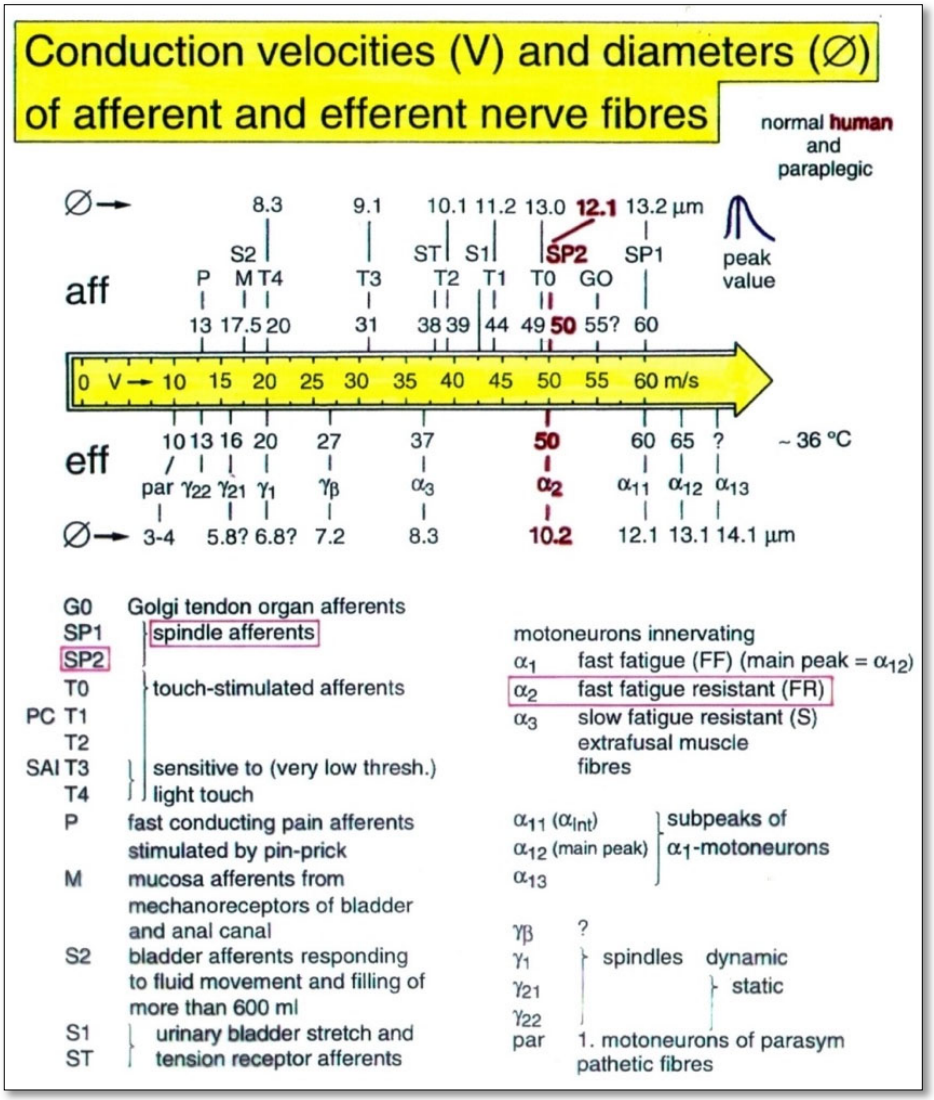

Figure 3. Conduction velocities (V) and nerve fiber diameters (∅) of afferent and efferent nerve fiber groups in normal humans and in patients with a traumatic spinal cord injury for 0.5 to 6 years. The splitting of the α_1-motoneurons into the three subgroups, α_{11}, α_{12}, α_{13}, has not yet been confirmed.

frequency of repeated firing with impulse trains and the interspike intervals of the impulse train **(Figure 4)**. If the afferent input to the neuronal network is too low to fire oscillatory or if the neurons in the circuitry are inhibited, the motoneurons are integrated in another organization form of the network. The motoneurons fire then in the occasional firing mode repeatedly approximately every three seconds or they fire transiently oscillatory.

Keywords: Human neurophysiology, Neuroanatomy, Electrophysiology, Single-nerve fibers, Conduction velocities, Nerve fiber diameters, Classification, Natural firing patterns, Oscillatory firing, Phase and frequency coordination, Surface EMG, Repair physiology, CNS repair, Urinary bladder

INTRODUCTION

From basic medical (human) research to health improvement

Medical research is designed to improve the health of human patients. 25 years ago, the Author published in the Journal of the Autonomic Nervous System basic human neuroscience, including the classification of human peripheral nerve fibers, following 10 years of research for a better understanding of urinary bladder functions under physiologic and pathologic conditions [1-4]. The present article represents an update of the classification of human peripheral nerve fibers after 25 years and documents that following 37 years of basic medical (human) research, the clinical application has fully been reached: the human

CNS can partly be repaired through movement-based learning **(Figures 5-10)**, including even cases of extreme severe brain injuries (potential organ donor) [122].

In spite of the rejection of official financial support, the Author went on with the research project to repair the human brain (CNS) and then fully reached the clinics25 years later, which means somatic and autonomic functions

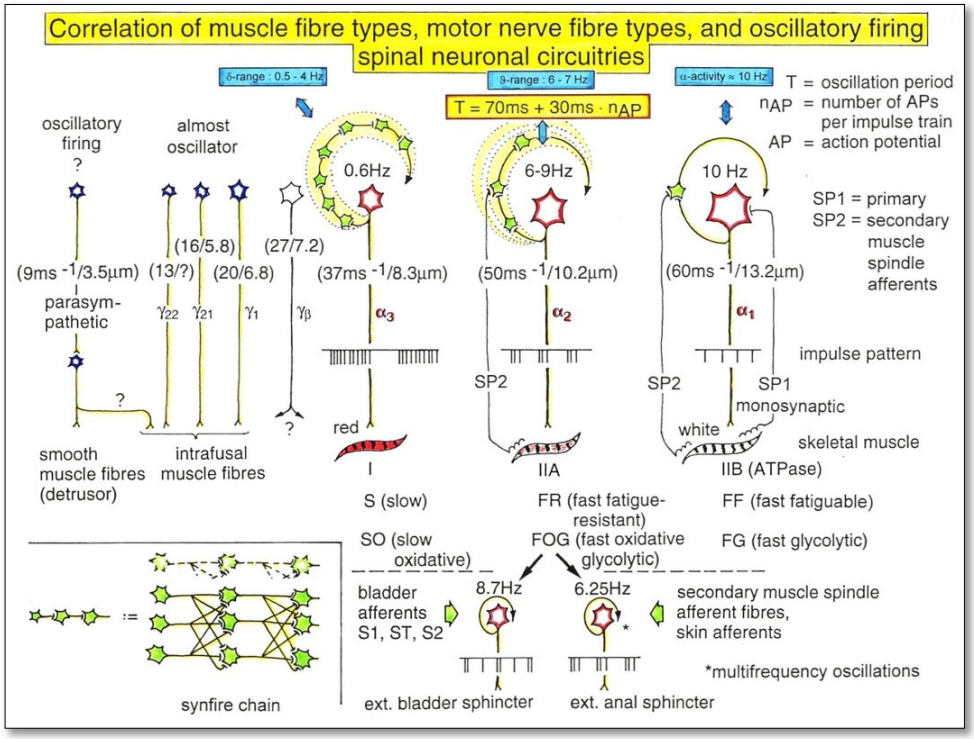

Figure 4. Correlation of muscle fiber types, motor nerve fiber types, and oscillatory firing spinal neuronal networks, based on histochemical, morphological and physiological properties. This figure provides a simplified correlation between muscle fiber, motoneuron and sacral premotor oscillator types. The existence of α_1-motoneuron (FF) oscillators firing at approx. 10 Hz (and higher) has been predicted, and they have been identified in this work. α, motoneuron; γ_1; γ_2, dynamic and static fusimotors; parasympathetic, parasympathetic preganglionic motoneuron; S1, ST, S2, stretch, tension and flow receptor afferents. α_2-Oscillators, innervating the striated ext. anal sphincter, show multifrequency oscillations (for example, f = 5.25, 6.25, 7.7 Hz). The dashed line neurons in the synfire chain, in the left lower part, indicate the functional fringe of subthreshold excitation of the synfire chain.

of the human nervous system can partly be repaired by a movement-based learning therapy called "Coordination Dynamics Therapy" (CDT) [5-7].

From the historical point of view it may be interesting for the reader to see medical research with no state support (1), judged mainly as unqualified and ethical not justified (Deutsche Forschungs-Gemeinschaft (DFG), Schweizer National-Fond, Max Planck Institution) (2), but still continued for another 25 years to show that the human nervous system can partly be repaired and that real qualified medical research, apart from statistics, is possible, even though not organized and not supported (3). The support from the former German president Richard von Weizsäcker could not change the decision of the DFG. The only country which really supported this research was the former East-Germany (GDR) (Ernst-Moritz-Arndt-University), which was officially not possible, because the Author was a subject from West-Berlin but was not involved in politics.

Since CDT can improve every nervous system at all ages in its functioning, the general health of patients and healthy persons can be improved, including cardio-vascular performance, urinary bladder functions and CNS injuries, malformations and degenerations [123].

To motivate the reader to attack the basic human neurophysiologic research and document the ethics of this research project, a few case reports of successful CNS repair are displayed at the beginning. It is not only important what research is allowed in humans but also what treatment and research is allowed to be left out. Only 0.3% of animal data have consequence for human patients.

Figure 5 shows CNS repair through CDT of an incomplete spinal cord injury (approximately 30% of the spinal cord remained), including transient spinal cord regeneration, following medical malpractice during a cancer operation [8]. The 9.5-year-old patient Nefeli (at the beginning of therapy) re-learned walking for managing well at school **(Figure 1)** and urinary bladder functions could be improved substantially through three years of therapy. Nefeli was proud to be able to learn and show hula-hoop, as she was the only one in the class of healthy children being able to learn it **(Figure 6)**. **Figure 7** shows the cerebral palsy girl Sophie with atrophied pons and cerebellum who learned the protection automatisms (when falling), walking, thinking and became fully continent through CDT [9]. An ageing man re-learned running after a stroke **(Figure 8)** [10]. The patient Dr. Cwienk suffered a very severe brain injury (frontal and parietal lobe) and lost 80% of his cerebellum **(Figure 9A and 9B)** in a traumatic brain injury (open scull) at an age of 55, but is still well up at the age of 80 **(Figure 9C)** [11]. An important part of CDT is the exercising on the special CDT device **(Figures 10, 58 and 59)** to improve the impaired phase and frequency coordination of CNS self-organization [12]. A now 74-year-old patient with Parkinson's disease was able to become better through CDT and could stop the progress of the disease for three years so far (unpublished). A permanent coma patient relearned speaking through 6 years of CDT [13] and the brain-cancer patient Hans, with an anaplastic oligodendroglioma WHO III (malign), re-learned **(Figure 9E)**, to walk **(Figure 1C and 1D)**, run **(Figure 9D)** and jump after the cancer removal operation; his cognitive functions improved to live independently and enjoy life with his friends [124]. It seems therefore possible to live longer with a better quality of life up to 20 years [123], if CDT is administered with approximately 15 h therapy per week continuously.

Figure 5. A. The 5.5-years-old girl Nefeli after suffering a spinal cord injury (Th10/11) during a cancer operation by medical malpractice. B. At school start. C, D. Nefeli at school following 1.5 years of Coordination Dynamics Therapy; she learned to walk again to the white board and write there.

Figure 6. The now 12-year-old spinal cord injury patient Nefeli during performing different hula-hoop patterns for training trunk stability and mobility.

Figure 7. A, B. The 6-year-old cerebral palsy girl Sophie with atrophied pons and cerebellum before starting CDT. She could not walk, crawl and had no protection automatisms when falling. Still incontinent. C. After learning the protection automatisms (located in the cerebellum?), Sophie learned to walk with some balance problems and became fully continent through CDT. Sophie, with the cerebellum atrophy, liked to walk and train together with the older spinal cord injury girl Nefeli.

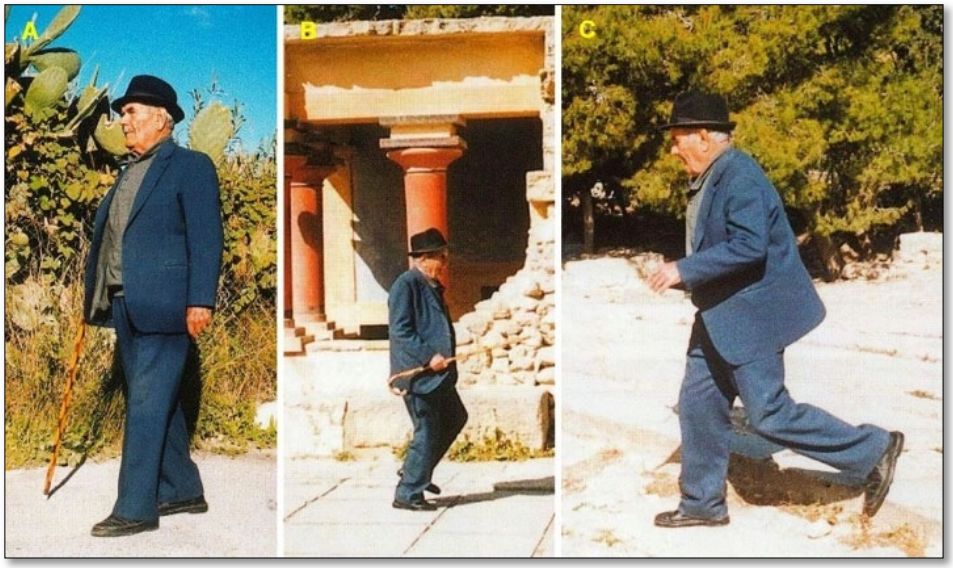

Figure 8. An ageing stroke patient re-learned running through Coordination Dynamics Therapy.

Altogether, CNS functioning could be improved or repaired through CDT so far after stroke [14], traumatic brain injury [15,16], spinal cord injury [8,17-19], cerebellar injury [10], cerebral palsy [19], hypoxic brain injury [21], in Parkinson's disease [22-23], spina bifida (myelomeningocele) [24] and scoliosis [25]. Speech had been induced and improved in a patient with severe cerebral palsy [4] and urinary bladder functions were repaired in patients with spinal cord injury [426]. In patients with cancer, especially breast cancer, cancer growth inhibition could be achieved via CDT [27]. A permanent coma patient, who lost approximately 50% of his brain, could be fully brought out-of-coma through 5 years of CDT and re-learned clearly to speak following 6 years of CDT [12]. An important property of the human CNS for neural network repair was the learning transfer from movements to urinary bladder and higher mental functions [28]. Obviously, basic medical research displayed below, and in following papers, has substantial health consequences for the whole world society.

In two articles it is tried to make understandable what scientific basis could generate such progress in human CNS repair and health improvement. Mainly the new recording technique, the single-nerve fiber action potential recording method, brought the progress in understanding human CNS functioning and its repair. This new recording technique, introduced below, made it

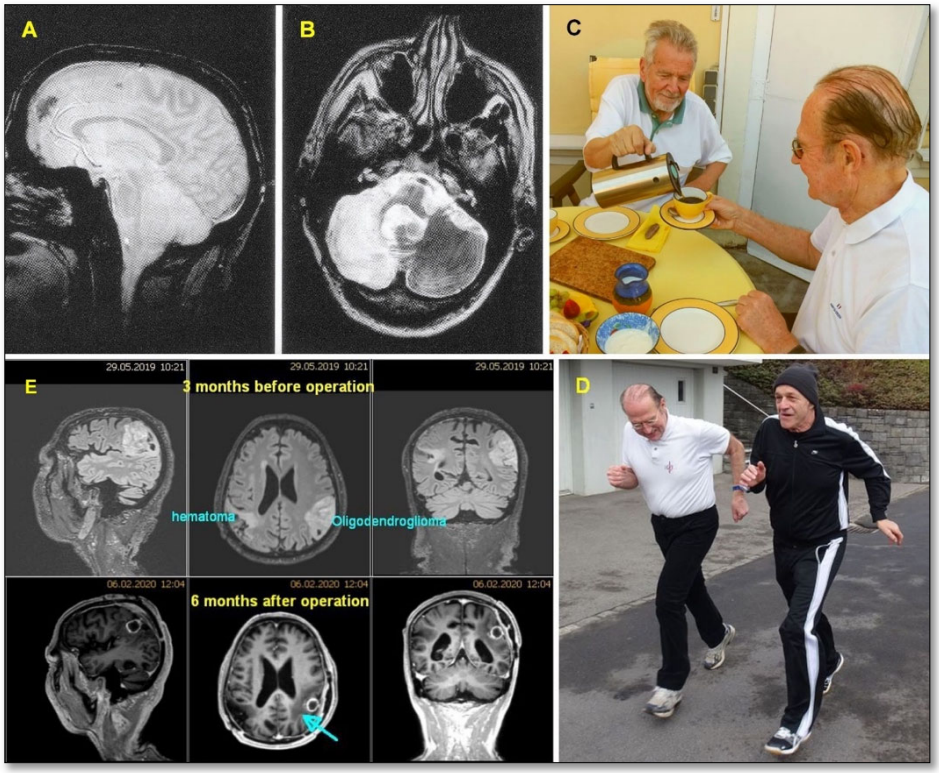

Figure 9. A, B. Dr. Cwienk suffered a frontal and temporal cerebrum injury with an open scull at the age of 55 and lost 80% of the cerebellum. He was given up by school medicine. Three years after the accident CDT was started. C. Through 21 years of Coordination Dynamics Therapy he is still having a meaningful life. In spite of coordination problems, he is able to give the Author coffee and have a high-level conversation with him. At the beginning of therapy, 20 hours therapy were administered to the very cooperative patient. Now with 80, he is training 9 h per week by himself to keep the level. If he would stop therapy for three days, his mental and physical performance would reduce dramatically, as the intelligent patient and his wife experienced before. D. The brain-cancer patient Hans during running again in interpersonal coordination with the Author through 4 months of CDT following the cancer removal (anaplastic oligodendroglioma WHO III). E. MRI's before and after the cancer operation. On the other side of the brain there is also damage from an old hematoma.

possible to develop in connection with anatomy and morphometry a qualified classification and identification scheme, with which it became possible to explore the functioning of the human CNS under physiologic and pathologic conditions at the single-neuron level and repair the human CNS by movement-based learning (CDT).

Human Neurophysiology

This research project to repair the injured, atrophied or degenerating CNS started from scratch. To explore the human CNS for repair, we need to identify the nerve cells from which we want to record and analyze the functions. In electroencephalography (EEG) it is recorded from millions of nerve cells, but it is still not clear which potentials are really recorded. To understand the functioning of the human brain it is also necessary to measure functions at the single-neuron level under natural conditions, as for example following touch or a pinprick. A new recording method has been developed with which it is possible to record single-nerve fiber action potentials from human nerve cells under natural conditions [29]. But to fully benefit from this new recording method, a classification scheme is needed and this will be given here at a further developed level for the identification of peripheral nerve fibers in cauda equina nerve roots. The nerve fibers (nerve cells) are characterized and identified by the group conduction velocity, the group nerve fiber diameter and the conducted natural impulse patterns. Since it is recorded simultaneously from a set of afferent and efferent single-fibers that means impulse patterns are recorded from several single fibers which are running simultaneously in and out of the spinal cord **(Figure 32)**, functions of the human CNS can be analyzed. It thus becomes partly possible to understand the functioning of the human brain and spinal cord at the neuron level under physiologic and pathologic conditions. According to the pathologic changes, treatment can be developed with which CNS functioning can be repaired. An efficient treatment is the developed "Coordination Dynamics Therapy" [31,32], with which it is possible to improve the

Figure 10. The cerebral palsy girl Sophie (pons and cerebellum atrophy) and Dr. Cwienk (loss of 80% of the cerebellum) during exercising on a special Coordination Dynamics Therapy device in the standing position. Both had severe balance problems at that time but were able to train in the up-right position without problems. The changing difficult coordination's between pace and trot gait when performing the coordinated arm and leg movements are efficient to repair urinary bladder functions and higher mental functions by learning transfer.

functioning of every nervous system and importantly to repair the CNS following injury **(Figures 5-10)**.

Another basic electrophysiological method for use in humans, the recording with tungsten electrodes of single-fiber extracellular APs [33,34], made it possible to record impulse patterns of single-nerve fibers innervating the skin. The method, however, rests on the classification schemes of animal peripheral nerve fibers, which do not apply to humans. Further, when recording from a skin nerve it is impossible to record simultaneously from motoneurons (efferents) to analyze brain functioning. Therefore, to record simultaneously from afferents and efferents under rather natural conditions is the new dimension in human neurophysiology, which lead to the repair of the human CNS **(Figures 5-10)**.

In this article it is concentrated on the classification scheme, the only existing one for humans. The classification schemes for animals are out-of-date, too inaccurate and are not holding in humans. The conduction velocities in animals are for example higher (up to 120 m/s) than in humans (up to 70 m/s). For a comparison between the conduction velocities of a human and a dog see Figure 54. Animal classification schemes are discussed in detail in the Discussion.

Because of the world-wide Covid-19 crisis, it is the duty of real medical research to contribute to the improvement of the Covid-19treatment of infected patients and how to reduce the risk of infection. This will be done in the Discussion. It will be shown that if patients would exercise in the lying position on the special CDT device, more patients could be cured. Further, through exercising outside in fresh not polluted air, the lung functions can be improved in the way that the immune function of the surfactant above the pulmonary epithelia can be improved with the consequence that healthy persons have a lower probability of getting infected because of the improved infection protection of the surfactant. It will be shown that the pollution of the breathing air contributed to the Covid-19 pandemic. The pandemic is partly self-made because of air pollution and missing basic medical (human) research organization and funding.

METHODS

Subjects recorded from

Pre-experiments were performed on frogs, rats and dogs (sharing experiment). The main measurements were collected from 7 brain-dead humans (HTs) and 9 patients (mean age 27 years) with a spinal cord injury (SCI), spastic bladder (hyperactive detrusor (nearly no bladder filling volume)), spastic pelvic floor (including external striated sphincters), dyssynergia of the urinary bladder, and general spasticity. Electrophysiologic measurements were performed during surgery, with the new method of recording single-nerve fiber action potentials (APs) extracellularly from undamaged nerve roots or nerve root fascicles. The patients underwent to have implanted a sacral anterior root stimulator (according to Brindley

[35]) to improve bladder control and to save the kidneys. The strategy of the surgery was to de-afferentiate the urinary bladder to increase its storage volume and to subsequently stimulate the motor roots (mainly S3 and S4) to empty the bladder. To de-afferentiate the bladder, afferents and efferents in the nerve roots were identified by electrical stimulation and partly by using the single-nerve fiber AP recording method to recognize afferents in certain (motor) roots. The surgical procedure involved extirpation of parts of the dorsal roots. Cut dorsal roots, from which was recorded, were fixated and prepared for morphometry. Light anesthesia was administered with Propofol. The implantation of anterior root stimulator (a destructive operation) is not justified anymore because bladder functions can be repaired now through CDT non-invasively [26].

Electrophysiologic principle of recording

Single-nerve fiber APs were recorded extracellularly **(Figure 2)** from nerve roots with 2 platinum wire electrode pairs (electrode pair distance (mostly) = 10 mm; electrode distance in each pair = 4 mm) at 2 sites, pre-amplified (x1000), filtered (RC-filter, passing frequency range 100 Hz-10 kHz) and displayed on a digital storage oscilloscope (Vuko Vks 22-16), and also stored using a PCM-processor (Digital Audio Processor PCM-501ES) and a video recorder. The beginning of a touch or a pin-prick was marked with an upward pulse; and the end with a downward pulse on trace "a" **(Figure 31A)**. These pulses were generated by a markation pulse generator connected to the digital scope, which was switched on and off with a touch sensor working on the basis of resistance changes. Also, the pulling and releasing of anal and bladder catheters were mostly marked with the help of a pull-switch connected to the catheters and working in connection with the same markation pulse generator. Trace "a" was the recording from the proximal electrode pair and trace "b" from the distal pair. Conduction velocities of single-nerve fibers were calculated from the conduction distance (electrode pair distance) and the respective conduction times, the time needed for an AP to cover the conduction distance (time difference between traces "a" and "b" for a particular AP) of 10mm. APs from afferents and efferents could clearly be distinguished from each other since for the used electrode arrangements the main phase (second phase) from afferent fibers is upwards and that of efferents downwards **(Figure 11)**. E.g., the AP of a skin afferent fiber reaches a pair of electrodes first as negative and then as positive. According to the electrode setting used, the main phase is upwards. An AP of a motoneuron, coming from the opposite direction, would reach the electrodes in the order positive-negative. The potential changes are therefore opposite and the main triphasic AP will point downwards. An AP in an afferent fiber reaches first the caudal electrode pair and then the rostral pair, whereas an AP of the efferent fiber reaches first the rostral electrode pair and then the caudal one. The conduction times are therefore also opposite. For further clarity, a change of the inputs to the preamplifiers does not change the ability to differentiate between afferent and efferent APs, because the amplitudes of both types of APs change their upward or downward direction **(Figure 11)**.

Figure 12 shows schematically how to get from a two-fiber recording to a recording from many afferent and efferent nerve fibers that means to the recording of the summed afferent and efferent impulse traffic in a thin root. The APs of the different nerve fibers add up algebraically.

In reverse, to get from a multi-unit recording to the simultaneous impulse patterns of the single fibers, the multi-unit recording has to be split up **(Figure 30)**. The splitting is achieved by recognizing the APs from the certain single fibers on the basis of wave form comparisons on the two recording traces and the conduction time which an AP needs to travel from one electrode pair to the other one (10mm) and selecting these APs out as is done in Figure 30. Being able to measure simultaneously the natural impulse patterns, generated by certain single receptors in the periphery, which run into the spinal cord (CNS) and those patterns which leave the cord in single fibers, it becomes possible to analyze integrative properties at the cellular level of the only little changed human CNS and its response to natural stimuli in the periphery. The use of this new electrophysiological recording technique brought the main progress in repairing the human CNS through the movement-based learning treatment, the coordination dynamics therapy.

Human nervous system research starts with animal research

To learn about the recording technique of measuring single-nerve fiber APs and the practical problems of recording, the Author started with frog measurements, went then to other animals and came only then to the measurements in human. In a human operation, one has only then a chance to successfully record single-nerve fiber APs, if one is familiar with all the practical problems of recording and has the necessary human anatomy in mind, especially the identification of the cauda equina nerve roots [36].

Since the recording of single-nerve fiber APs from frogs' peripheral nerves is comparably easy [37], such electrophysiology could be used for teaching medical students. Since 40% of the oxygen consumption in frogs is supplied by oxygen diffusion through the skin, not much care has to be taken with frog preparations for sufficient oxygen to be supplied, allowing afferent and efferent single-nerve fiber AP conduction in peripheral

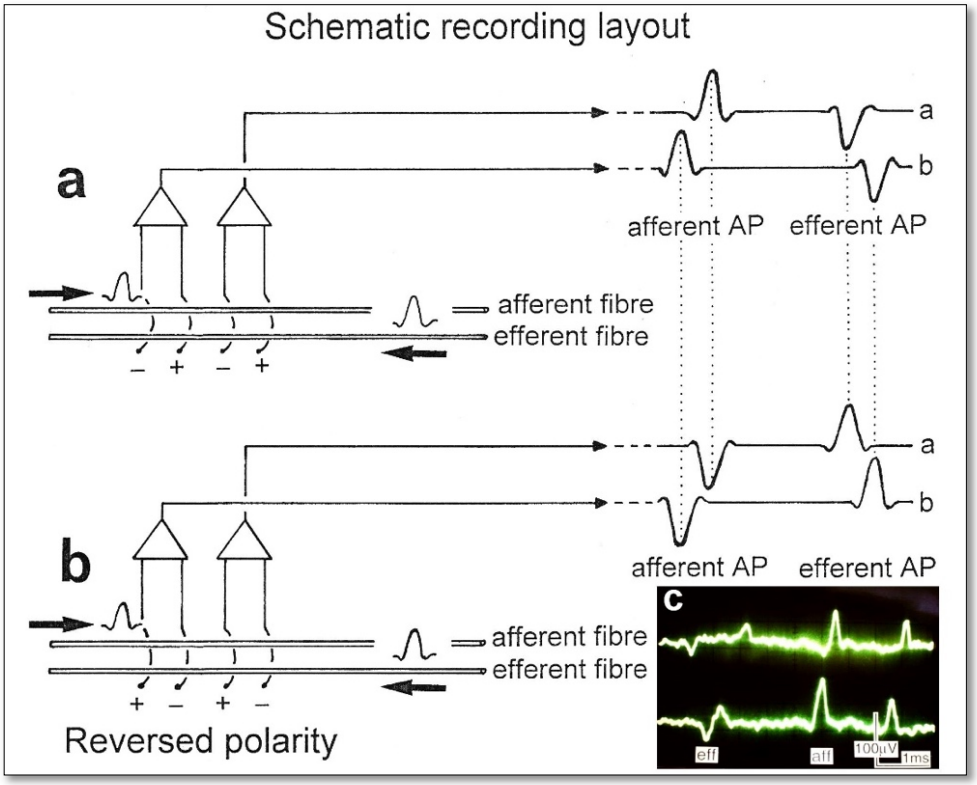

Figure 11. a. Schematic layout for recording single-nerve fiber action potentials (APs). b. The reversing of the inputs to both preamplifiers does not change the ability to differentiate between afferent and efferent APs. c. Original scope recording.

nerves to be demonstrated to medical students or physicians.

There is no problem with oxygen supply to record from patients in an operation, because the anesthetist is taken care of. The recordings from brain-dead humans was a problem, even with the assistance of an anesthetist, a surgeon, a physician or medical student, apart from mental problems. With the brain death often, but not always, the rest functions and regulations faded rather quickly, so that no action potentials could be measured any more.

Since human nerve roots have no epineurium **(Figure 20A)**, single-nerve fiber action potentials (APs) could be recorded from un-dissected nerve roots and systems functions explored. Since frog's peripheral nerves have also nearly no epineurium, single-nerve fiber APs can be easily recorded also from thin un-dissected frog nerves.

Such a recording from a frog is shown in **Figures 13A and 13B**. The relation between conduction velocity and AP amplitude can be seen in **Figure 13A** and seems to be similar to the human case **(Figure 14)**. Conduction velocity distributions can also be constructed **(Figure 13C)**. Skin afferent activity can nicely be recorded upon the stimulation of the skin **(Figure 13B)**. Since the AP recording quality is high, a classification scheme for the frog, similar to that in humans, could be constructed and nervous system functions explored. But since the understanding of the functioning of the human nervous system is more important for a repair of the human nervous system than that of the frog, the functioning of the human nervous system was the focus.

Relation between conduction velocity, action potential (AP) amplitude and action potential duration in human

The first fundamental step in repairing the human CNS was achieved, when it turned out, in a pre-measurement in human, that it is possible to record single-nerve fiber action potentials from human nerve roots because membrane properties are different in different species. The recording in the frog **(Figure 13)** was made at approximately 18°C, whereas in human at 32°C **(Figure 14)**. Optimal recording temperature in human would be 36°C. Even though the APs look similar, the neuron properties are different. The single-nerve fiber action potential recording method in human opened the possibility to clarify functions of the human brain at the single-neuron level which is a prerequisite for its repair. The next important step, the identification of nerve fibers (the classification), is tackled in this article.

In accordance with animal data [38] and frog data **(Figure 13A and 13D)**, the AP amplitude of single afferent APs decreases and the AP duration increases with decreasing conduction velocity (increasing conduction time)

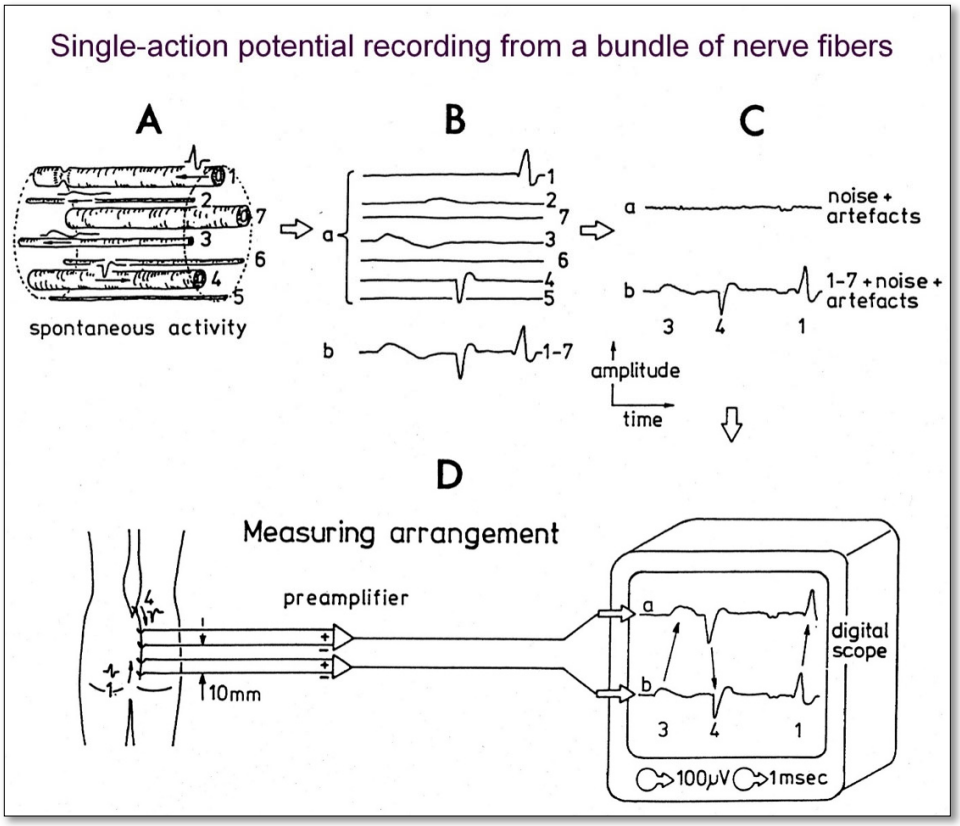

Figure 12. Schematic layout of the recording of extracellular single-nerve fiber action potentials from a bundle of 7 nerve fibers. A. The afferent nerve fibers 1, 2 and 3 and the efferent fiber 4 are occasionally active as indicated by the arrows and the single-unit potentials; fibers 5, 6 and 7 are not active. Large single-nerve fiber potentials from thick fibers are indicated by larger potential changes and small potentials from thin fibers by small potential changes. B. Traces 1 to 7 (a) show the theoretical recordings of the single fibers. Trace b shows the arithmetic sum of the 7 recordings. C. Trace a show the noise and artifact background levels; trace b is the constructed recording (sum of traces b (B) and a (C)) of 3 single unit potentials from 3 nerve fibers in a bundle of 7 nerve fibers. The potential of fiber 2 is lost because of low amplitude. D. Stimulation and recording layout. The numbers at the single-nerve fiber potentials correspond to the nerve fiber numbers in A, B and C. Traces a and b are now the records from the 2 sites of the nerve root; downward arrow (4) of the scope = efferent, upward arrow (3,1) = afferent. The stimulation used were touch, pin-prick, anal and bladder catheter pulling.

(Figure 14), if the different nerve fibers have the same distance to the recording electrodes [37].

Similar relationship between conduction velocity, AP amplitude and AP duration hold for efferent APs. With increasing conduction velocity (and increasing diameter) the AP amplitude increases, and the AP duration decreases. The scatter in these relations is large because the different fibers in a root are at different distance from the recording electrodes. Also nerve fibers change their diameter slightly from internode to internode **(Figure 27A)**. And as a matter of fact, damaged nerve fibers have strongly reduced conduction velocity and increased AP duration. Poor digitalization and too strong filtering will reduce large AP amplitudes. Nevertheless, good recordings clearly demonstrate that average AP amplitude decreases and AP duration increases with the reduction of the conduction velocity when changing from one nerve fiber group to another. These relations are of interest, since with known expected conduction times, AP amplitude and AP durations, it is much easier to identify or to pick up certain APs on the recording traces a and b, in particular if the AP amplitudes are small and the level of noise and artefacts is high.

From different recordings it was calculated that the AP duration increased from α_2 through γ_1 to parasympathetic motoneurons (1:3:6) and the AP amplitude decreased in the same sequence (1:1/3:1/8) **(Figure 28)**.

Also, in the case of parasympathetic efferents, AP amplitude, duration, and conduction time can be

calculated as long as the APs can be recognized **(Figures 28 and 35)**. Therefore, high quality recordings are necessary for detecting the APs from thin fibers. They can be obtained from the thin and long lower sacral nerve roots **(Figure 21)**.

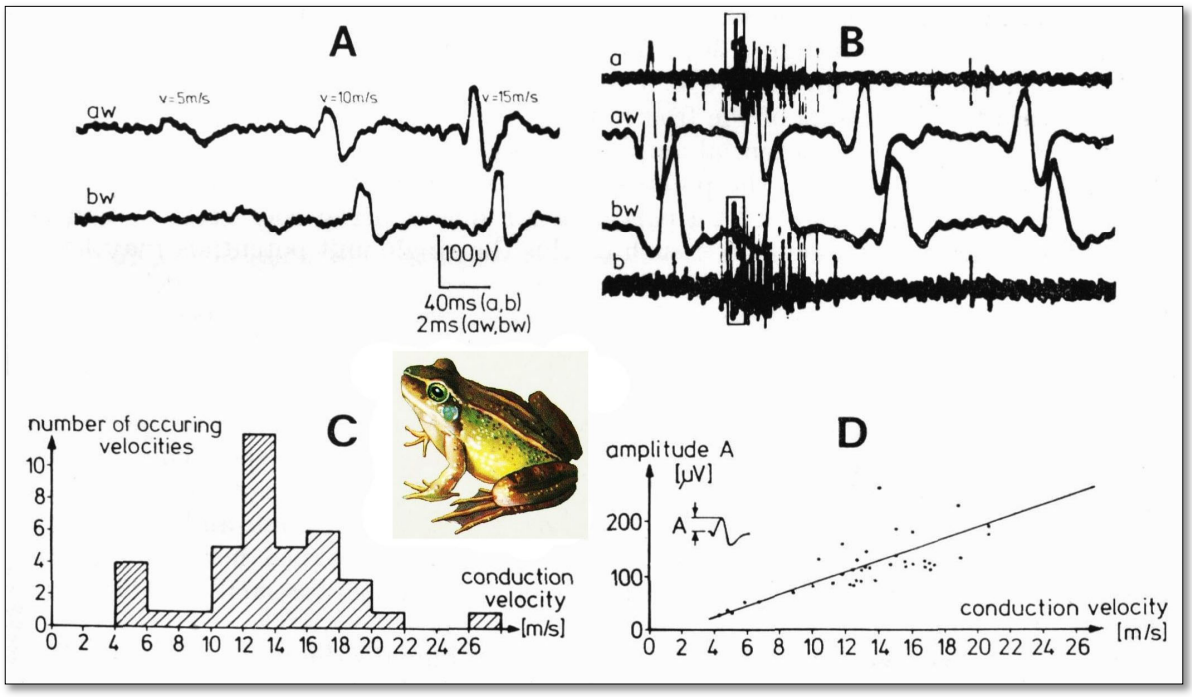

Figure 13. Recording of single-nerve fiber action potentials (APs) from the frog (rana temporaria). A. Recording of three single APs of different conduction velocities and different amplitudes. Note, the AP with the highest conduction velocity (shortest conduction time from one electrode pair (trace a) to the other one (trace b)) has the largest amplitude. B. Overall view of the activity increase on the traces a and b upon touching the skin of the frog. On the window traces aw and bw (stretched traces) the waveform of the APs of the touch afferents can nicely be seen. C. Conduction velocity frequency distribution histogram at room temperature of spontaneous and stimulated activity. D. AP amplitude in relation to conduction velocity in human **(Figure 14)**. The polarity in the frog recording is different to that in the human recordings.

RESULTS

THE CLASSIFICATION SCHEME OF HUMAN PERIPHERAL NERVE FIBERS

Anatomy and Morphometry

Cauda equina: Unique anatomy for recording single-nerve fiber action potentials

The author dissected more than 50 human cadavers to clarify the necessary anatomy, including morphometry of nerves and nerve roots and urinary bladder innervation, for establishing a classification scheme for human peripheral nerve fibers and measuring afterwards CNS functioning. The development of this new human recording technique was possible because of the unique anatomy present in the human spinal canal. Because of the Ascensus of the spinal cord, the lumbosacral nerve roots have become very long and form the cauda equina **(Figure 15)**.

Since the caudal sacral nerve roots are very thin **(Figures 15B, 15C and 15a)** and nerve roots are only sheathed by a thin layer of cells **(Figure 20A)**, they are ideal for recording single-fiber APs from undissected nerve roots. It is also possible to record single-nerve fiber APs from thin human and animal peripheral nerves, but the epineurium has to be removed and the quality of recording cannot reach that of root recordings, because the perineurium is still shunting AP currents, and tissue parts may give rise to resistance artefacts.

Since further, humans have no tail, mainly continence (mainly S2 to S5) and sexual functions are located in the conus medullaris only. Those functions are therefore represented in the lower sacral nerve roots, and they don't mix with tail functions as, for example, in rat, cat or dog [56].

A few nerve fibers to leg muscles run through the lower sacral nerve roots (not mentioned in anatomy books), as can easily be verified by electrical and manual nerve root stimulation and the observation of foot or toe movements

in an operation. Root thicknesses of dorsal and ventral roots can be seen in **Figures 15 and 15a**. The lower sacral nerve roots show quite a lot of variation, including root interconnections **(Figure 15C, right)** and ventral root

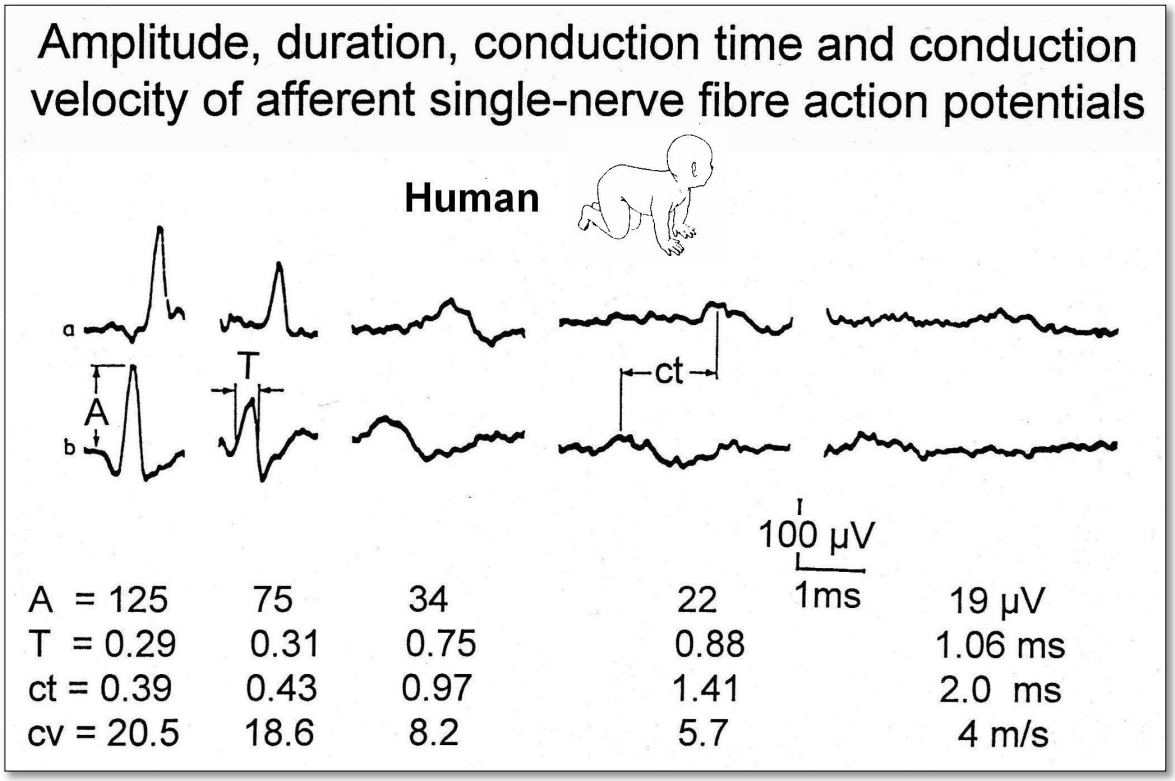

Figure 14. Extracellular AP waveforms of different amplitude (A), duration (T), conduction time (ct) and conduction velocity (cv). The different nerve fibres, in which these APs were conducted, had approx. the same distance to the recording electrodes. The afferent nerve fibres were stimulated by touch, pain, and bladder and anal canal-catheter pulling and releasing. Brain dead human HT4, 56 years, 32°C (approximate measuring temperature), recording made from a dorsal S5 root (diameter = 0.17 mm).

afferents and dorsal root efferents [56] (violation of Dales principle). With respect to electrical nerve root stimulation for urinary bladder control, the functions in the roots have to be identified functionally, including electrical nerve root stimulation and recording of afferent APs, to cut the afferents to the bladder and stimulate later the efferents in ventral roots, after the surgery, for efficient bladder control. The implantation of an electrical bladder stimulator [35] is not justified anymore because the urinary bladder can be repaired through CDT non-destructively [26].

Number of axons in nerve roots

Values of nerve root diameters, axon densities, root cross sections and numbers of myelinated nerve fibers per root [49] are given in **Figure 15a**. It can be seen that the dorsal roots are much thicker than the ventral roots in the lower sacral range and that the root diameters strongly decrease in the caudal direction **(Figures 15a, Figure 15B and 15C)**.

In one case, it was even possible to obtain similar myelinated nerve fiber numbers with the morphometric method as described below and the electrophysiologic method [58] (see below). Taking into account the number of unmyelinated nerve fibers **(Figures 20 and 26)**, then the number of axons and the axon densities in the dorsal roots will be much higher than in ventral roots, may be by a factor of 5.

Functional morphometry

Nerve root pieces a few cm lengths were removed from dorsal roots of patients during surgery and from roots of brain-dead humans (HTs) and used to record from, fixated for four hours in 4% glutaraldehyde in cacodylate buffer, after-fixated in 1% OsO_4 for four hours, and dehydrated and embedded in Araldite according to standard techniques. Pictures of semi-thin sections (approximate depth = 1µm), stained with Thionin acridine-orange, were taken with a light microscope (x1000). Nerve fiber diameters $\varnothing = 1/2(\varnothing_1 + \varnothing_2)$ ($\varnothing_1$ and $\varnothing_2$ is the larger and the smaller diameter of non-round shaped fibers) and the

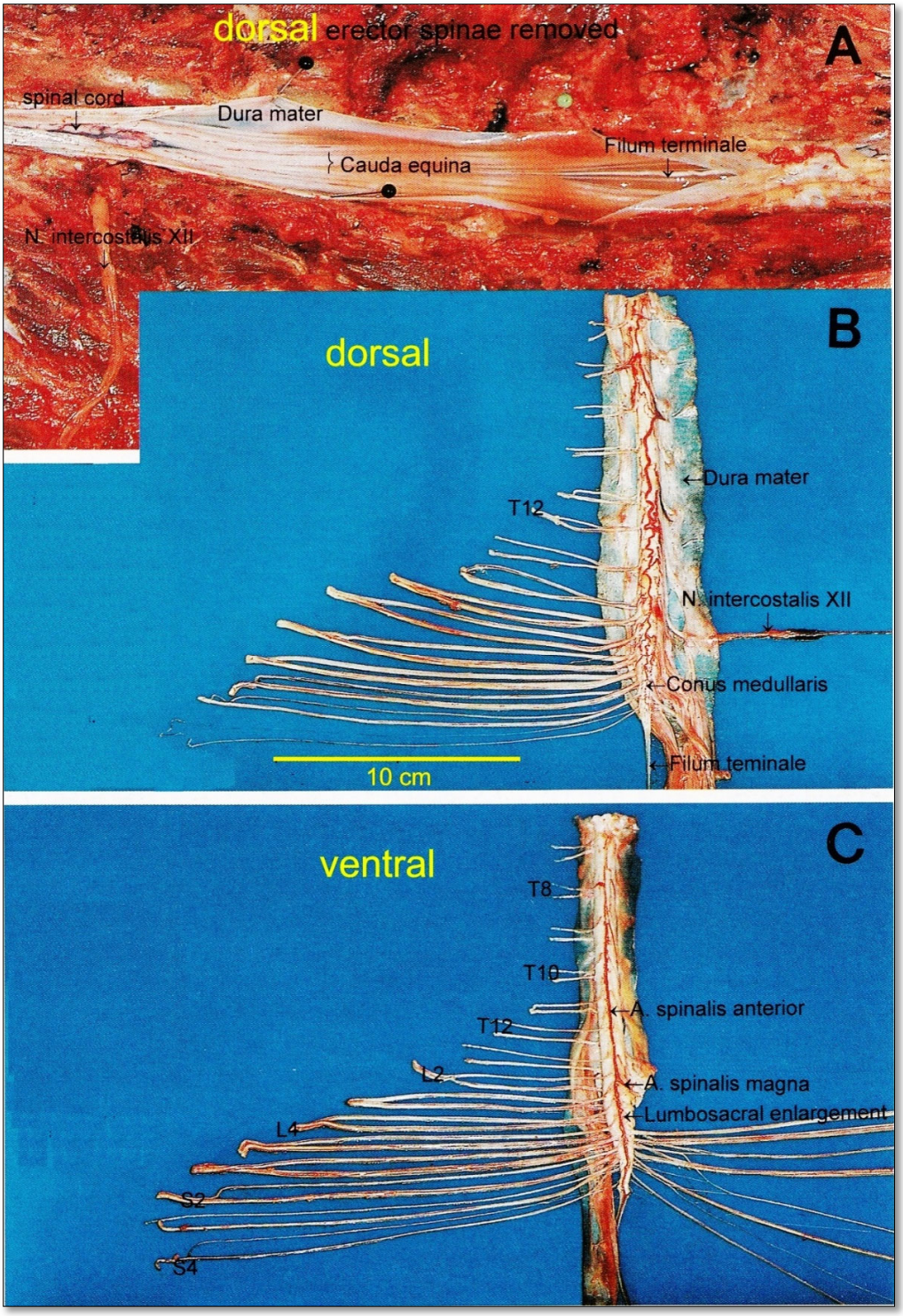

Figure 15. A. Cauda equina and the intercostal nerve XII (subcostalis). Laminectomy, the dura mater spinalis opened and the erector spinae removed. Nerve roots lie in a position similar to a horse's tail (cauda equina). Cadaver dissection by the Author. B. The dorsal spinal cord, the cauda equina nerve roots, the dura mater and the intercostal nerve XII removed and split up. The roots are cut at the dura mater. Note that the caudal ventral roots are thinner than the dorsal roots. C. The ventral spinal cord and the cauda equina nerve roots. The passage of the artery spinalis magna is indicated. Note the root interconnections on the left side.

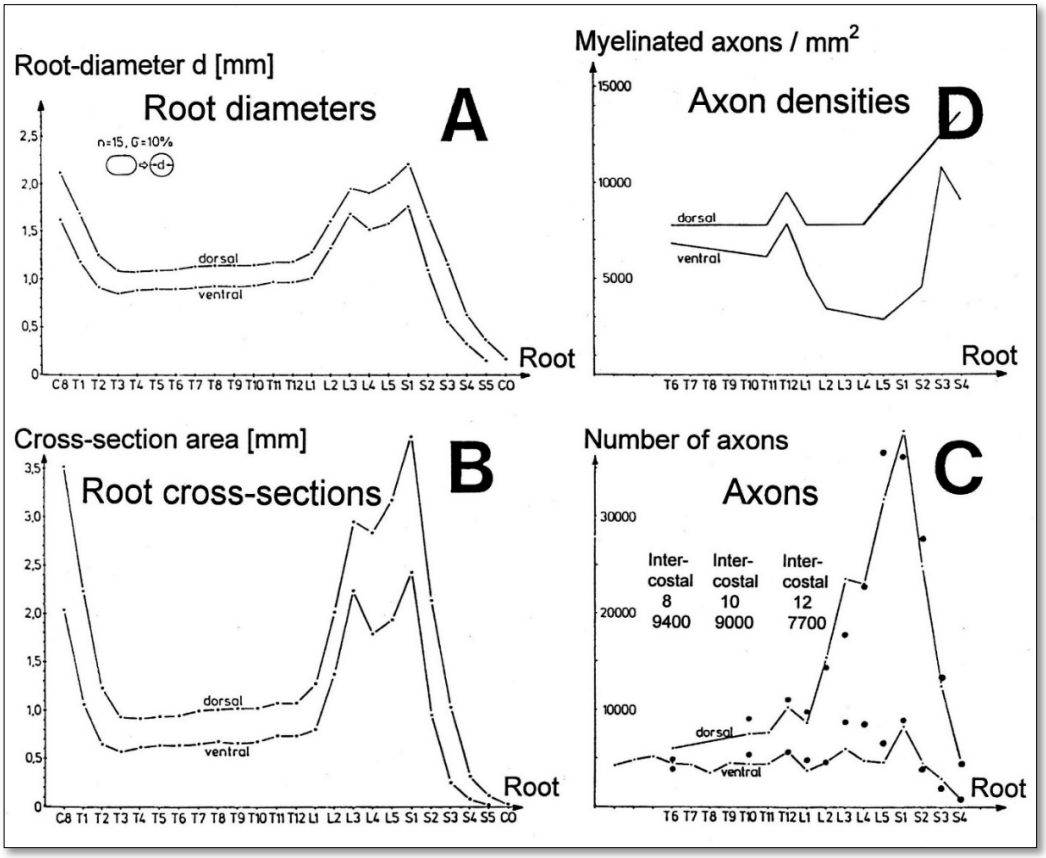

Figure 15a. A. Dorsal and ventral mean root diameters of 15 cadavers in relation to the root level. In the case of elliptic-shaped cross sections, the diameters of the circle with the same area were taken. The standard deviation was 8 - 10%; 10% for the smaller roots. B. Dorsal and ventral mean root cross section areas, calculated from A, in relation to the root level. C. Number of myelinated axons of dorsal and ventral roots. The line for dorsal roots is the average of two van Gieson stains and the Tuloidin blue stain. The line for the ventral roots is the average of three ventral root counts. The large dots are counts from the Tuloidin blue stain; upper dots are the dorsal counts; lower dots are the ventral counts. The deviation of the dots indicates the variation of the axon counts. The inserted axon counts from the intercostals 8, 10, and 12 are from a Tuloidin blue stain count. As viewed under the light microscope, the intercostals 8 and 12 had about the same cross section area; the tenth intercostals had about a 10% smaller one. D. Approximate densities of myelinated axons in relation to the root level, calculated from B and C (density = number of axons/cross section area).

mean myelin sheath thickness "d" were measured by hand. A correction of 8% for shrinkage was allowed.

The nerve fiber diameters measured were divided into four classes of myelin sheath thickness: 0.25µm ≤ d < 0.8; 0.8 ≤ d < 1.3; 1.3 ≤ d < 1.8; 1.8 ≤ d < 2.5µm. For each range of myelin sheath thickness, a diameter distribution histogram was constructed. In the case of damaged fibers (split myelin sheath), the myelin sheath thickness was measured at the most preserved part. Very strongly damaged fibers were not considered. The morphometry was performed manually. Computer-assisted morphometry would have less accuracy, since computer programs cannot handle artefacts and altered nerve fibers as if they were normal fibers.

Relation between nerve fiber diameter and myelin sheath thickness

In order to identify possible nerve fiber classes in the nerve fiber diameter distribution histograms, the diameter spectra were split according to different myelin sheath thickness ranges. To choose feasible ranges, the relation between nerve fiber diameter and myelin sheath thickness of the nervi pelvini was constructed and shown in **Figure 16**.

The myelin sheath thickness roughly increased with the diameter. But the correlation points indicate that there may be different populations of nerve fibers with their own correlation between myelin sheath thickness and diameter. Correlation lines for possible nerve fiber populations are drawn into **Figure 16**. It can be seen from

the large scatter of the correlation points that it is difficult or impossible to identify different nerve fiber populations on these morphological data alone. The myelin sheath thicknesses were therefore lumped together in four classes characterized by the myelin sheath thickness ranges $0.3 \leq d < 0.8$, $0.8 \leq d < 1.3$, $1.3 \leq d < 1.8$ and $1.8\mu m \leq d < 2.3\mu m$. Nerve fiber diameter distribution histograms were then calculated for these myelin sheath thickness ranges. With the chosen classification ranges, it is still possible that a certain population of nerve fibers covered more than one myelin sheath thickness range, as is indicated in **Figure 16**.

As **Figure 16** indicates, the choice of the myelin sheath thickness ranges was not arbitrary. And therefore, the split histograms separate different nerve fiber groups better than a whole diameter histogram.

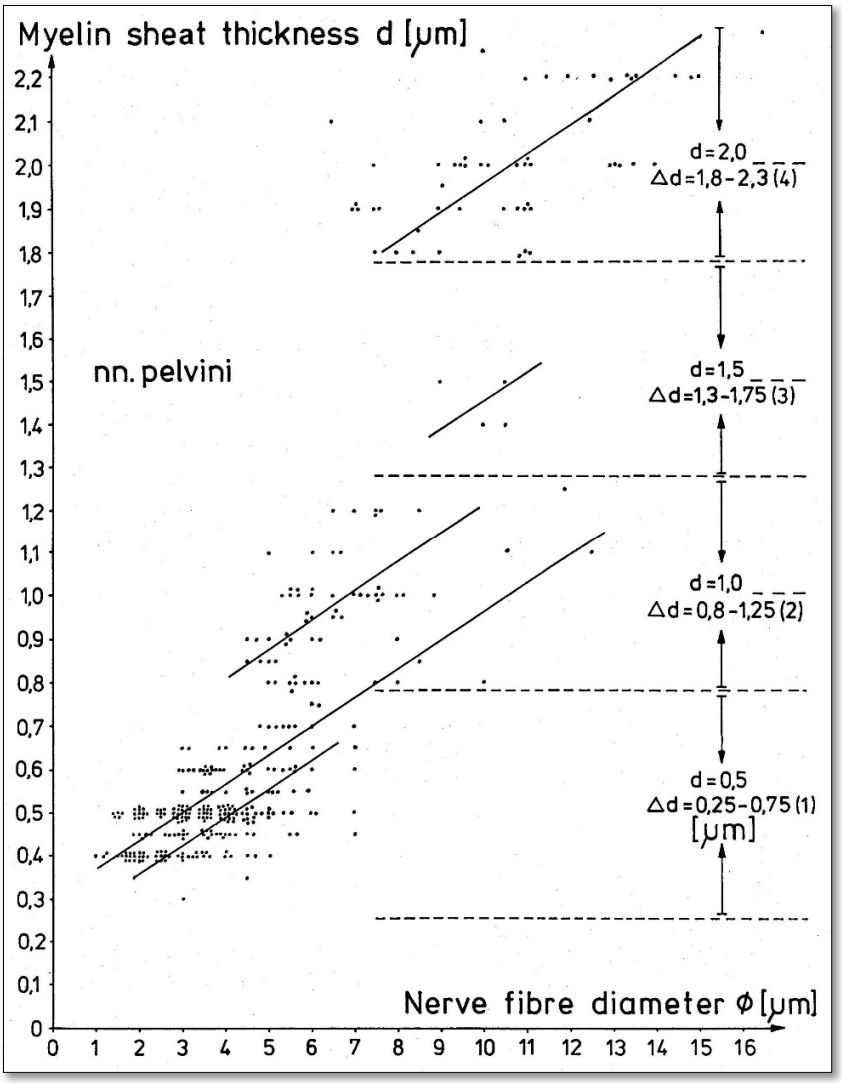

Figure 16. Myelin sheath thickness in relation to the nerve fiber diameter Ø of the nervi pelvini. Lines indicate suggested correlation between d and Ø for different nerve fiber groups. Note, there may be several nerve fibers groups in one class ($0.3 \leq d < 0.8\mu m$), and a nerve fiber group may extend into another class. Correlation dots in class $0.3 \leq d < 0.8\mu m$ are shifted slightly because of closeness.

Nerve fiber diameter distribution histograms to identify nerve fiber groups and estimate urinary bladder sphincter innervation [39,40]

Nervi rectales inferiors and perineales

Figure 17C shows the nerve fiber diameter distribution histograms of the nervi rectales inferiors and perineales for the four myelin sheath thickness ranges according to **Figure 16**. In **Figure 17Cb,** a characteristic cross section area is shown and in **Figure 17Ca** the corresponding spectra are shown. To analyze the diameter spectra of the

nervi rectales inferiors and perineales, the spectra of an L4 ventral nerve root are shown for comparison in **Figure 17Ba**, with the identified three α-motoneuron peaks [41,42] for myelin sheath thicknesses between 1.8 and 2.3µm. The nerve fibers of the L4 dorsal root are distributed differently over the four myelin sheath thickness ranges **(Figure 17Aa)**. The majority of fibers are thin and have a thin myelin sheath and lay therefore in the histogram with sheath thicknesses 0.3 and 0.8µm. Since this spectrum shows two peaks, at least two populations of very thin afferent nerve fibers can be expected to exist in this range. For the mixed (afferent and efferent) nervi rectales inferiors and perineales **(Figure 17Ca)**, the majority of fibers lie in the class with myelin sheath thicknesses between 0.3 and 0.8µm. Several fiber groups can be expected in this histogram.

From the nerve fibers of the histogram with $1.8 \leq d < 2.3$ µm, an estimation of the number of nerve fibers leading to the external bladder sphincter muscle fibers can be obtained. Sphincter muscles have muscle fibers mainly of the slow twitch type (FR) **(Figure 4)**. These muscle fibers are innervated by α_2-motoneurons with a nerve fiber diameter range of 9.5 to 12µm (hatched in Figure 17Ca). In these nerve fiber diameter and myelin sheath thickness ranges are about 4% of the nerve fibers of the nervi rectales inferiors and perinales, namely 68 fibers (0.04 x 1700). This number of nerve fibers contains α_2-motoneurons and afferent fibers with the same nerve fiber diameter and myelin sheath thickness range.

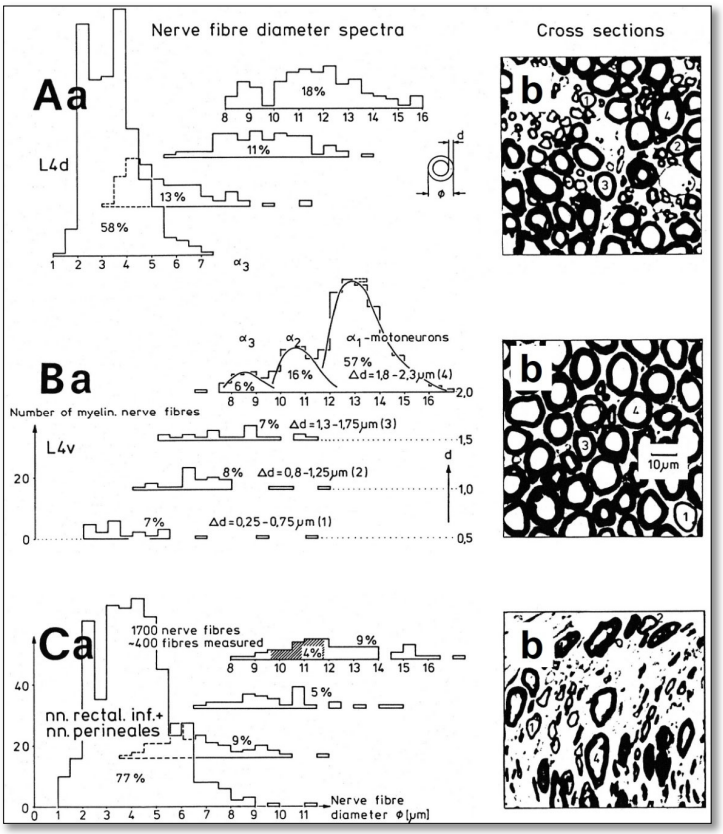

Figure 17. a. Nerve fiber diameter distribution histograms classified by four classes of myelin sheath thicknesses as indicated in Ba. % indicates percentage of fibers in classes or subgroups. b. Corresponding characteristic cross sections. A few fibers are numbered by their myelin sheath thickness range to which they belong. Dimension scale for A, B, and C is drawn in Bb. 8% shrinkage correction. For the definition of fiber diameter Ø and myelin sheath thickness d, see insertion in Aa. – A. Nerve fiber diameter spectrum of a fourth dorsal lumbar root of a 47-year-old female human cadaver, removed two to five hours after death, 660 fibers were measured. B. Spectra of a fourth ventral lumbar root (same case as in A), 320 fibers were measured. In the myelin sheath thickness range $1.8 \leq d < 2.3$µm, the distribution curves of the three α-motoneuron classes are drawn into the histogram. C. Spectra of the nervi rectales inferiores and perineales. Note, the majority of fibers (77%) has a very thin myelin sheath ($0.3 \leq d < 0.8$µm) with a relatively large amount of thick fibers. In the histogram of very thick myelin sheaths ($1.8 \leq d < 2.3$µm), the diameter range of α_2-motoneurons, to which sphincter motoneurons belong, is cross hatched (4% of the fiber).

If one assumes a similar distribution of afferent and efferent fibers in this myelin sheath thickness range (1.8µm ≤ d < 2.3µm), then one can expect to have an upper limit of sphincter α_2-motoneurons leading to the anal sphincter and possibly to the external bladder sphincter through the S3 to S5 ventral and dorsal roots [43] of 30 fibers on one side. The number of additional necessary γ-motoneurons will not exceed 30 [42] since there are no or only few spindles in the sphincter muscles [44]. The α-motoneurons to the pelvic floor muscles normally do not lead through the pudendal nerves [45, 46]. Such fiber numbers are helpful, if one plans a qualified nerve anastomosis to re-innervate the urinary bladder in patients with a spinal cord injury (see Discussion).

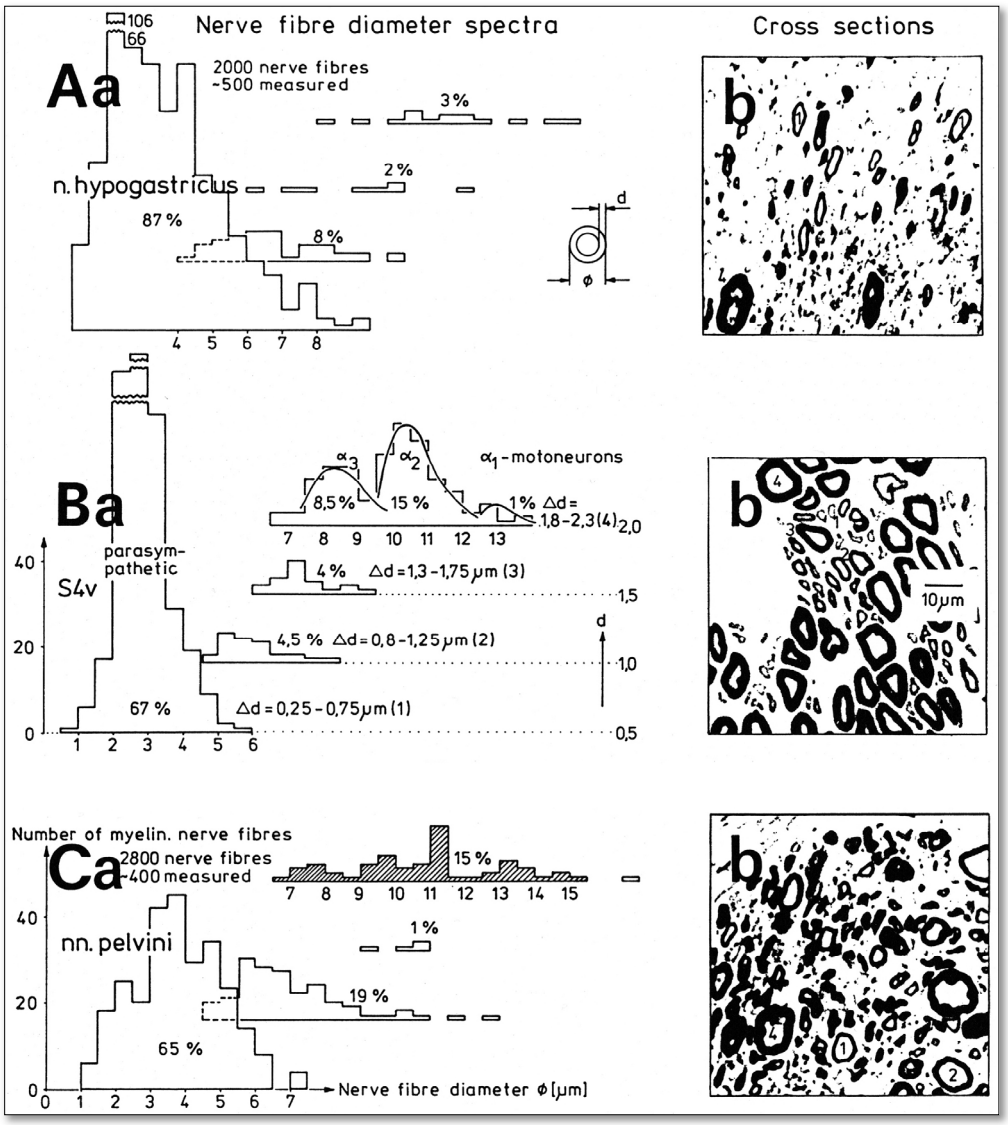

Figure 18. a. Nerve Fiber diameter distribution histograms of the nervus hypogastricus, a S4 ventral root and the nervi pelvini, classified by four ranges of myelin sheath thicknesses, indicated in Ba. % indicates percentages of fibers in classes or subgroups; b. Corresponding cross sections. A few fibers are numbered by the class of myelin sheath thickness to which they belong. Dimension scale is drawn in Bb. 8% shrinkage correction. – A. Nerve fiber diameter spectra of the nervus hypogastricus. Note, the nerve fiber diameter histogram class 0.3 ≤ d < 0.8µm (87% of the fibers) shows a large proportion of thick fibers. B. Nerve fiber diameter spectra of a fourth ventral sacral root. In the distribution histogram of class 1.8 ≤ d < 2.3µm, the distribution curves of the three α-motoneuron classes are drawn. C. Diameter spectra of the nervi pelvini. Note, 15% are thick and have a very thick myelin sheath (class 1.8 ≤ d < 2.3µm, crosshatched). α_1, α_2,α_3, SP1, T1 = peak group diameters of α-motoneurons, primary spindle afferents and T1 skin afferents.

Nervus hypogastricus

Figure 18Aa shows the nerve fiber diameter spectra of the nervus (plexus) hypogastricus **(Figures 56, 57)**. The majority of myelinated fibers are contained in the spectrum with myelin sheath thicknesses between 0.3µm and 0.8µm. Most sympathetic efferent fibers will be unmyelinated since the hypogastric nerve lies caudal to the sympathetic chain **(Figure 19)**. The two nerve fiber peaks at about 2.3 and 4.3µm lie at similar diameters as the two peaks of afferent fibers in the L4 dorsal root of **Figure 17Aa** and contain therefore most likely afferent fibers. Probably a few preganglionic parasympathetic fibers will be intermingled. Their diameters lie also in that range **(Figure 18Ba)**. The nervus hypogastricus contains thicker but thinly myelinated afferents in comparison to the afferents of the L4 dorsal root **(Figure 17Aa**; 0.3µm ≤ d < 0.8µm).

Nervi pelvini

The nerve pelvini **(Figure 19)** of Figure 18Ca have nearly no fibers in the spectrum for myelin sheath thicknesses between 1.3 and 1.8µm. The fibers in the myelin sheath thickness ranges 0.3µm ≤ d < 0.8µm and 0.8µm ≤ d < 1.3µm mainly represent parasympathetic afferent and efferent fibers. For the efferent parasympathetic fibers, this becomes clear by comparing Figure 18Ca with **Figure 18Ba.** For the afferent parasympathetic fibers, such direct comparison is not possible. The large number of thick fibers in the myelin sheath range 1.8 ≤ d < 2.3µm (hatched in Figure 18Ca) is unexpected. It is likely that these fibers are all of parasympathetic afferent type. One would expect the thickest parasympathetic afferents innervate mechanoreceptors, flow receptors, Pacinian corpuscles (distributed over large areas in the tissue [47, 48]) and tension receptors in the detrusor wall. Their diameters probably range up to values of about 12µm (Figure 3). The largest at 11.3µm and the existence of nerve fibers with diameters larger than 12µm suggest that there are also motoneurons and may be a few spindle afferents in the spectrum with myelin sheath thicknesses between 1.8 and 2.3µm. It will be discussed below that these thick nerve fibers could innervate the external urethral sphincter.

Number of efferent parasympathetic fibers in the nervi pelvini

The parasympathetic peak of S4 ventral root fibers of Figure 18Ba contains about 380 fibers. The number of parasympathetic efferent fibers in the nervi pelvini on one side is therefore about 800, if one assumes that parasympathetic fibers are contained in three roots (S3, S4, S5 or S2, S3, S4) and that 20 to 30% of the fibers are ventral root afferents [41,42,49] ((380 x 3) x 0.7 ≈ 800). Taking the value for myelinated fibers in the nervi pelvini **(Figure 19)** and disregarding the existence of possibly a few thick somatic motoneurons, then one finds that among the myelinated fibers of the nervi pelvini about 20% are efferents (case 1: 2800x0.2 = 560; case 2: 4700x0.2 = 940). In the monkey, it was found that the parasympathetic nucleus on one side contained approximately 410 motoneurons [50].

Innervation of the external bladder sphincter

In the nervi pelvini and in the nervus (plexus) hypogastricus are thick fibers with a thick myelin sheath (1.8 ≤ d < 2.3µm) **(Figure 18)**. At least for the nervi pelvini, it is unlikely that all these fibers are afferent fibers. In the nervi pelvini, these fibers make up 15% (hatched in Figure 18Ca). The possibility that a thin direct muscle branch to the pelvic floor [45,46] was removed with the nervi pelvini is unlikely, since the direct branch to the pelvic floor tends to lie more laterally and the nervi pelvini more medially [51], and such thick fibers were found in all sub nerves. It is possible that these thick fibers of the nervi pelvini innervate the external bladder sphincter. It has been reported that the external bladder sphincter could also be innervated through a direct branch from the S3 and S4 roots [46] or via the pelvic nerves [52]. In five male cadaver dissections, the author could not find the branch from the nervus pudendus or nervus dorsalis penis leading to the external bladder sphincter, situated caudally to the prostate gland. To learn more about the innervation of the human urinary bladder by a comparison with animal data caution is necessary, since it was reported that similarly named muscles (for our purpose the external sphincter muscle) may not have homologous functions in humans and cats [53]. The representation of the urinary bladder in the sacral nerve roots is different in dogs and humans [54-56]. With the single-nerve fiber action potential recording method the nerve fibers leading to the external bladder and anal sphincters could be found in the lower sacral roots and their activation patterns measured.

As emphasized in **Figures 56, 57 and 19**, it is important to be able to measure in nerve roots through electrophysiology single-fiber action potentials and innervations of the urinary bladder and other internal organs in the complexity of networks and connections.

The innervation of the urinary bladder and its functioning is important, because continence is a big problem in the world society and also for the patients of this report. Morphometry contributes to the knowledge for a natural repair of the bladder. Morphometry of the human vagal nerve would be needed for a comparison with the other nerves.

Nerve anastomoses to repair the urinary bladder

Nerve anastomoses to repair the urinary bladder (for example, from the intercostal nerves to cauda equina nerve roots or bladder innervating nerves) and other

functions in SCI are partly destructive operations (even if highly qualified) and no longer necessary anymore because via CDT, including structural repair, the bladder and other functions can partly be repaired naturally. For further details of a nerve anastomosis see Discussion [39,40,57.58].

Number of myelinated nerve fibers innervating the urinary bladder

In six human cadavers, the nervus pudendus, the nervi pelvini and the nervus (plexus) hypogastricus were dissected to study the gross anatomy. In further two human cadavers, a few centimeters of the whole nerves of the nervi rectales inferiores and perinealis, the nervi pelvini and the nervus hypogatricus (at the sacral promontorium) were removed.

The nerve pieces were fixated, embedded, stained (fixated in 4% glutaraldehyde in cacodylate buffer, after-fixated in 1% OsO_4, embedded in Araldite) and cut, and the myelinated nerve fibers counted. Figure 19 shows the obtained nerve fiber numbers. The nervi pelvini had 2,800 and 4,700 myelinated fibers and consisted of 6 and 13 sub-nerves. The nervi rectales inferiores and perineales contained 1,700 myelinated fibers and consisted of five and one sub-nerves. The thick nervus (Plexus) hypogastricus contained only 2,000 myelinated nerve fibers. Most fibers of this vegetative nerve were most likely unmyelinated. The unmyelinated fibers were not counted here. From the number of sub-nerves of the two cadavers of the nervi pelvini (6 and 13) and the nervi rectales inferiors and perineales (5 and 1) **(Figure 19)**, one can expect many variations of these nerves.

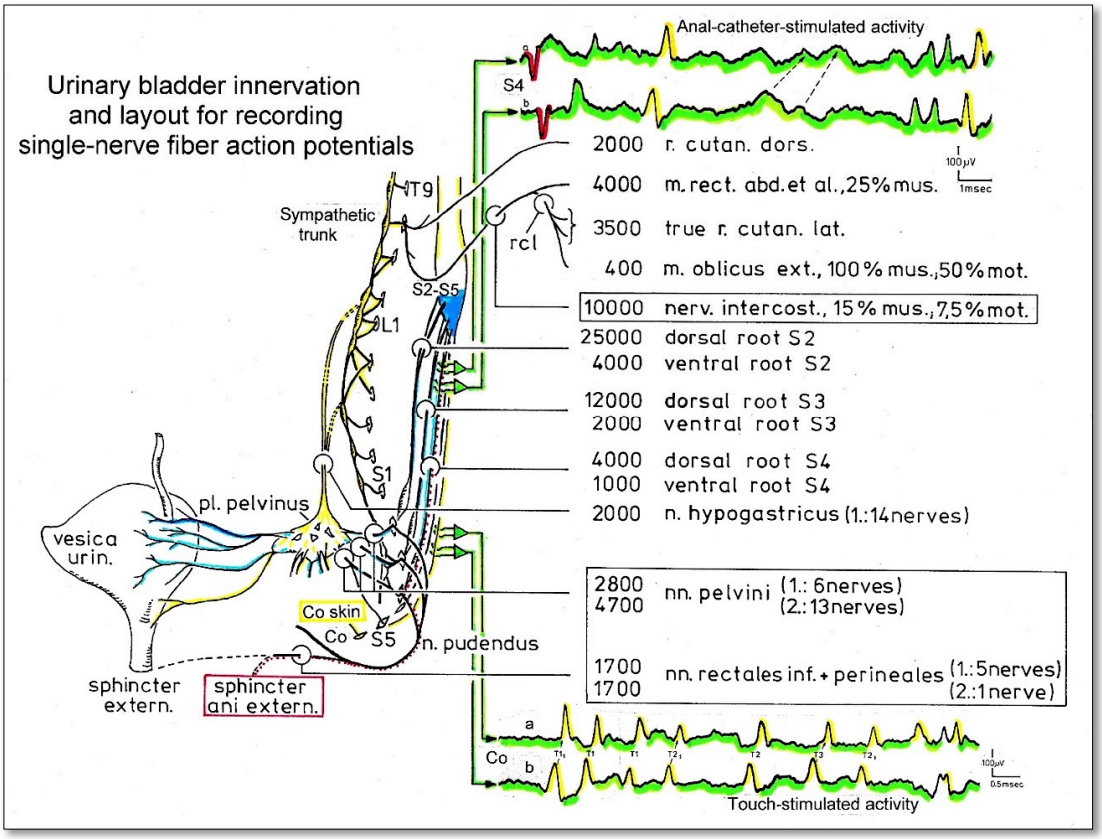

Figure 19. Urinary bladder innervation (anatomy; structure) and recordings of single-nerve fiber action potentials from a S4 and a coccygeal root (electrophysiology; function). Number of myelinated nerve fibers of the nervi rectalis inferioris and perinalis, the nervi pelvini and the nervus hypogastricus. T = thoracal; L = lumbal; S = Sacral; rcl = ramus cutaneus lateralis, no pure skin nerve; %mus = % of nerve fibers leading to muscles; %mot = % of nerve fibers which are motoric; 1 and 2 = Nerve fiber counts from cadavers 1 and 2. Number of nerves in the bracket gives the number sub-nerves of which the nerve consisted. The innervation pathway of the external bladder sphincter is unclear. The S4 root recording informs about single-nerve fiber activity running into the spinal cord (from the bladder receptors) and running out of the cord to the urinary bladder (bladder efferents) upon natural stimulation. Functions of the urinary bladder and the sacral micturition center in the spinal cord, as a part of the human CNS, can therefore be analyzed. The Co root (no efferents; something like a skin nerve) recording informs about skin receptor activity in the coccygeal dermatome.

Thickness of nerve fibers at different distances from the soma (tapering of nerve fibers)

Nerve fiber diameter distributions of nerve roots and peripheral nerves (outside the spinal canal) were compared here, assuming that the nerve fibers have the same diameter along their length. If the peaks in Figure 18Ca at diameters of 7.8 and 9.8 µm ($1.8 \leq d < 2.3$µm) are really the distribution peaks of α_2 and α_3-motoneurons, then these values would indicate that the motoneuron axons are distally slightly thinner, because in the cauda equina they are 8.3 and 10.2 µm **(Figure 3)**.

In the comparisons made here, it was assumed that the reduction in nerve fiber diameters at distal parts is small in comparison to other errors or variations. It will be measured below that the reduction of nerve fiber diameters with increasing distance from the soma is really small. If there is no splitting or branching of fibers. The tapering is 0.2% per 13 cm (see below). A 100cm long fiber, for example of the pyramidal tract, would only reduce the diameter from 10 µm to 9.8 µm.

Tapering of nerve fibers

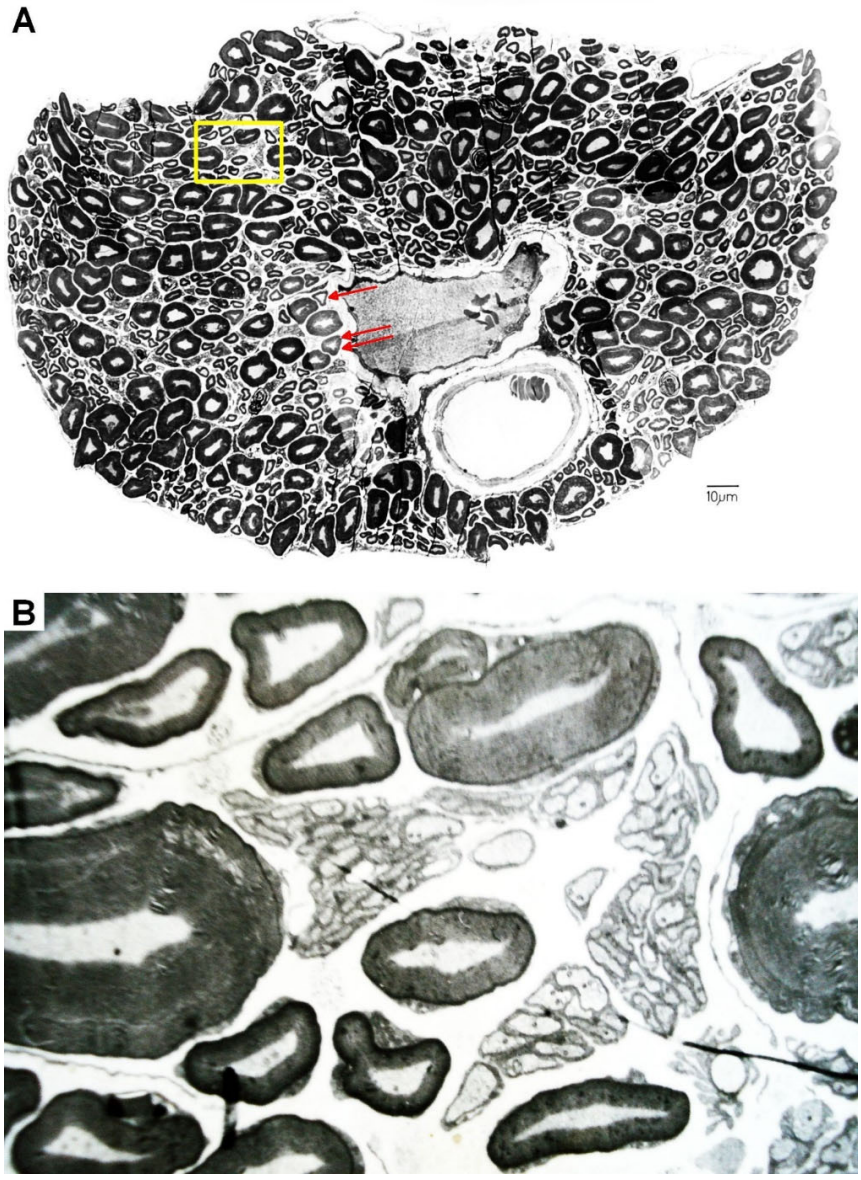

Figure 20. Montage of several electron microscope photographs of an S4 ventral root from HT1. Single arrow marks a nerve fiber with a comparably thin myelin sheath; double arrow marks a nerve fiber of similar size with a comparable thick myelin sheath. Scale not corrected for shrinkage. B. Enlarged scale of the rectangle in A to make unmyelinated nerve fibers visible.

An exact classification of peripheral nerve fibers by the diameter is only helpful if their thickness is changing only little with increasing distance from the soma. It is measured here that the so-called tapering is only little.

Summary of tapering

To determine the tapering [59] of human nerve fibers **(Figure 20)**, rostral and caudal root pieces of cauda equina nerve roots were removed from four cadavers **(Figure 21)** with no known neurological disease, and nerve fiber diameter distributions constructed for four myelin sheath thickness ranges for the two sites and compared with each other **(Figures 22,23)**. The reduction of the group diameter in the different α-motoneuron groups was 0.2 % per 13cm. Accounting for systematic errors, there may be even less tapering. An identified single-nerve fiber showed no tapering. Further, there is indication that γ-motoneurons, preganglionic sympathetic and parasympathetic fibers and skin afferents also reduce their fiber diameter by 0.2 % per 13 cm or less. Consequently, a nerve fiber with a diameter of 10 µm would be reduced to approximately 9.8 µm at 1m from the cell soma. Preganglionic parasympathetic fibers were found to be represented in the roots S1 to S5. At similar distances from the spinal cord, the mean diameter of ventral root α_1-motoneuron (FF) axons increased in the roots from the thoracic towards the lumbo-sacral region before decreasing again in the lower sacral region **(Figure 25)**. Usually no α_1-motoneuron axons were found in S5 roots. The diameter distribution of unmyelinated nerve fibers of a ventral S5 root showed three peaks at 0.25, 0.95 and 1.2 µm.

The unmyelinated fibers with diameters around 0.25 µm may represent parasympathetic fibers. In six selected areas of the ventral S5 root, on average 6.6 times more unmyelinated nerve fibers than myelinated fibers were found.

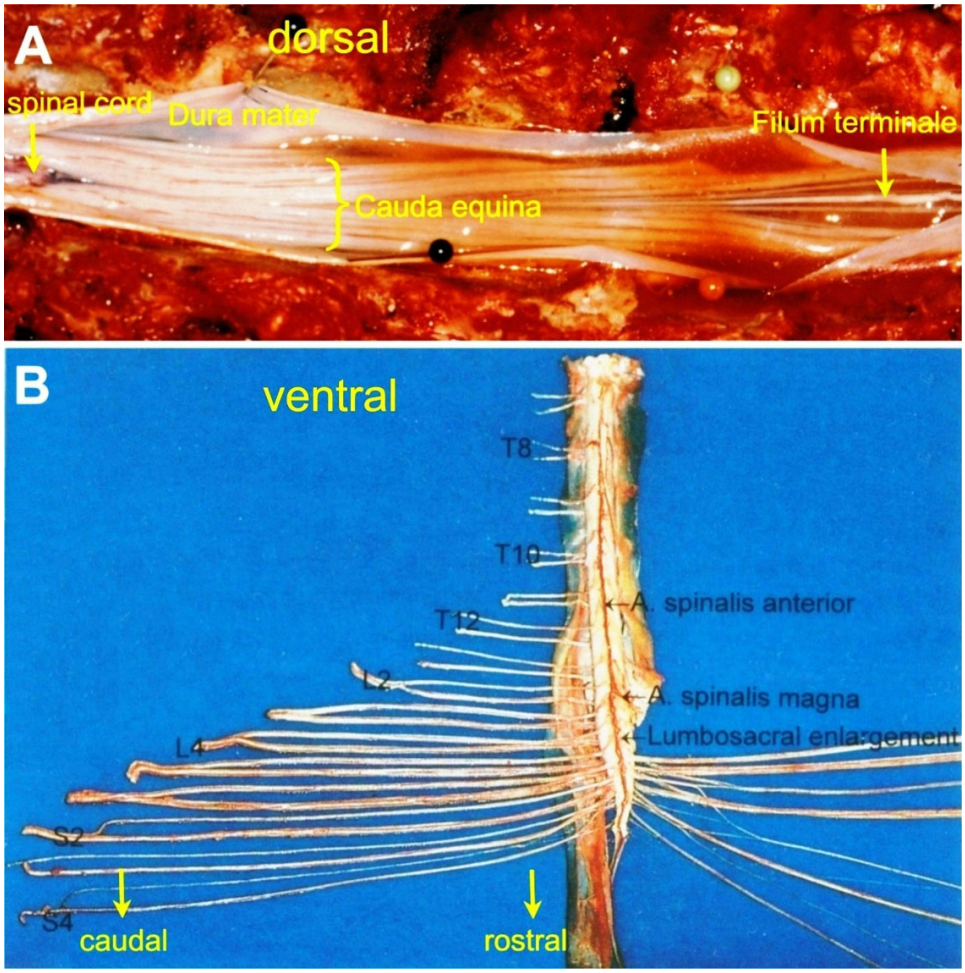

Figure 21. Schematic layout for measuring the tapering of human nerve fibers. After opening the spinal canal (A) and removing of the lower spinal cord with the cauda equina nerve roots and the dura mater (B), rostral and caudal nerve root samples of 1 to 2cm length were removed from identified dissected and fixed nerve roots (mounting in some similarity to B).

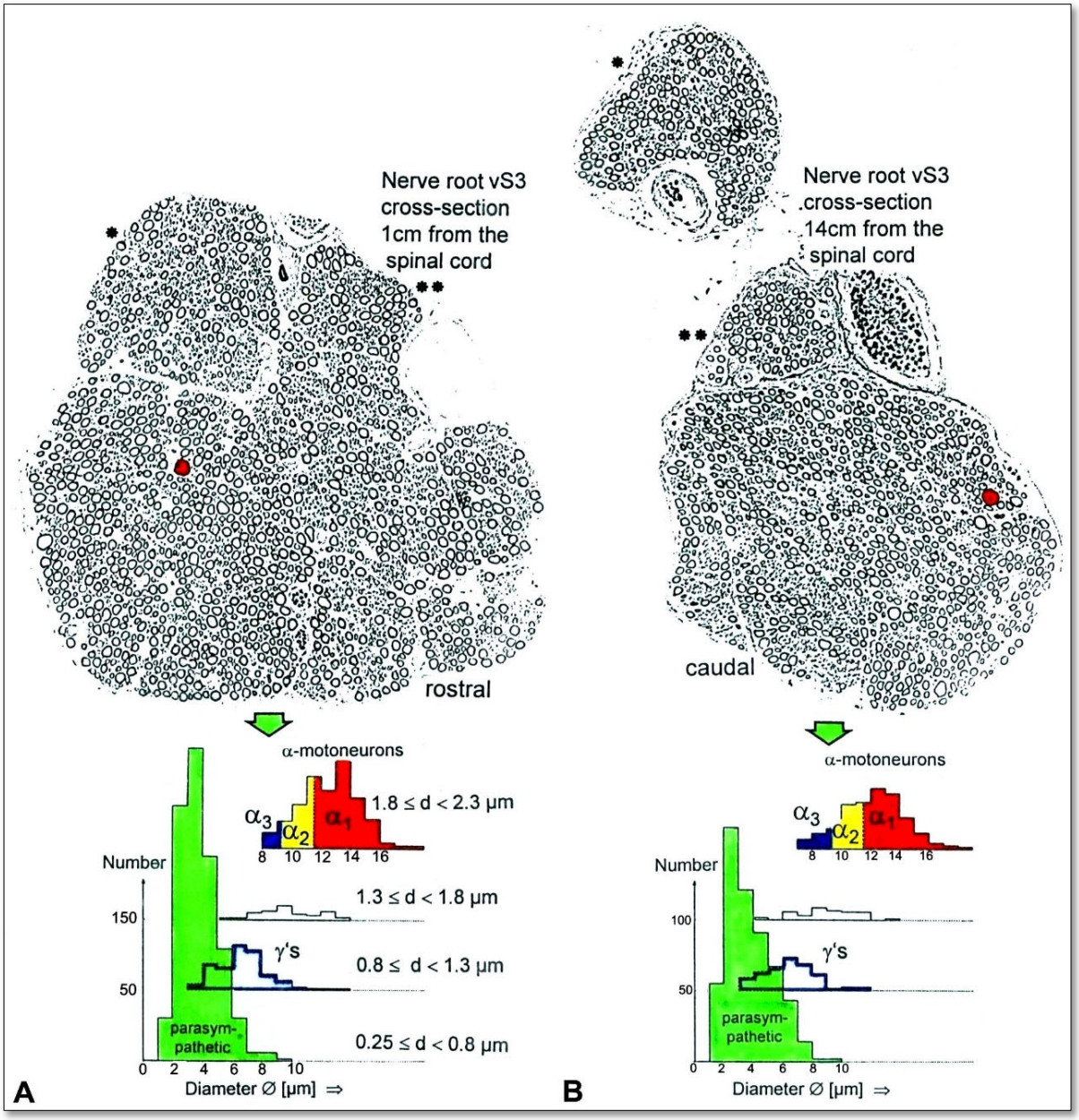

Figure 22. Comparison of nerve fiber diameter distributions of a vS3 root rostral (A) and caudal (B) to measure tapering. After embedding, cutting and staining (Thionin acridine-orange), the cross sections were photographed (x1000), and mean nerve fiber diameter and myelin sheath thickness were measured for the whole cross section or parts of it. Nerve fiber diameter distribution histograms with nerve fiber group characterizations (α's and γ's) from the rostral and caudal cross sections for the four myelin sheath thickness ranges (d) and the corresponding rostral and caudal distributions were compared with respect to tapering. Probable fasciculation of the vS3 root is marked by one or two stars. An identified single fiber in the rostral and caudal cross sections is also marked. If only a few ventral root afferents are present in the ventral S3 root, then the fiber diameter distribution of the myelin sheath thickness range 0.25 µm ≤ d < 0.8 µm represents mainly parasympathetic fibers.

Measuring Procedure

To measure the tapering of human nerve fibers, the spinal cords were removed together with the cauda equina nerve roots from four cadavers **(Figure 21)**, fixated, and the nerve roots were then dissected to a maximum extent under the dissecting microscope in a chamber filled with the fixative.

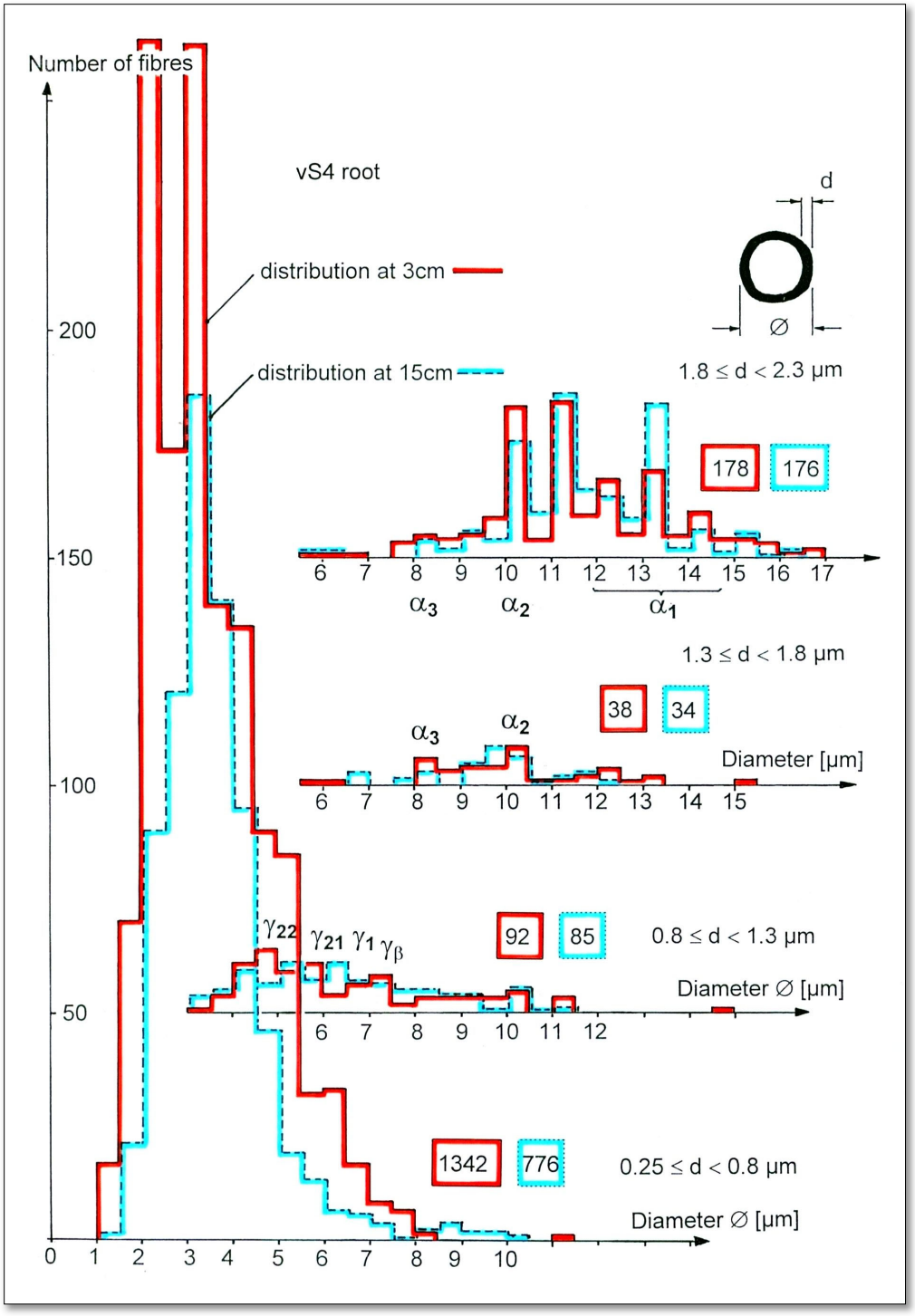

Figure 23. Nerve fiber diameter distributions for four myelin sheath thickness ranges "d" of the rostral (solid line) and the caudal (dashed line) cross section of a ventral S4 root. Nerve fiber groups are partly marked at the corresponding distribution ranges or peaks. Figures in the solid and dashed line rectangles give fiber numbers from the fiber distributions of certain myelin sheath thickness ranges rostrally and caudally. α_1, α_2 and α_3 = α_1 (FF), α_2 (FR) and α_3-motoneurons (S). γ_1 = dynamic γ-motoneuron. γ_{21}, γ_{22} = static γ-motoneurons.

The thin roots were of special interest because they are long and thin and can be expected to allow morphometry of the whole root cross sections over a long distance between the rostral and the caudal root parts. After freeing the root from one another, samples of rostral and caudal roots were taken, post-fixated, embedded, stained, and photographed, and the mean diameter and myelin sheath thickness measured, and nerve fiber diameter distribution histograms constructed **(Figures 22 and 23)**.

The nerve fiber diameter distributions for the rostral and the caudal part were compared quantitatively to find out whether human nerve fibers do or don't taper. The data of all analyzed roots are summarized in **Table 1**.

For thicker roots, the fibers were only measured in a part of the cross sections, and only nerve fiber diameter distributions were compared for the different myelin sheath thickness (d) ranges. The different α-motoneuron groups were mainly compared for the myelin sheath thickness range $1.8 \leq d < 2.3$ µm. Since there was often a considerable re-organization and fasciculation of the roots on their way caudally **(Figure 22)**, the same root cross section area could not be identified safely rostrally and caudally. Only comparable areas were chosen for the analyses. In five cases, the root cross sections could be measured completely, and the rostral and caudal distributions compared.

Reduction of the mean diameter of completely and partially measured roots

The reduction of the mean diameter of α-motoneurons was mainly measured in the diameter range from 8 µm to 16 µm. The mean diameter of the α-motoneurons in all measured cases dropped by -2.3 % to 3.8 % between the cord and, on average, 13 cm caudally on the roots **(Table 1)**. A mean value of tapering of 0.6 % per 13 cm was obtained for the α-motoneurons (and afferent fibers in one case).

Reduction of the mean diameter of completely measured roots

In the roots that could not be measured completely, there sometimes were slight differences in the composition of α_1, α_2, and α_3-motoneurons in the chosen areas of the cross sections. More reliable tapering values are therefore obtained from **Table 1** by only selecting cases in which the whole root or the fascicle have been analyzed rostrally and caudally. In **Figure 23**, the nerve fiber diameter distributions are shown for a ventral S4 root for the four myelin sheath thickness ranges, measured close to and at a distance from the spinal cord. The distributions for the different myelin sheath thickness ranges are very similar, apart from the distribution for the myelin sheath thickness range $0.25 \leq d < 0.8$ µm. It seems that at 3 cm from the spinal cord, there is a thin myelinated fiber population (d ≈ 2 to 2.5 µm), which on its way to the caudal parts leaves the root via root interconnection. From the five cases for which the whole cross sections could be measured (in Table 1 marked by the thick frame), a mean tapering of 0.2 % per 13 cm of α-motoneurons was obtained. If one considers that, on average, distal parts of the roots showed a stronger desiccation in places where the cauda equina consisted of fewer thinner roots, then the tapering of the nerve fibersmay have even be smaller than 0.2 %.

No tapering of an identified single α-motoneuron axon

In one case (ventral S3 root), it was possible to identify a single α-motoneuron axon rostrally and caudally by its size (the thickest fiber), its thin myelin sheath thickness (1.8 µm) and its close location to two thin blood vessels (marked red in Figure 22A, B). The measured mean diameter was 23.5 µm both rostrally and caudally and showed, therefore, no tapering. The single-fiber measurement makes it likely that there may be very little or no tapering at all of nerve fibers if there is no branching of nerve fibers in between the sites where the measured root samples were taken.

Tapering of afferents, γ-motoneurons and preganglionic parasympathetic and sympathetic fibers

The rostral and caudal nerve-fiber diameter distributions of the same root **(Figure 23)** and other cases seem to indicate that the γ-motoneurons and the preganglionic parasympathetic fibers do taper only little or not at all.

The tapering of the preganglionic sympathetic fibers, probably leaving the spinal cord via the TH10 to L2 roots, is more difficult to measure since these roots are much thicker than the lower sacral roots in which the parasympathetic fibers are contained. Since, however, the preganglionic sympathetic and parasympathetic root fibers had very similar nerve-fiber diameter distributions rostrally and caudally **(Figure 24)**, it seems that also the preganglionic sympathetic fibers (contained even more caudally in the ramus albeus) taper only very little or not at all. The much thinner and unmyelinated postganglionic sympathetic fibers (contained in the ramus griseus) have not been measured here.

Sacral neurons reassigned: The sacral autonomic outflow is sympathetic

It has been reported that the sacral autonomic outflow is sympathetic in mice [60] and not parasympathetic. If this is so, then probably the sacral visceral nervous system is the caudal outpost of the sympathetic outflow probably also in human. The importance of the paper is that we need to re-measure the whole human (and animal) nervous systems to up-grade the human neurophysiology and get more safety about its functioning. The drawing back of this publication is that human neurophysiology

Table 1. Reduction of the mean diameter of α-motoneurons (diameter range 8 to 16 µm; myelin sheath thickness range 1.8 to 2.3 µm) from rostral (distance from the spinal cord 1 to 3 cm) to caudal site (distance from the spinal cord 12 to 16 cm) of the cauda equine nerve roots **(Figure 21)**. Presence symp. Or parasymp. = Presence of sympathetic or parasympathetic fibers in the nerve root, symp. = sympathetic, para = parasymp. = parasympathetic. vS3 = ventral S3 root, dS5 = dorsal S5 root, Para 5 = paraplegic patient 5, α-mot = α-motoneurons, prox = proximal, γ's = γ-motoneurons. Number of α-motoneurons (in the entirely or partly measured root cross sections) rostral → caudal = α-motoneurons in the diameter range 8 to 16 µm. Column 4 indicates the presence of sympathetic or parasympathetic fibers in the nerve root or nerve root fascicle.

Case	Root	Part measured	Symp. or para. fibres	Reduction of mean diameter rostral → caudal distance from cord	%	Number of α-mot rostral → caudal	Special notes
1	vT12	whole spectrum	symp.	3 cm –			
1	vS1	whole spectrum	para.	3 cm –			
1	vS3	whole spectrum	para.	12.0 µm → 11.7 µm 1 cm 14 cm	2.5	282 → 205	
1	vS3	single fibre		23.5 µm → 23.5 µm 1 cm 14 cm	0		identified by thin myelin sheath and 2 blood vessels
1	vS4	whole crosssection, only α-mot	para.	11.4 µm → 11.4 µm 1 cm 13 cm	0	37 → 30	more fibres prox., root connections should exist
2	vL1	whole spectrum	symp.	1 cm –			
2	vL5	whole spectrum	–	12.0 µm – 1 cm –			
2	vS4	whole spectrum of whole root	para.	11.5 µm → 11.3 µm 3 cm 15 cm	1.7	174 → 175	73 % more fibres rostrally for $0.25 \leq d < 0.8$ µm
3	vL1	whole spectrum	symp.	3 cm –			
3	vL5	whole spectrum	–	13.2 µm → 12.7 µm 1 cm 13 cm	3.8	129 → 119	
3	vS1	whole spectrum	para.	2 cm –			
3	vS4	whole spectrum of whole root	para.	11.7 µm → 11.7 µm 1 cm 16 cm	0	27 → 52	root fascicle of 20 µm measured
3	vS4	whole crosssection, only α-mot	para.	12.3 µm → 12.3 µm 1 cm 11 cm	0	23 → 15	
4	vL5	whole spectrum	–	12.8 µm → 13.1 µm 1 cm 12 cm	2.3	163 → 159	no tapering for γ's
4	vL5	α-mot spectrum	–	16 cm			
4	dS5	whole root, α-mot	/	13.4 µm → 13.5 µm 1 cm 16 cm	–0.7	26 → 22	
Para 5	S5	whole spectrum, whole fascicle S5	para.	8.3 µm ↔ 8.2 µm 3 cm 6 cm $7 \leq d < 11$ µm	1.2	70 → 70	

was not cited even though the authors propose treatment in human.

The Science Editor's summary is also not convincing: "Sacral neurons reassigned. The autonomic nervous system regulates the function of internal organs such as the gut. The parasympathetic and sympathetic arms of this system tend to operate antagonistically. Espinosa-Medina et al. [60] used anatomical and molecular analyses to reevaluate the assignment of neurons in the sacral autonomic nervous system. Previously categorized as parasympathetic, these neurons are now identified as sympathetic. The results resolve a persistent confusion about how the two systems developed and open the avenue to more predictable outcomes in developing treatments targeted to the pelvic autonomic nervous system."

The Editor of Science has no problems to switch easily from animal data to human treatment. Probably he has never heard anything about 'Translational Medicine'. The biggest difference between mice and men is the nervous

system. The human nervous system needs something like 20 times more time to develop than the one of mice to achieve full complexity and this will have consequences for the treatment of human patients. For a reassignment one could have expected also the measuring of function at the neuron level. If the parasympathetic neurons are really sympathetic, then in the pictures of the Author, parasympathetic has to be replaced by sympathetic. The reassignment has no consequences for the measured organization of the human CNS, because the Author measured how populations of neurons organize themselves. The Authors assignment was done by functional aspects and to be in accordance with standard medical knowledge. If the human bladder for example is filled retrogradely, stretch and tension receptors will fire. Since the identification of groups of neurons with their properties is not sufficient exact in human and animals for further qualified research, the nervous systems of humans and animals have to be clarified from the scratch. The Author had started it.

Since myelinated preganglionic sympathetic and parasympathetic nerve root fibers have very similar nerve fiber diameter distributions **(Figure 24)**, it could well be, from the point of view of group nerve fiber diameters, that the sacral parasympathetic fibers are really sympathetic fibers.

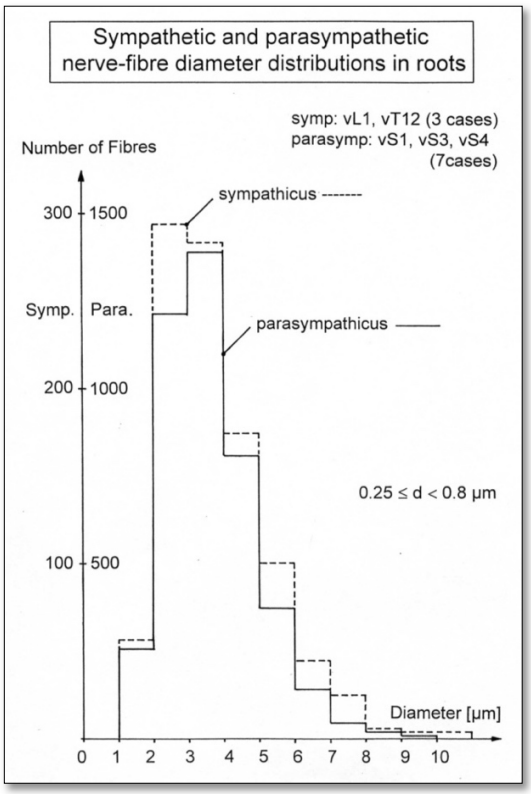

Figure 24. Sympathetic (dashed line) and parasympathetic (solid line) efferent nerve-fiber diameter distributions of several roots indicated in the upper right Figure. Myelin sheath thickness between 0.25 µm and 0.8 µm. Note that the sympathetic and parasympathetic distributions are very similar. sympathicus (symp): vL1, vL2 (three cases); parasympathicus (para): vS1, vS3, vS4 (seven cases).

Representation of preganglionic parasympathetic fibers in nerve roots S1 to S5

The measurements summarized in **Table 1** indicate that the S1 roots also contain a substantial number of preganglionic parasympathetic fibers. The S1 root was identified by counting from the 12th intercostal nerve (subcostal) downwards and by the fact that the ventral S1 root is the last thick root in the caudal direction **(Figures 15a, 21B)**. Parasympathetic fibers were found earlier in thin S5 roots. Since S5 roots are very thin (much thinner than the S4 root), their fiber numbers are not as important as those in the S1 root.

Representation of differently sized α_1-motoneuron axons at different spinal cord levels

Figure 25 shows that the mean of the α_1-motoneuron axon diameter distributions (indicated by an arrow) increase from the ventral (v) TH12 root towards the lumbar roots, before decreasing again in the lower sacral

roots. In the ventral S5 root, there were no α_1-motoneuron axons at all; this agreed with the electrophysiologic identification, when recording single-nerve fiber action potentials from undissected nerve roots during surgery. In the ventral L1 root, there were only a few α_2 and α_3-motoneuron axons contained. Even though these measurements were obtained from an arbitrarily selected set of cross-sectional areas, and the fiber distributions could vary in other sets, these measurements still reflect somehow the different distributions of differently sized α_1-motoneuron axons at different spinal cord levels. The different representation of α_1, α_2 and α_3-motoneuron axons in muscle nerves has consequences for the understanding of the size principle of motor unit recruitment. But all α_1-motoneurons fire with one action potential at 10Hz or higher **(Figure 4)** and the possible subgroups of α_1-motoneurons are indicated in **Figure 3**.

Unmyelinated nerve fibers in a ventral sacral S5 root

In the cross sections of a ventral S5 root of the paraplegic patient 5 (24 years of age), unmyelinated nerve fibers

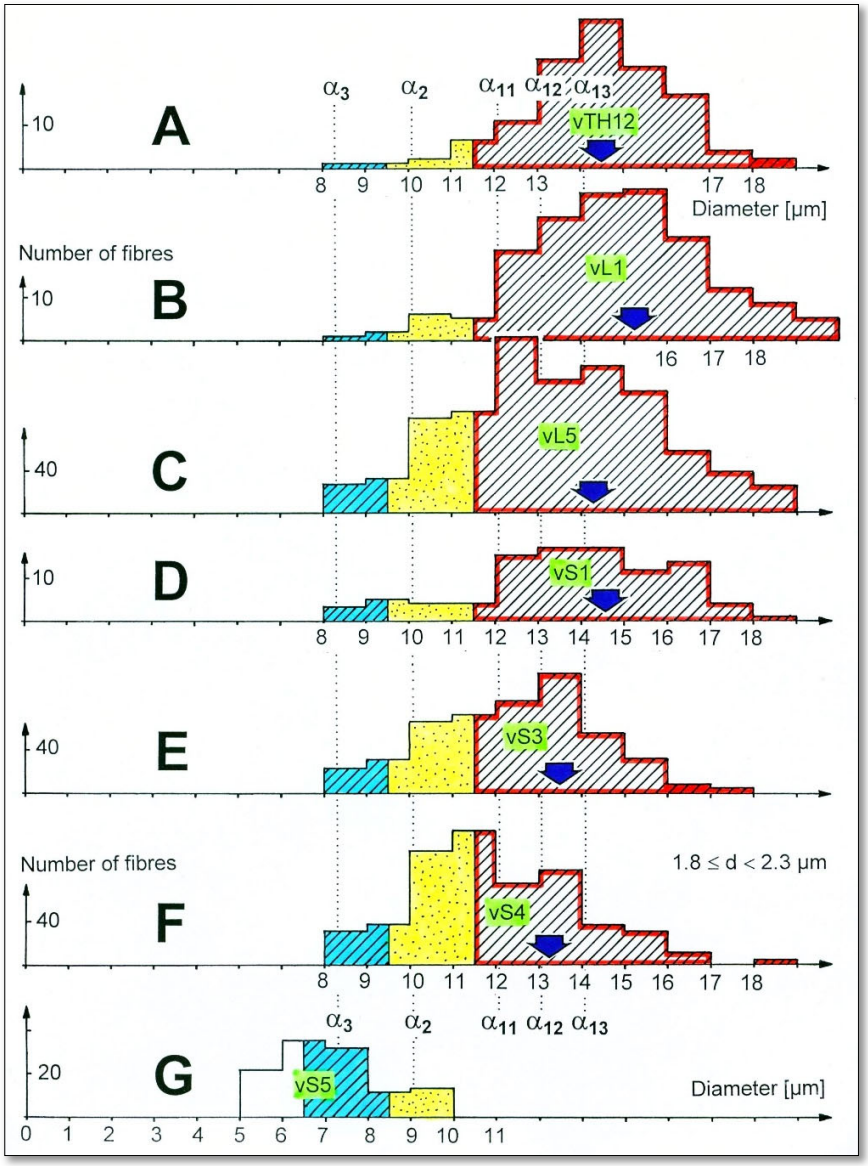

Figure 25. α-Motoneuron type representation in nerve roots (A-G). Composition of sub-motoneuron groups in a number of diameter distributions of ventral roots in the myelin sheath thickness range 1.8 µm ≤ d < 2.3 µm. α_1, α_2, α_3 = α_1 (FF), α_2 (FR), α_3-motoneurons (S). α_{11}, α_{12}, α_{13} = possible subgroups of α_1-motoneurons. Arrow indicates mean of the α_1-motoneuron axon diameter distribution.

were observed **(Figure 26A)**. Because of the existence of ventral root afferents in the lower sacral nerve roots [42, 43], the finding of unmyelinated fibers was to be expected. Since in different cross sections there seemed to be sometimes mainly thick or mainly thin unmyelinated fibers, mean diameter of unmyelinated fibers were measured, and diameter distributions constructed **(Figure 26B)**.

The distribution in one area of unmyelinated fibers showed three peaks (solid line distribution) at 0.25, 0.95 and 1.2 µm. In another part of the cross section with

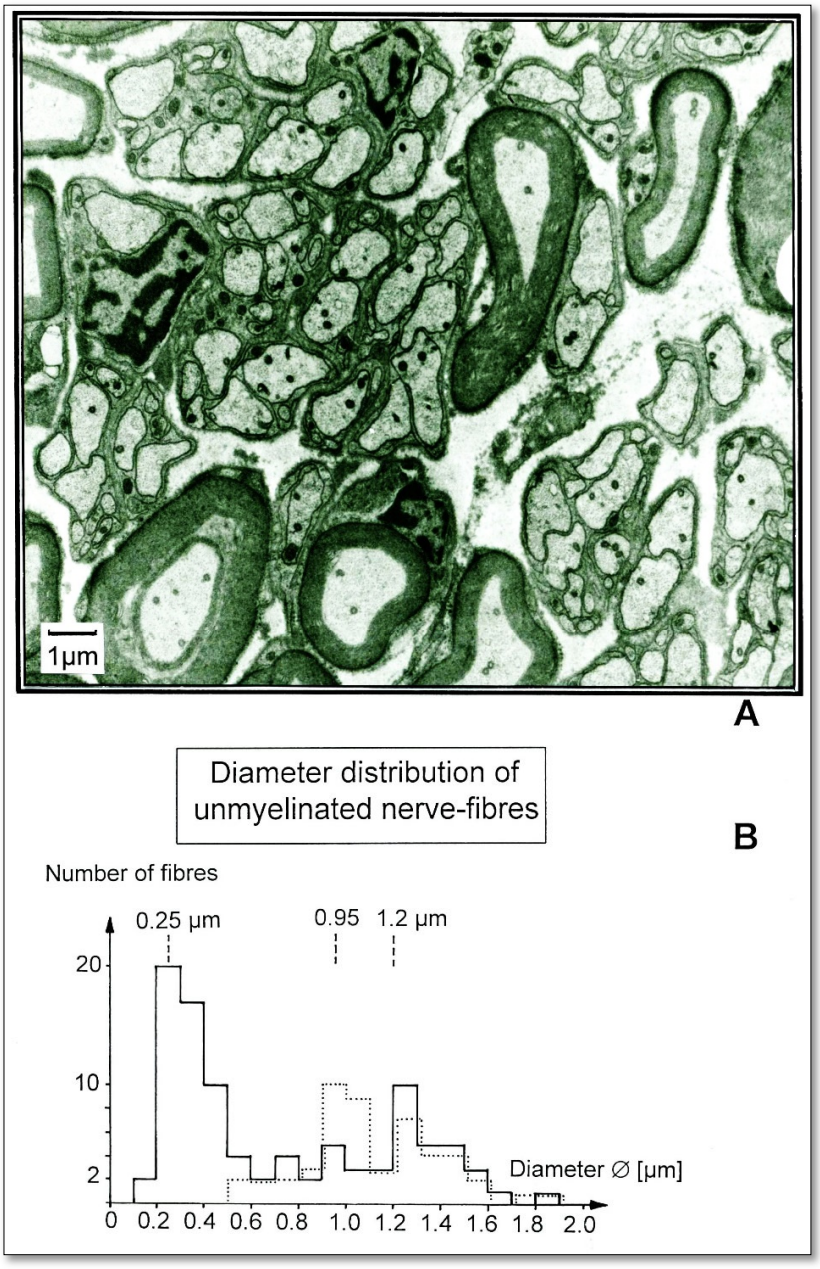

Figure 26. A. Section of a ventral sacral S5 root of a 24-year-old female paraplegic patient (para 5). Thin and thick unmyelinated nerve fibers can be seen besides myelinated nerve fibers. B. Nerve fiber diameter distributions of unmyelinated nerve fibers. The solid line distribution was taken from an area of which the section in A was a part. The dotted line distribution stems from an area in which mainly only thick myelinated fibers were present. Note that the peak at 0.25 µm is missing in the distribution marked by the dotted line.

mainly thick unmyelinated fibers (dotted line), the distribution showed only peaks at 0.95 and 1.2 µm. Because of the three distribution peaks at least three groups of unmyelinated nerve fibers seem to exist in the lower sacral nerve roots, which may belong to the somatic and parasympathetic nervous system divisions.

For including unmyelinated nerve fibers into the classification scheme **(Figure 3)**, much more research is necessary. Morphometry can be performed, but to measure the conduction velocities is the problem. Single-fiber action potentials cannot be recorded extracellularly from single unmyelinated nerve fibers. But maybe compound action potentials (see below) can be recorded.

Numbers of unmyelinated nerve fibers in relation to myelinated fibers

In six areas of the ventral S5 root of the paraplegic patient 5, the number of unmyelinated fibers was counted, and diameters measured. The fiber number varied quite much according to whether more thin fibers with a group diameter around 0.25 µm were contained or more thickly unmyelinated fibers were contained with probable group diameters of 0.95 or 1.2 µm. In the chosen areas (approx. 23 µm x 17 µm), the number of unmyelinated fibers ranged from 42 to 173, and the number of myelinated fibers from 10 to 16. The relation between unmyelinated and myelinated fibers ranged from 3.5 to 14. The mean ratio was 6.6. The ratio between unmyelinated and myelinated fibers depended therefore strongly on the number of thin myelinated fibers contributing to it.

Tapering of nerve fibers of nerve roots and peripheral nerves

A tapering of nerve fibers of nerve roots by 0.2% per 13 cm was identified by the present measurements when the whole cross sections were measured. Concerning the systematic error due to the mostly better fixation rostrally as a result of a slightly different osmotic pressure and different autolysis, and taking into account that an identified single fiber showed no tapering, it is safe to conclude that the tapering of nerve fibers is 0.2% per every 13 cm of length or smaller. First measurements show that the phrenic nerve fibers (0.8µm ≤ diameter) reduce their diameter by 0.2 % per every 10 cm of length. There is indication for human nerve fibers showing a slight tapering tendency. The conclusion that nerve fibers only show little tapering is in accordance with an earlier comparison of morphometric measurements on skin nerve branches of intercostals and a coccygeal nerve root [58] through which mainly skin nerve fibers run to the coccygeal dermatome. The nerve fiber diameter distributions of the nerves and the root were very similar, even though the coccygeal root piece was taken approximately 10 cm away from the ganglion and the spinal cord, whereas the skin nerve branch sample of the intercostal was taken approx. 25 cm away from the ganglion. In **Table 1**, the dS5 root of case 4 shows a negative tapering value of 0.7%. This negative value does not mean that afferent fibers get thicker the farther they are measured from the ganglion. Most likely, the systematic errors of fixation and staining gave rise to the negative value of tapering. By taking the rostral root sample at a distance of 1 to 3 cm from the spinal cord, the central-peripheral transition zone [61] was not touched. The analyzed fascicle of the S5 root of paraplegic 5 was most likely a ventral one, since a dorsal root fascicle would have thicker fibers, at least from the T1 (PC) skin afferents. The distance of approx. 3 cm between the rostral and the caudal (it is unclear what is rostral and what is caudal) cross sections is too small in comparison to the variation of the morphometry due to the systematic error, even though as expected, the quality of the root cross sections from the patient was better than those from the cadavers (no autolysis). Long distances are needed to measure tapering.

Saltatory conduction of myelinated nerve fibers

Saltatory conduction and nerve fiber diameters for different internodes (teased fiber dissection)

Measurements of nerve fiber diameters in general and tapering especially depend on the assumption that the nerve fiber diameters are very similar along different internodes. Internodal lengths and their nerve fiber diameters have to be measured for clarification [41].

With normal effort, 130 **(Figure 27B)** of the 570 myelinated fibers of a S4 ventral root **(Figure 21B)** were teased and, additionally, the diameters of 95 of these were measured **(Figure 27D)**. As the similar shape of the diameter histogram of the teased fiber dissection **(Figure 27D)** in comparison to that of **Figure 18Ba** indicates, a somewhat representative selection was teased. In order that several internodal lengths could be determined, as much of a length of a fiber as possible was teased. **Figure 27A** shows a montage of three photographed teased single fibers of different thicknesses. It can be seen that the internodal lengths are not always similar. It seemed that every third to fifth was markedly different from the other ones. At three thick fibers, it was found that the longer internode corresponded with a thicker nerve fiber as is shown in **Figure 27A**, fiber 1, so that the ratio of internodal length to nerve fiber diameter **(Figure 27C)** was not changed. Figure 27B shows the frequency distribution histogram of the internodal length. This distribution also shows four characteristic peaks, as the frequency distribution of the nerve fiber diameters does **(Figure 18Ba,** motoneurons). This similarity can be understood since the nerve fiber selection of the teased fiber dissection of Figure 27D was somewhat representative, and the relation between internode length L and fiber diameter d was proportional **(Figure 27C)**. By

dividing the internodal length in Figure 27B by L/d = 100, one gets a somewhat similar histogram as in Figure 18Ba, if the four histograms are added. By teased fiber dissections therefore it is shown [41] **(Figure 27C)** that in human sacral nerve roots the internodal length L is related to the nerve fiber diameterd, including myelin sheath, by L/d = 100. Therefore, in frequency distribution histograms of internodal lengths, grouping of nerve fibers can also be observed **(Figure 27B)**.

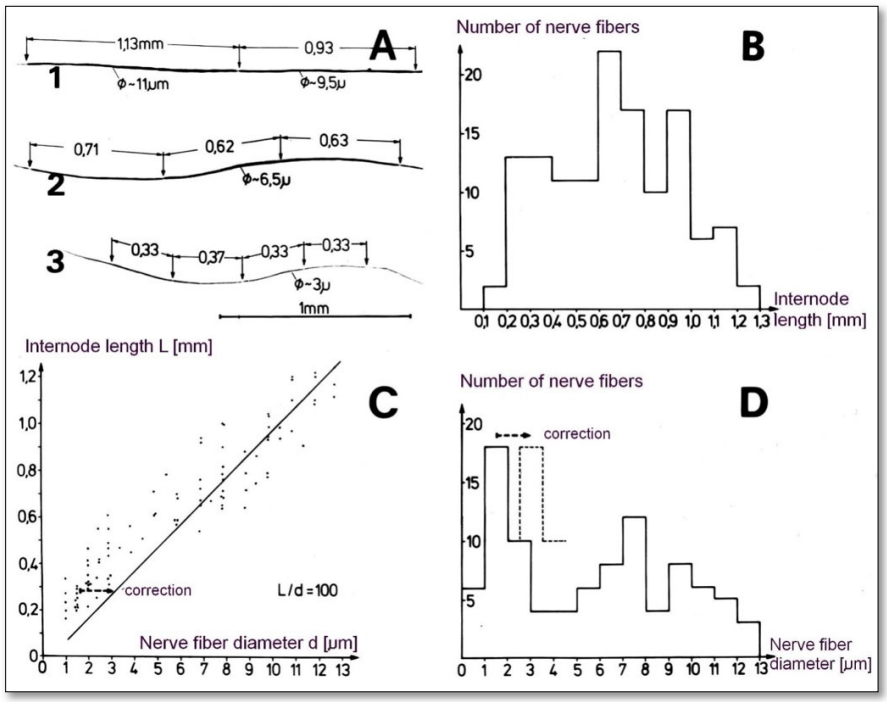

Figure 27. Quantified results of a teased fiber dissection of a whole S4 ventral root from HT1. No shrinkage correction. A. Three original nerve fiber dissections, several internodes are measured and marked. Approximate fiber diameters (Ø) are indicated. The teased fiber dissection, the Author learned from Stämpfli [62]. B. Frequency distribution histogram of internode lengths. Numbers indicate peaks. Class borders are < and ≤. If more than one internode length of a nerve fiber was measured (30% of the cases), then the mean value was used. C. Internode length in relation to its nerve fiber diameter. A small correction for small nerve fibers was performed (see D). D. Very approximate nerve fiber diameter frequency distribution. Since the diameter of the nerve fibers were measured under the stereomicroscope with a 100 times magnification, the thin nerve fibers were estimated more than measured. Comparing this diameter frequency distribution of the S4 ventral root with that of a S4 ventral root measured with a light microscope **(Figure 18Ba)**, a correction for small nerve fiber diameters was performed and indicated in the Figure.

Action potential waveform changes due to saltatory conduction

The action potential waveform may vary a bit along the nerve fiber, according to the different localization of the node of Ranvier with respect to the recording electrodes [62, 63]. Only three internodes lie between the electrodes of a pair of electrodes for the nerve fibers contained in peak 1 of Figure 18B (mean internodal length = 1.2mm **(Figure 27B)**; electrode distance in a pair = 4mm). Furthermore, the measurement of several internode lengths from one fiber indicated that every third to fifth internode length was quite different from the other ones **(Figure 27A)** and, also, the nerve fiber diameter was then different from the other ones. Therefore, one cannot exclude some changes in the action potential wave form from differences of the internodes, even though the nerve fiber could have partly compensated for such differences by a different internodal cleft or a different sodium and/or potassium channel density.

Space distribution of single-nerve fiber action potentials

Even though the electrophysiology is presented only in the next section, a recording is needed to show that in a first approximation, one can disregard the saltatory conduction, because the APs are distributed over several until many internodes.

Figure 28 shows the action potential (AP) durations of an α_2-motoneuron, a γ_1 (dynamic), a γ_{21}-motoneuron (static), and a parasympathetic efferent fiber at a measuring temperature of 33°C. The main peaks of the triphasic waveform are approximately 0.15, 0.4, 0.5, and 0.6ms long, respectively. The space distribution (length) (v = s/t; s = v times t) of the single-fiber APs along the fibers were approximately six (40m/s times 0.15ms = 6mm; α_2), 5.3, 5, and 3.2 (par) mm, respectively. With the approximate nerve-fiber diameters of 10.2, 6.8, 5.8, 3.5µm **(Figure 3)**, we obtain internode lengths of (L/d = 100) 1.02, 0.68, 0.58, and 0.35mm, respectively. The main peak of the triphasic AP was approximately distributed over five (6mm:1.2mm = 5; α_2), 7.8, 8.6, and 9.1(3.2:0.35 = 9.1; par) internodes, respectively.

With this result that we can disregard in a first approximation the saltatory conduction, because the action potentials are space-distributed over several internodes. We change now to the electrophysiology to establish a qualified classification scheme of human peripheral nerve fibers to explore on its basis the functioning of the human CNS and in turn its repair.

Conclusion with respect to COVID-19 treatment

Even though the morphometry of human nerve roots and nerves has no direct consequences for the treatment of Covid-19 infected patients, but it shows on what level basic medical research has to be started and performed. Further, in the medical study it is also started with the anatomy, followed by the physiology and then the treatment of human patients. With the following step to human electrophysiology based mainly on the new recording method, we come nearer to the treatment of patients. Mostly, a basic new measuring method brought progress in science or medicine and it was also so with the single-nerve fiber action potential recording method (Introduction).

ELECTROPHYSIOLOGY: SINGLE-NERVE FIBER ACTION POTENTIALS AND CONDUCTION VELOCITIES

Principle of recording single-afferent and efferent nerve fiber action potentials

The development of the single-nerve fiber action potential recording method was possible because of the unique anatomical landscape of the human spinal canal. Because of the Ascensus of the spinal cord, the lumbosacral nerve roots have become very long and form the cauda equina **(Figures 15, 21)**. Since the caudal sacral nerve roots are very thin **(Figures 15aA, 21)** and are only ensheathed by a thin layer of cells **(Figure 20A)**, they are ideal for recording single-nerve fiber action potentials (APs) from undissected nerve roots. Since humans have no tail, continence (mainly S2 to S5) and sexual functions are mainly located in the conus medullaris only. Those functions are therefore represented in the lower sacral nerve roots and they are not intermingled with tail functions as they are for example in rats, cats and dogs.

Recording of single-nerve fiber action potentials from nerve roots and splitting of the multiunit recording into natural impulse patterns of several single afferent and efferent fibers

The schematic recording layout was shown in **Figure 11** to record single-nerve fiber action potentials (APs) extracellularly from undissected nerve roots (in that case from two fibers) with two pairs of platinum wire electrodes.

A real recording arrangement during an operation is shown in Figure 29. To obtain natural impulse patterns simultaneously from several single afferent and efferent nerve fibers to analyze CNS functioning, the summed impulse traffic of several afferent and efferent fibers in a nerve root has to be split into the impulse patterns of single fibers **(Figure 30)**. The splitting is achieved by recognizing the APs from certain single fibers on the basis of wave form comparisons on the two recording traces and the conduction time which an AP needs to travel from one electrode pair to the other one (10mm) and selecting these APs out. The summed impulse traffic of the recording in **Figure 29** is split into the impulse patterns of 5 single afferent and efferent nerve fibers **(Figure 30)**. This procedure is somehow the opposite of the adding up of impulse patterns of several single fibers **(Figure 12)**.

In the thin lower sacral nerve roots, there are afferent and efferent fibers in the ventral and dorsal roots.

The splitting of the skin afferent activity upon touch or pin-prick into the natural impulse patterns of the different single touch receptors is shown in **Figure 31**. Such messages inform the CNS about changes in the periphery. Similar natural impulse patterns inform the CNS about changes in the urinary bladder or anal canal, stimulated by bladder filling or bladder or anal canal catheter pulling **(Figure 2)**.

Simultaneous recording of afferent and efferent action potentials to analyze integrative properties of the human CNS

As we can measure the natural impulse patterns, generated by certain single receptors in the periphery, which run into the spinal cord (CNS) (afferents) and those patterns which leave the cord (efferents) in ensembles of single fibers simultaneously **(Figure 32)**, it becomes possible to analyze the integrative properties of the largely unchanged CNS of brain-dead humans (HTs) at the cellular level. This also means that the change in function, caused by CNS injury, can be identified.

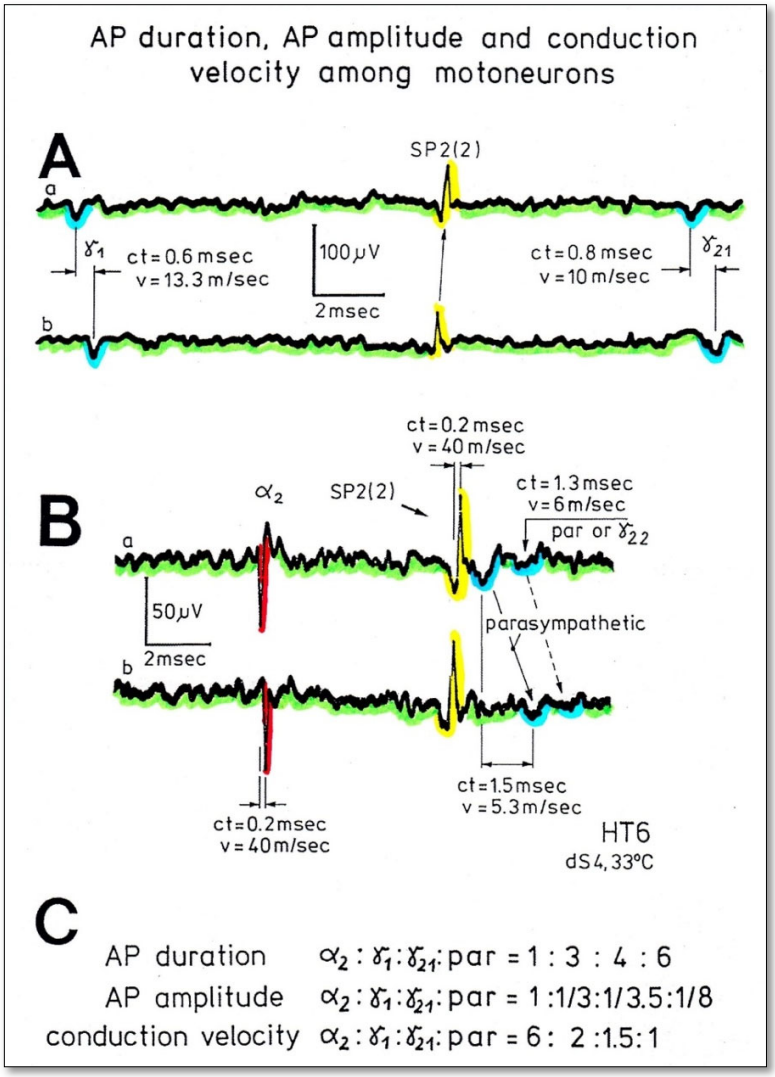

Figure 28. A, B. Recordings of single-nerve fiber action potentials (APs). C. Relation between the AP durations, AP amplitudes and conduction velocities of single α_2, γ_1, γ_{21} and parasympathetic motoneurons. HT6, dS4-root, 33°C.

Conduction velocity distribution histogram to classify nerve fiber groups electrically and identify single-nerve fiber APs

Through morphometry, nerve fiber groups could be identified in nerve fiber diameter distribution histograms **(Figures 17, 18)**. By measuring conduction velocities of recorded single-nerve fiber action potentials during a certain time period and plotted conduction velocity distribution histograms, one can recognize different nerve fiber groups in the distributions **(Figure 33)**. With the identified group conduction velocities, one knows for the actual recording in what kind of nerve fiber the action potential was generated. For a safe identification, calibrations are necessary. One calibration relation is that the secondary muscle spindle afferents (SP2) conduct at the same velocity as the α_2-motoneurons **(Figure 33)**. Since in caudal sacral nerve roots only few primary spindle afferents (SP1) and α_1-motoneurons, this identification is easy. But if in more rostral roots are more primary spindle afferents and α_1-motoneurons, then the additional calibration relation holds that the primary spindle afferents conduct with the same velocity as the α_1-motoneurons **(Figure 34)**.

These calibration relations are easily to apply because the spindle afferents and the motoneurons are thick fibers and conduct fast with large action potentials **(Figure 14)**. But the thinner fibers, conducting more slowly and having a small action potential amplitude, are the problem in identification. **Figure 35** shows that parasympathetic APs are just recognizable. The group conduction velocity peaks of the parasympathetic fibers can be distinguished from those of the different γ-motoneurons. But if, when

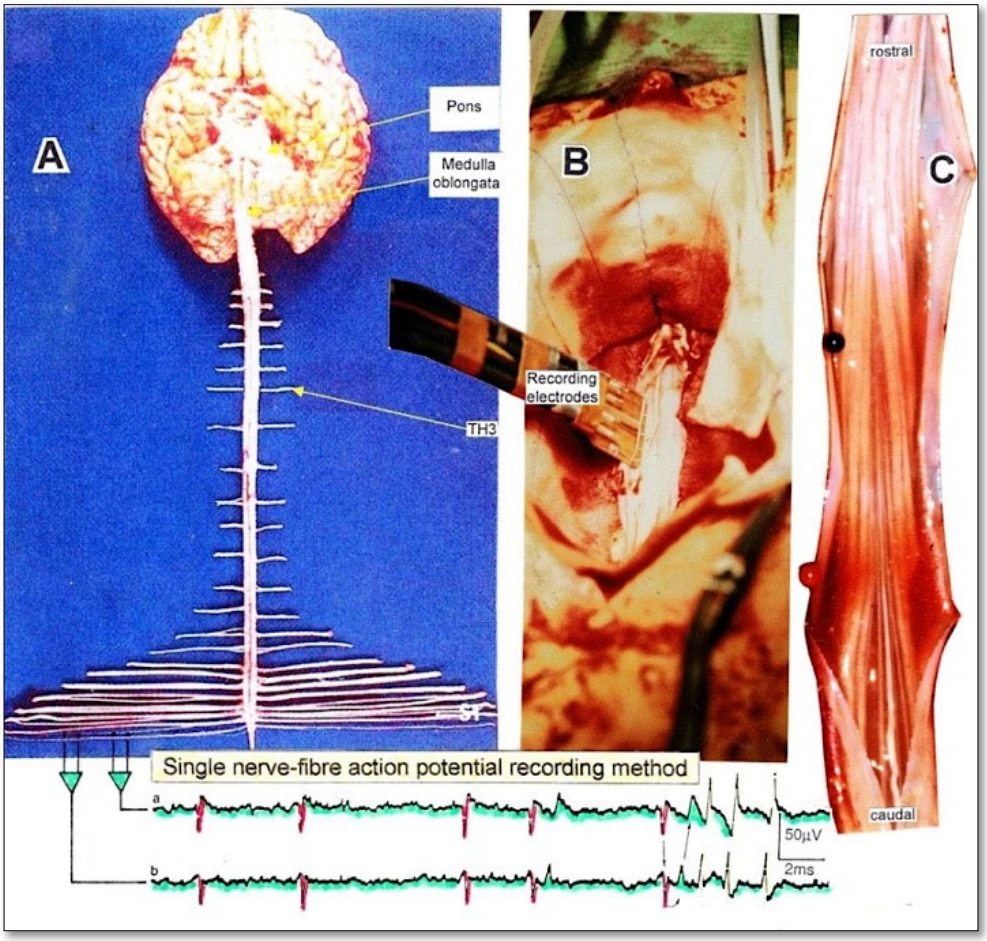

Figure 29. Anatomical layout for the recording of single-nerve fiber action potentials to analyze the self-organization of neuronal networks of the human CNS under physiologic and pathophysiologic conditions. A,B,C. By recording with two pairs of platinum wire electrodes (B) from sacral nerve roots (cauda equina, C) containing between 200 and 500 myelinated nerve fibers, records were obtained in which single nerve-fiber action potentials (APs) were identified from motoneurons (main AP phase downwards) and afferents (main AP phase upwards). Note, in B there is in between the electrode pairs a sensor for the temperature measurement.

especially the temperature is low (see below) the different peaks do not separate (they are fused), then a logarithmic plotting will help.

Identification of peaks of γ-motoneurons and parasympathetic fibers in conduction velocity distributions on a log scale

On a linear scale the conduction velocity peaks may fuse and canonly partly be separated by their different functions **(Figure 36Da, Ea)**. By constructing first histogram classes for conduction times however and plotting them then on a log scale from the column values, the velocity peaks separate. Figure 36D, E shows that the fused γ-peaks of the linear plots (Da, Ea) split up into different peaks on the log scale (Db, Eabc). Since first histogram classes of conduction times were constructed, using a linear scale, it was also possible to study the dynamics of peaks or peak values upon stimulation. The group identification of single-nerve fiber action potentials is necessary to explore human CNS self-organization and learning.

Figures 36Db and 36Eb show several distribution peaks in which the γ_1 and γ_{21}-peaks could be identified from earlier functional considerations. By comparing the velocity distributions obtained upon stimulation with those without stimulation **(Figure 36E)**, and reasonably assuming that the dynamic intrafusal motoneuron peaks are higher upon stimulation **(Figure 36Ed)** and the static ones are higher with no stimulation **(Figure 36Ec)**, a second static γ_2-peak (γ_{22}) could be identified and at least one further rather dynamic motoneuron peak (para) can be seen. This peak distribution observed in the paraplegic patient could also be found in the measurements in HT6 **(Figure 36Db)**. That the "Para" peak contains really

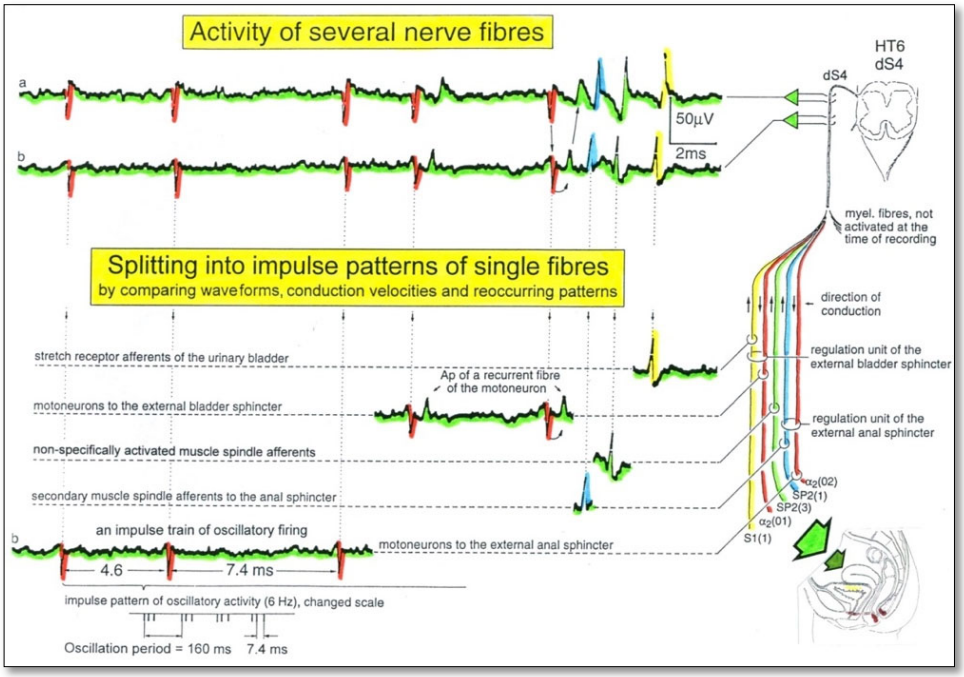

Figure 30. Schematic splitting of the activity of several nerve fibres into simultaneous impulse patterns of single fibres by comparing wave forms, conduction velocities and reoccurring characteristic impulse patterns (rhythmic firing of sphincter motoneurons). The different conduction times and wave forms were recognized on an expanded time scale. Stretch receptor and secondary muscle spindle afferents contribute to the drive of sphincter motoneurons and form, together with other afferents, regulation units.

activity from parasympathetic fibres was shown other publications [4, 5]. The identification of parasympathetic efferents contributes substantially to the understanding of urinary bladder functions under physiologic and pathophysiologic conditions and its repair by coordination dynamics therapy. The nerve fibre groups obtained from conduction velocity distributions for single fibres are in accordance with the sub-compound action potentials of compound action potentials, which will be shown in the next section.

To get more safety in classifying nerve fiber groups through conduction velocities and the identification of single-action potentials, so far induced by natural stimulation, electro-stimulation will be used additionally.

Nerve compound action potentials analyzed with the simultaneously measured single-nerve fiber action potentials [64]

Summary

Compound action potentials (CAPs) and single-nerve fiber APs were recorded with two pairs of wire electrodes from an S5 root from a paraplegic patient during surgery. The compound APs were evoked by electrical nerve root stimulation.

Frequency distribution histograms of single-nerve fiber conduction velocities were constructed, and nerve fiber group conduction velocities were compared with the conduction velocities of the peaks of the CAPs. By increasing the strength of the stimulation, the peaks in the CAP could be identified, and the threshold order of efferent nerve fiber groups determined. Using additional literature data, it is likely that the primary spindle afferents have the lowest threshold due to electrical nerve root stimulation followed by the α_1-motoneurons (FF), the secondary muscle spindle afferents, the α_2-motoneurons (FR), the α_3-motoneurons (S), the γ_β, γ_1 (dynamic), γ_{21} (static), γ_{22} (static), and the parasympathetic motoneurons.

By comparing the mean area of a single-nerve fiber AP with the areas of the peaks of the compound APs, it was found that 230 single-nerve fiber APs contributed to the compound AP. In the secondary spindle afferent fiber and α_2-motoneurons groups, 53 fibers were stimulated (23%). The α_3-motoneuron peak and the afferents in the same velocity range contained 101 fibers (44%), the γ_β peak contained nine fibers (4%), the γ_1 32 (14%), the γ_{21} 23 (10%) and the γ_{22} 12 (5%) fibers. Additionally, two primary spindle afferents and two α_1-motoneurons most likely contributed to the compound AP. Since the large peaks in the compound APs did not change their area with increasing stimulation, most likely all muscle spindle afferents and α-motoneurons were activated to contribute to the compound AP.

Electrical intravesical stimulation evoked single-nerve fiber action potentials (APs) and compound action potentials (CAPs) of stretch (S1) and tension receptor afferents (ST). From the latencies (7.4ms and 9.5ms) and the group conduction velocities (41 (S1) and 35m/s (ST)), it can be calculated that the afferent activity travelled from the urinary bladder approximately 320mm to reach the recording electrodes of an dS2 root.

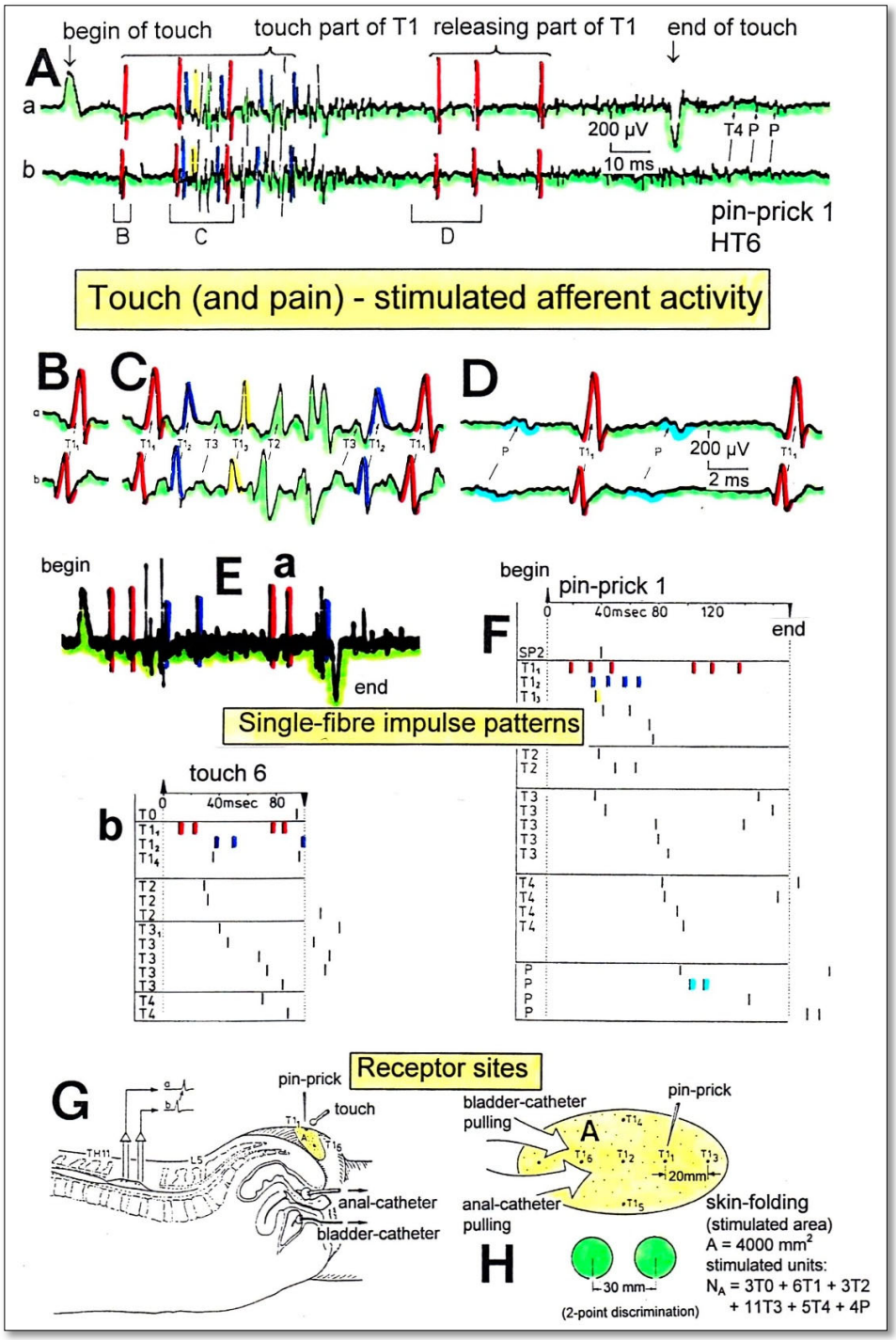

Figure 31. Touch and pain activity stimulated by pin-pricking (A) and touching (Ea) S5 or Co dermatomes and recording extracellularly from a dorsal coccygeal root (brain-dead human HT6). T1, T2, T3, T4, P = mark action potentials (APs) from single touch and pain fibers. Subscripts 1, 2, 3-mark single fibers. --- A. Whole sweep following pin-prick 1 at a slow time

base. The large upward artifact on trace 'a' mark electronically the beginning of the pin-prick/touch. The large downward artifact on trace 'a' marks the end of the pin-prick. Note that 2 intervals of high activity of large APs occurred, one after the beginning of the pin-prick with 1 AP in front, and a second before the end of the pin-prick; potentials with small amplitude follow potentials of large amplitude. Time intervals B, C and D are time-expanded. --- B, C, D. Time expanded sweep pieces of 'A'. Identified APs are indicated. Note that the APs from the $T1_1$ touch unit can be safely identified by the waveforms in B, C, D. --- Eb, F. AP occurrence patterns of single touch and pain fibers following short touch 6 and pin-prick 1. No pain afferents are stimulated upon touch 6. Upon pin-prick 1, the single-fiber AP activity of the different touch and pain groups is identified by the AP waveforms on traces 'a' and 'b', and by the conduction times. The single touch afferents of the T1 group are marked with subscripts. One active secondary muscle spindle afferent fiber (SP2) could always be identified in F. Note that for pin-prick 1, touch and pain afferents are stimulated whereas for touch 6 only touch afferents. --- G. Recording and stimulation arrangement for simultaneous recording of several single touch and pain units. A = area stimulated by skin folding, drawn in H in more detail. $T1_1$, $T1_6$ = suggested touch points of the $T1_1$ and $T1_6$-units. --- H. Drawing of the very approximate skin area stimulated by skin folding. $T1_{1\text{-}6}$ = suggested focal T1 touch points. Two-point discrimination indicated for the sake of comparison. N_A = number of stimulated units in the dorsal coccygeal root. Skin tractions evoked by anal and bladder-catheter pulling are indicated by the large open arrows.

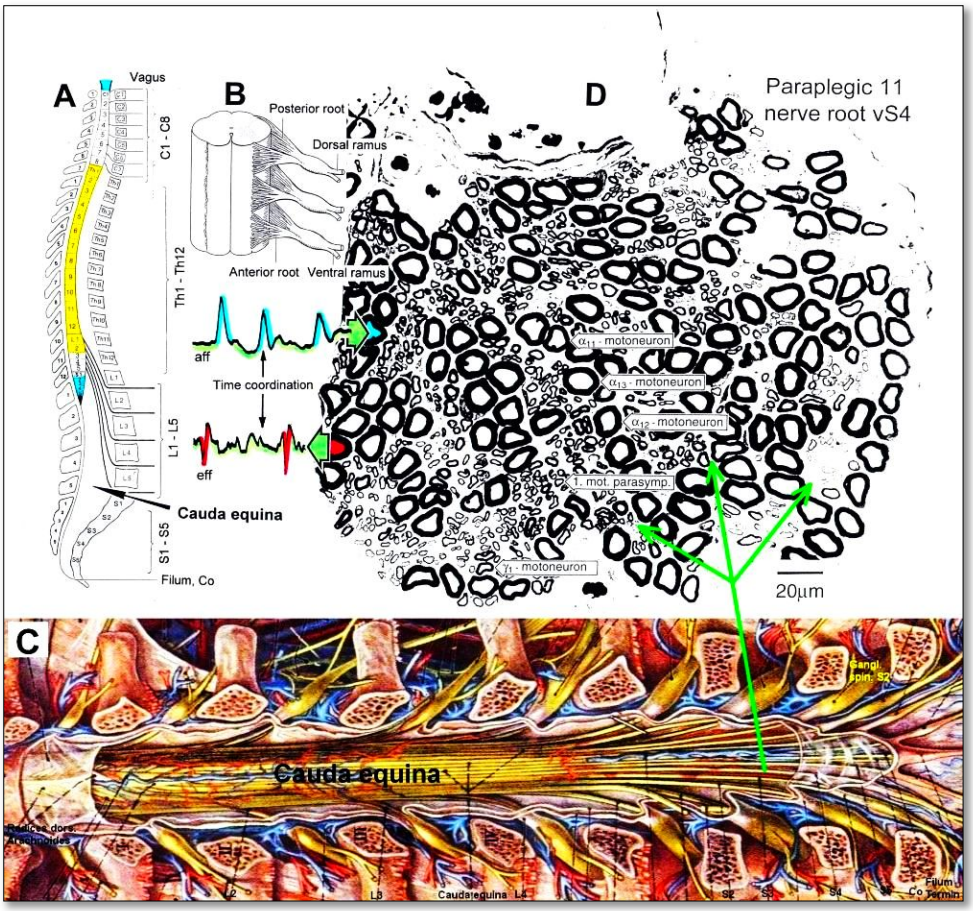

Figure 32. Anatomy to record single-nerve fiber action potentials. A. Ascensus of the human spinal cord gives rise to long nerve roots in the lumbar and sacral range. B. But the nerve roots in the cervical range are short. C. Picture of the opened spinal canal with the cauda equina nerve roots, ganglions and spinal nerves. D. Real ventral S4 nerve root cross section with single-nerve fiber action potentials of afferent (aff) and efferent (eff) fibers and their time coordination. Principle sizes of different nerve fiber cross sections are indicated.

Single-nerve fiber action potentials and compound action potentials measured simultaneously from a nerve root

By recording simultaneously single-nerve fiber APs following natural or no stimulation and compound nerve action potentials (CAPs) elicited by electro-stimulation of a nerve root **(Figure 37D)**, single-nerve fiber conduction

velocity spectra can be constructed, and nerve fiber groups identified and compared with the subpeaks of CAPs.

Figure 37 shows schematically how a compound action potential (CAP) is generated. The by electro-stimulation elicited single-nerve fiber APs in the different nerve fibers (Figure 37A) add up algebraically to give rise to a triphasic compound AP. Near to the site of stimulation it looks like in Figure 37C. APs of the single fibers or fiber

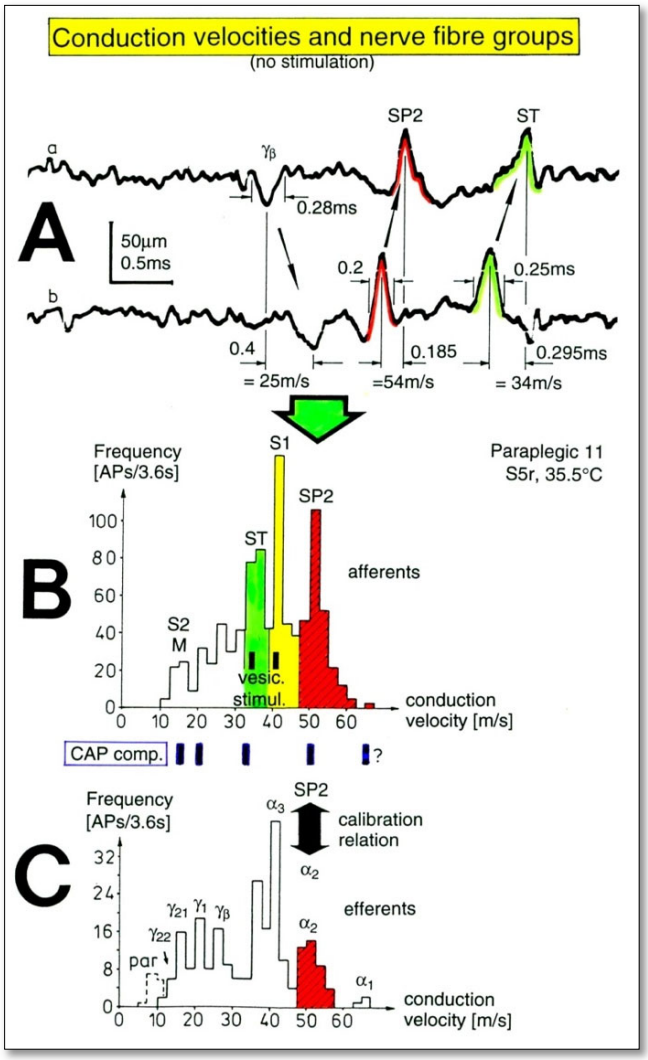

Figure 33. A. Sweep piece of action potential recording. Conduction times and corresponding conduction velocities are indicated. Root temperature at recording electrodes is 35.5°C. --- B, C. Conduction velocity distributions of afferents (B) and efferents (C) obtained for a time interval of 3.6s with no additional stimulation. SP2 = secondary muscle spindle afferents, S1 = stretch receptor afferents of bladder, ST = tension receptor afferents, M = mucosal afferents, S2 = afferents responding to fluid movement; α_1 = α_1-motoneurons (FF), α_2 = α_2-motoneurons (FR), α_3 = α_3-motoneurons (S), γ_β = γ_β-motoneurons, γ_1 = γ_1-fusimotors (dynamic), γ_{21} = γ_{21}-fusimotors (static), γ_{22} = γ_{22}-fusimotors (static), par = preganglionic parasympathetic motoneurons. CAP comp. = group conduction velocities obtained from the components of compound action potentials (CAPs). Vesic. stimul. = group conduction velocities of bladder afferents obtained upon electrical intravesical stimulation (see Figures 39 and 40). Calibration relation indicates the same peak group conduction velocity of secondary spindle afferents and α_2-motoneurons (cross-hatched). Velocity histogram classes ≤ and < (half closed (left) interval).

groups cannot be recognized in the CAP. Distant to the site of electro-stimulation, the CAP changes its shape due to the contribution of the different fast conducting fibers **(Figure 37B)**. Under suitable real recording conditions, sub CAPs of groups of nerve fibers can be identified **(Figure 38)** and correlated to the group conduction velocities, obtained from single-nerve fiber conduction velocity distribution histograms.

In a paraplegic patient, sub peaks of compound APs could be recorded from a S5 root and sub peaks could be identified **(Figure 38)** by comparing them to the single-nerve fiber conduction velocity group values and to the available knowledge concerning electrical stimulation thresholds. Using additional literary data, it was found that the primary spindle afferents likely have the lowest threshold upon electrical nerve root stimulation, followed by α_1-motoneurons (FF), secondary muscle spindle

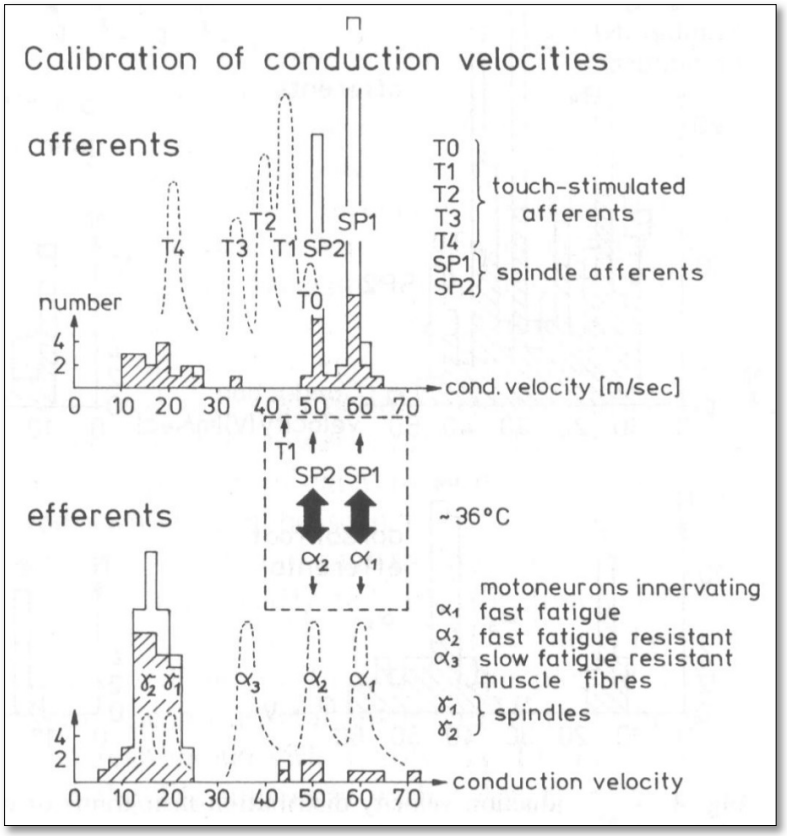

Figure 34. Calibration of conduction velocities of afferent and efferent nerve fibers. Black double arrows mark similar conduction velocities of afferents and efferents. Note, the α_2-motoneurons have about the same conduction velocity as the secondary muscle spindle afferents (SP2), the T1 touch afferents conduct about 10% slower. L4 plus S4 roots, HT3. Root-temperature ≈ 36°C.

afferents, α_2-motoneurons (FR), α_3-motoneurons (S), $\gamma\beta$, γ_1 (dynamic), γ_{21} (static), γ_{22} (static), and parasympathetic motoneurons. In a first approximation, the AP duration increases in the same way as the AP amplitude decreases with the decreasing conduction velocity **(Figure 14)**, and the area between the average single-fiber AP curve and the baseline is the same for all single-fiber APs with the same distance to the recording electrodes in the root cross section. By comparing the mean area of a single AP with the areas of the peaks of the compound APs, 230 single-fiber APs were found to contribute to the compound AP in the measured case. In the group of secondary spindle afferent fibers and α_2-motoneuron groups, 53 fibers were stimulated (23%). The α_3-motoneuron peak and the afferents in the same velocity range contained 101 fibers (44%), the $\gamma\beta$ peak contained nine fibers (4%), the γ_1 32 (14%), the γ_{21} 23 (10%), and the γ_{22} contained 12 (5%) fibers. Additionally, two primary spindle afferents and two α_1-motoneurons most likely contributed to the compound AP. Since the large peaks in the compound APs did not change their area with the increasing stimulation, all muscle spindle afferents and α-motoneurons were most likely activated to contribute to the compound AP [64]. The different sub-compound APs comprised in the compound AP (CSP1, Cα_1, CSP2, Cα_2, Cα_3, C$\gamma\beta$, Cγ_1, Cγ_{21}, Cγ_{22}) **(Figure 38)** provide more conclusive information with respect to splitting of nerve fiber groups. In unfavorable recording conditions (for example, low temperature), the compound AP can give additional information that can be used to identify nerve fiber groups [64].

If the distance between the stimulation and the recording electrodes would have been longer, the splitting into sub-peaks would have been better, but the S5 nerve root was no longer. That the α_3-motoneuron peak is that prominent in Figure 38 for stronger stimulation is understandable because in a ventral S5 root there are mainly only α_3-motoneuron axons **(Figure 25G)**.

Single-nerve fiber action potentials and compound action potentials recorded from nerve roots elicited by electrical stimulation of urinary bladder receptors or afferents

Electrical intravesical stimulation of the nearly empty urinary bladder with up to 30V evoked single-nerve fiber action potentials (APs) and compound action potentials (CAPs) of stretch (S1) and tension receptor afferents

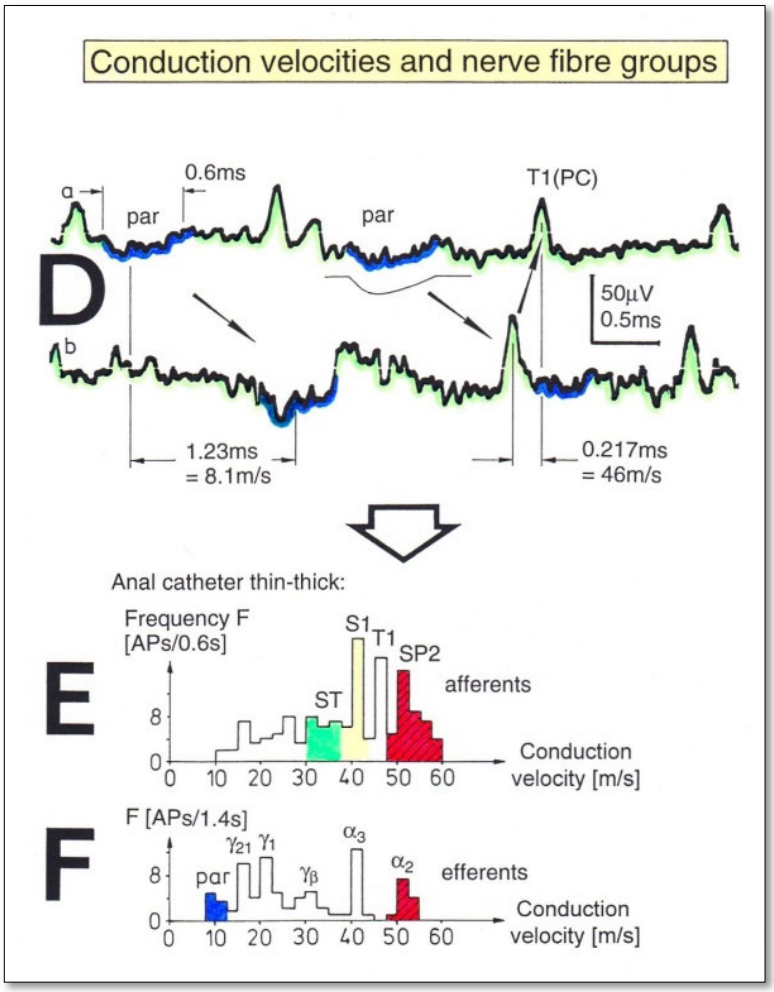

Figure 35. Sweep piece of recording (D) and conduction velocity distributions (E,F) taken from time intervals following a change (pulling) of a thin anal catheter (∅ = 12 mm) for a thick one (∅ = 20 mm). Note, the parasympathetic APs are just recognizable in D and also the parasympathetic peak (par) manifests itself in the corresponding conduction velocity distribution (F). For symbols, see legend of **Figure 3**.

(ST). In the recording from a dS2 root, mainly two CAPs followed the stimulation artefact with latencies of 7.4ms and 9.5ms **(Figure 40AB)**. The CAP conduction velocities were 41 and 35m/s. From the latency and the group conduction velocity, it can be calculated that the afferent activity travelled approximately 320mm to reach the recording electrodes. This value is of interest because the anatomical pathways of bladder innervation is not fully clear **(Figure 19)**.

Electrical intravesical stimulation

In **Figure 39**, the recording and stimulation layout for electrical intravesical stimulation is shown. The negative electrode was connected to the tip of the bladder catheter but was in no direct contact with the bladder mucosa. The indifferent positive electrode was attached to the leg of the patient. Following stimulation with 30V compound action potentials (CAPs) of stretch (S1) and tension

receptor afferents (ST) could be evoked. In the recording from the root dS2 **(Figure 40A)**, mainly two CAPs follow the stimulation artefact, with latencies of 7.4 ms and 9.5 ms.

The CAP conduction velocities in **Figure 40C** were 41 and 35m/s. According to Figure 40AB, the stretch receptor afferents (S1) contributed to the CAP with a latency of 7.4ms and the tension receptor afferents (ST) to the CAP with a latency of 9.5ms. The faster conducting S1 afferents give rise to the CAP with the shorter latency, as they would be expected to. From the latency and the group conduction velocity, it can be calculated that the afferent activity travelled approximately 320mm to reach the recording electrodes, as indicated in Figure 39A. The surgeon estimated a distance of 300mm.

With a slightly increased electrical stimulation, the S1 and ST-CAPs increased slightly **(Figure 40B)**, probably because more afferents were stimulated in the bladder wall. A recording from root S5 (same electrical stimulation) showed no pronounced CAPs. By schematically plotting S1 and ST- CAPs from Figure 40A into Figure 39B and by calculating the conduction velocities of the single-fiber APs in the latency range of the ST-CAP, it was found that the single-fiber APs were conducted by tension receptor afferents, as can be seen from the time-stretched Figure 39C. Thus, at least the ST-CAP was composed of the single-fiber APs of the ST afferents. Normally, subpeaks in CAPs do not represent single-fiber APs, as is indicated in Figure 40C. The arithmetic addition of single-fiber APs of different triphasic AP waveforms often results in large amplitude potential changes, which do not represent single-fiber APs, as can be learned from recordings of high skin afferent activity. To obtain CAP recordings from stretch and tension receptor afferents, a substantial number of bladder afferents have to be stimulated simultaneously through the nerve root that is used to record from.

Conduction velocities of urinary bladder afferents measured via bladder filling

Urinary bladder afferent activities for constructing conduction velocity distribution histograms were recorded at bladder fillings of up to 200 or 400ml, depending on the compliance of the bladders measured preoperatively. The thin bladder afferents with small AP amplitudes and long AP durations (M, S2; **Figure 14**) (possibly also activated by the bladder catheter) could not reliably be detected so far because of insufficient recording conditions.

Activity of urinary bladder afferents induced through retrograde bladder filling

For measuring bladder afferent activity increase upon retrograde bladder filling, the bladder was emptied and then filled while recording (time-consuming procedure, successful so far only in two cases). With the groups of nerve fibers identified from conduction velocity distribution histograms, the increase in activity of the urinary bladder stretch (S1) and tension receptor afferents (ST) in response to retrograde bladder filling could be measured. **Figure 41** shows the activity increases following filling of the bladder of Para 7, via a catheter, with up to 400 ml fluid.

The bladder was filled to the maximal acceptable value as determined pre-operatively by compliance (bladder filling volume / bladder pressure) measurements. Figure 41B shows the sum of the individual velocity distributions for different filling stages for afferents and efferents. The peaks are identified by two calibration relations; α_2-motoneurons conduct with the same velocity as the secondary muscle spindle afferents (~50 m/s); and α_3-motoneurons conduct with the same group velocity as the stretch receptor afferents S1 (41 m/s) at about 35.5°C. Figure 41A gives the velocity distributions for certain bladder filling stages. The most important obvious feature is that the bladder stretches and tension receptor afferents fired considerably even with no bladder filling.

By setting up conduction velocity borders of the S1 and ST groups according to the distribution curve **(Figure 3, inset and Figure 41B)**, the activity of each group could be measured for different filling volumes and plotted **(Figure 42A)**. As can be seen in **Figure 42A**, the stretch (S1) and tension receptor afferents (ST) in the left root S5 fired with 15 APs during 0.2s at no bladder filling.

The bladder afferents increased their firing rate with the increasing bladder storage volume. At 160 ml filling, a transient very strong firing of ST afferents occurred. This was the filling volume at which before the surgery the detrusor was activated in a urodynamic measurement. So far, it has not been possible to activate the detrusor with retrograde bladder filling during the surgery, even despite the light anesthesia, as paraplegics with a complete spinal cord injury feel no pain below the injury level.

From a ventral S3 root in paraplegic 11, a similar undulating activity increase of S1 and ST bladder afferents was obtained with retrograde bladder filling. When the bladder was empty, the afferents (S1 and ST) fired already with 10 APs/0.2s. At 50 ml filling, they fired with 23, at 200ml with 6 at 250ml with 25 and at 500ml with 12 Aps/0.2 s.

The detrusor was activated pre-operatively at a filling volume of 80ml (continuously undulating contractions (0.08Hz) started). As in the para 7, the first high afferent input falls approximately together with the onset of the pre-operative detrusor contraction, when filling the bladder. The occurrence of bladder afferent APs in the ventral S3 root was higher (166 APs/2.2s) during the

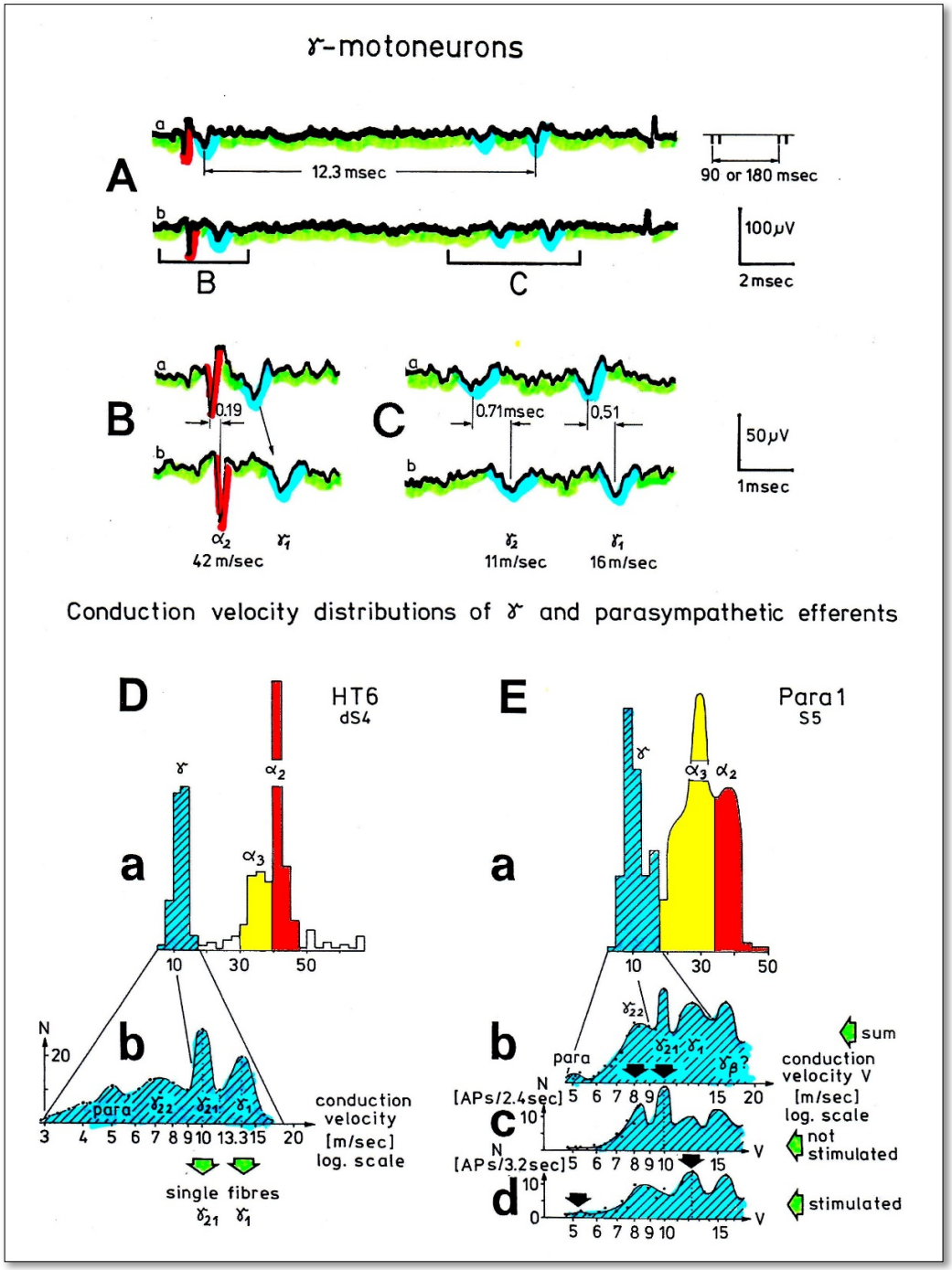

Figure 36. A. Activity from two γ-motoneurons and one α_2-motoneuron. The γ_1-motoneuron may have fired in the oscillatory mode for a few cycles with a period duration of 90ms or 180ms. Interspike intervals of the possible impulse train, consisting of two APs, are indicated (12.3ms). The insert shows the possible oscillation cycle period. HT6; dS4. --- B,C. Time and amplitude expansions of A. Conduction velocities are indicated. Note that with the increasing conduction velocity, the AP amplitude increases and the duration decreases. --- D,E. Conduction velocity distributions of motoneurons for the brain-dead human HT6 (D) and paraplegic 1 (E). To make intrafusal motoneuron and parasympathetic peaks visible, the main γ-peak of Da and Ea was plotted on a log scale in Db and Eb. The distribution peaks are labeled with the groups, they most likely represent. In E, the distribution Eb is split into the distribution upon no additional stimulation (Ec) and upon

additional stimulation (Ed). Note that in the non-stimulated distribution (Ec) the static γ-motoneuron peaks (γ_{22}, γ_{21}) are highest, whereas for no stimulation (Ed) the parasympathetic (para) and the dynamic γ-motoneuron peaks (γ_1) are highest. When plotting the velocities in Db and Eb logarithmically, the conduction times were first grouped by a conduction time histogram and the column values were then used to construct conduction velocity distribution curves.

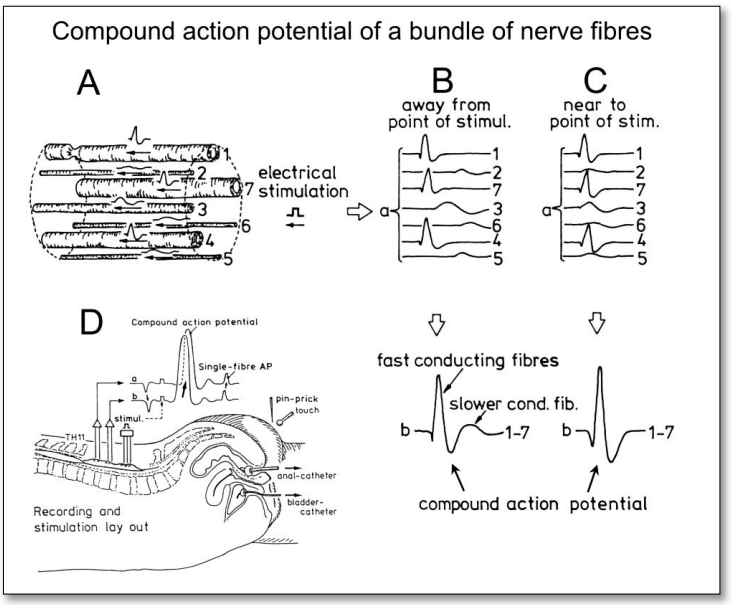

Figure 37. A, B, C. Schematically generated compound action potential. The real compound action potential (CAP) generated in a nerve root corresponds to the case 'B'. Subcomponents of the CAP are not drawn in 'B'. --- D. Layout for stimulation and recording of single-fiber action potentials (APs) and CAPs. Traces a and b are records taken from the two sites; downward arrow = efferent, upward arrow = afferent, the natural stimulation used were touch, pinprick, and anal and bladder catheter pulling. Following electrical (artificial) stimulation with a "Brindley" stimulator (stimul.), the CAP passes the two electrode pairs as a large afferent-like AP.

bladder filling than those of □-motoneuron APs (70 APs/2.2s); the secondary muscle spindle afferents fired with 64 APs/2.2s. The speed of filling in Para 11 was 300ml/min. In this ventral S3 root, there were at least a few percent of the fiber's afferent.

Comparison of bladder afferent activity increase to bladder filling between a paraplegic and a brain-dead human.

The pathology of the bladder afferent activity in the paraplegic 7 analyzed in Figure 42A, with a dyssynergia of the bladder, is fully revealed by a direct comparison with the activity increase of the bladder afferents following retrograde bladder filling in the brain-dead human HT6 **(Figure 42B)**. The dependence of the bladder afferent activity on the bladder filling volume in paraplegic 7 shows four main differences in comparison to those in HT6. (1) The bladder afferents fired already with no bladder filling, which was not the case in HT6. (2) The activity increased more smoothly in the HT than in the paraplegic, even though the bladder filling was stopped twice in HT6 but was not stopped in Para 7. (3) In Para 7, the tension receptor afferent activity was higher than the stretch receptor afferent activity, which was not the case in HT6. (4) The bladder afferent activity was higher in the paraplegic than in the HT6. By taking into account the different measuring times of the activity, the ST-activity in Para 7 was approx. 40 times higher than those in HT6 (5APs/1.2 in HT6 against 210APs/1.2s in Para 7). The recording conditions are not directly comparable. There are on average more bladder afferents in a dS4 root (HT6) than in a S5 root (Para 7). The 40 times higher tension receptor afferent activity is probably overestimated. It is nevertheless safe to conclude that in some paraplegics, the bladder afferent activity, especially from tension receptor afferents, was several to many times higher than that in the brain-dead human, the latter probably representing the physiologic case in this respect. The finding of an increased afferent activity in two paraplegics is in accordance with the experience that in brain-dead humans, activity from bladder afferents was recorded only occasionally, whereas in paraplegics, the activity from S1 and ST-afferents was always obvious and prominent in the velocity distributions, rather independent of the extent of bladder filling. Paraplegics with dyssynergia of the bladder suffer from high bladder pressure and have often bladder infections of antibiotic-resistant bacteria. These infections will stimulate bladder

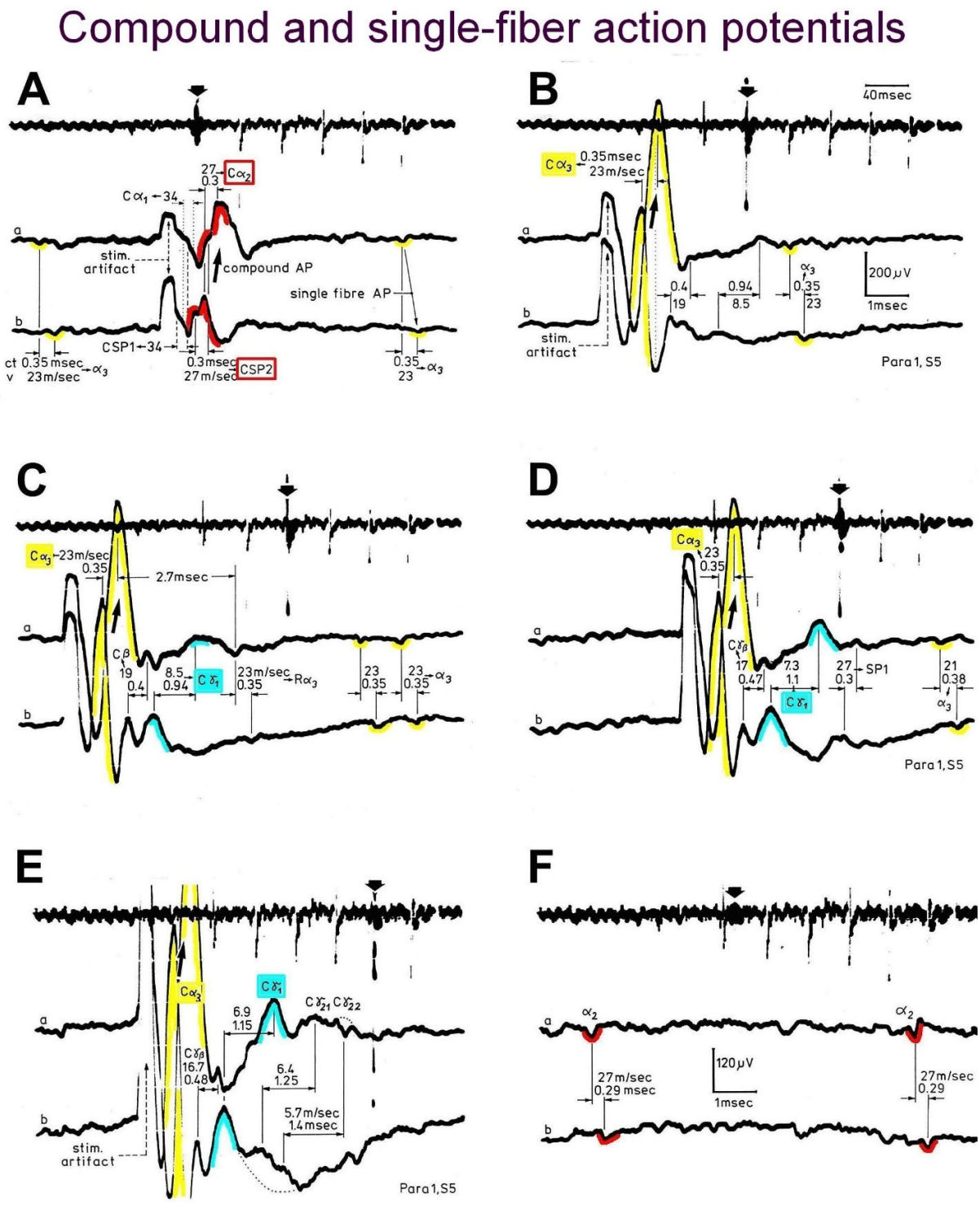

Figure 38. Size and form of real compound action potentials (AP) in dependence on the strength of the stimulation and in relation to single-fiber APs. Single-fiber APs are labelled according to the group to which they belong (e.g., SP2, α_2); components of the compound AP are labelled according to the nerve fiber group to which they belong, namely CSP2, Cα_3. R α_3 designates possible reflected antidromically propagating α_3-motoneuron APs. Conduction time (ct) and conduction velocity (v) are indicated at single-fiber APs and peaks of compound APs. The large arrows in A, B, C, D indicate the main compound AP. Note that with increasing stimulation artefact (stim. artefact) from A through D, also the more slowly

conducting nerve fiber groups got excited. The small thick arrows on the summary trace (trace 'a'; time scale 40 ms) on top of A to F marks the first (A), second (B), third (C), fourth (D) and fifth (E) stimulation artefact. In E, the amplitudes are stretched (120 μV) to make compound AP components $C\gamma_{21}$ and $C\gamma_{22}$ visible. F shows single-fiber APs recorded between the first and the second stimulation. Para 1, S5 root, root temperature unknown.

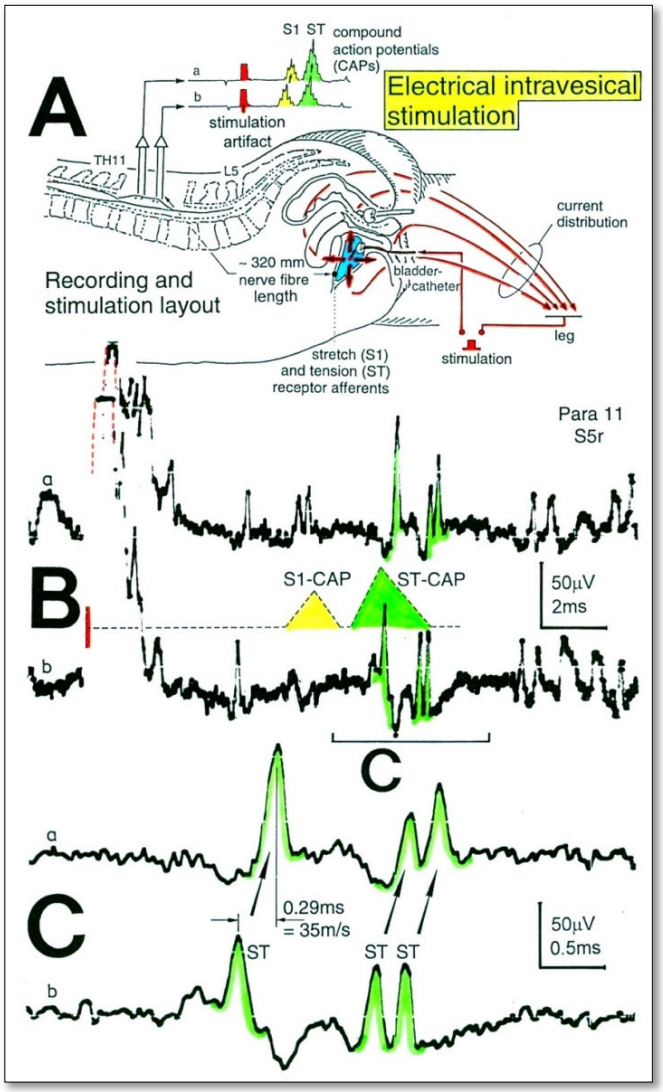

Figure 39. A. Recording and stimulation layout for electrical intravesical stimulation; the electro negativity is in the bladder. B. Recording from an S5 root following electrical stimulation. Compound action potentials (CAPs) of S1 and ST afferents schematically redrawn from Figure 40. C. Time-stretched sweep piece of the recording in B. Single tension receptor afferent APs (ST) are indicated.

receptors and ruin the bladder wall. The stiffer bladder wall activates in turn especially more stretch receptors. This increased afferent activity will have consequences on the excitation/function of the sacral and pontine micturition centers. The desire to void will change and the activation of the striated sphincters of bladder and rectum will change. For urinary bladder repair through movement-based learning, one must also get rid of continuous bladder infections.

Temperature dependence of group conduction velocities

In all measured cases, the AP durations decreased and the conduction velocities of the single-nerve fibers increased with increasing temperature. It seemed further as if the different nerve fiber groups had different temperature dependences, because at lower temperatures, it was much more difficult to identify the different nerve fiber groups

by their peaks in the velocity distributions. The operational field was, therefore, often warmed with an infrared lamp to bring the root temperature as close as possible to 36°C.

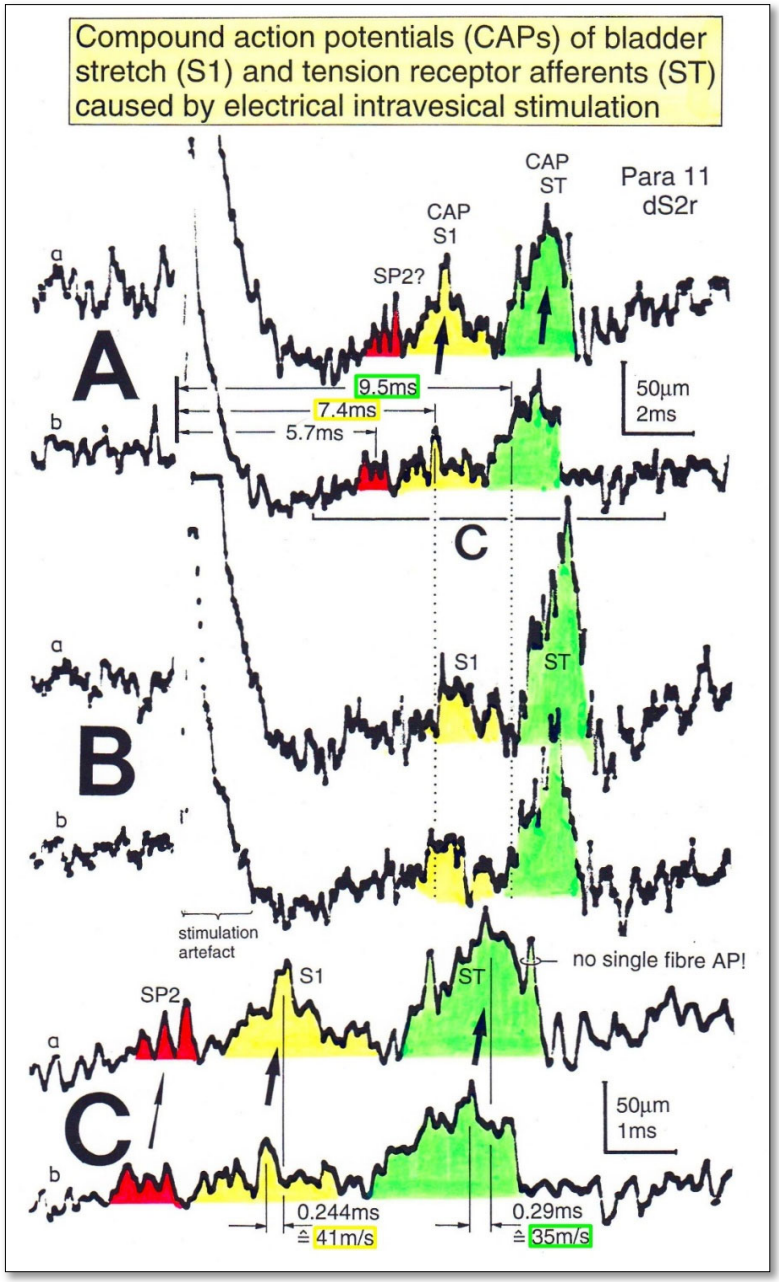

Figure 40. Compound action potentials (CAPs) of urinary bladder stretch (S1) and tension receptor afferents (ST) following electrical intravesical stimulation. Stimulation in B was slightly stronger than in A. The recordings in C represent a time-stretched portion of A. Mean conduction times and calculated mean conduction velocities of CAPs are indicated. In C, three single secondary muscle spindle afferent fibers are marked (SP2). The stimulation pulse (not rectangular) was 0.3ms long; no earthing between recording and stimulating electrodes. Earth electrodes positioned 5 to 10mm away from the recording electrodes reduced stimulation artefact and single-fiber AP amplitudes and were therefore not used. Horizontal line of stimulation artefact is due to the limited input range.

In paraplegic 11, good conduction velocity distribution histograms from the same root under the same recording conditions were obtained for low (32°C) **(Figure 43C, D)** and for high (35.5°C) **(Figure 43E, F)** root temperature. The secondary muscle spindle afferents (SP2) and the α_2-motoneurons increased their conduction velocity from 40 to 50 m/s (25% increase), the S1, ST and M afferents from 31.3 to 40 (28%), from 25 to 33.8 (35%) and from 12.5 to 13.8 m/s (10%) respectively, with increasing temperature (Figure 43G). The α_3-motoneurons increased their conduction velocity from 33 to 40 m/s (21% increase).

In the original recording piece of Figure 44, an ST nerve fiber increased its velocity of conduction from 29m/s (32°C, A) to 34m/s (35.5°C, B). Even though only one set of good quantitative measurements could be obtained so far, the two sets of velocity values clearly show that different nerve fiber groups have different temperature dependences of their group conduction velocity. The SP2 afferents and the α_2-motoneurons showed the same temperature dependence of the group conduction velocity. The calibration relation of the velocity distributions of afferent and efferent fibers, namely that the SP2 fibers conduct with the same velocity as the α_2-motoneurons, is therefore temperature independent. To make the different temperature dependence of nerve fiber groups better visible, values of group conduction velocity values and group nerve fiber diameters will be plotted into the conduction velocity – nerve fiber diameter plane **(Figure 45)**.

Correlation between group nerve fiber conduction velocities and group nerve fiber diameters in dependence of temperature

Exact temperatures of the measured roots were not known. Absolute conduction velocity dependency could, therefore, not be calculated. But relative dependency could still be studied since the two temperatures in Figure 45, even though only approximately known, were the same for the α-motoneurons and the touch afferent groups, because conduction times were measured simultaneously. In Figure 45A, the temperature dependence of the touch afferent groups changed from 16%/4°C to 34%/4°C when going from the T0 group to the T4 group. This clearly indicates that in thinner touch afferents, the conduction velocity depends more strongly on the temperature. α2 and α3-Motoneurons (Figure 45B) showed a similar behavior, namely that the group with the thinner fibers and the lower conduction velocities are more temperature dependent. Another observation from Figure 45 is that the conduction velocities of the α-motoneurons are about only half as dependent on the temperature as the touch afferents.

CORRELATION BETWEEN ELECTROPHYSIOLOGY AND MORPHOMETRY

Correlation between group nerve fiber conduction velocities and group nerve fiber diameters

In **Figures 2 and 3**, the classification of human peripheral nerve fibers was obtained by measuring single-nerve fiber action potentials in brain-dead humans (HTs) and patients with cancer and spinal cord injury in the spinal canal during an operation. Nerve fiber diameters were measured in HTs, human cadavers and some patients.

By correlating the peak group values of distributions of velocities and diameters and taking the temperature dependence of the single-fiber velocities into account, this qualified classification scheme was obtained. Part of the measured values are summarized in **Table 2**.

Unchanged group nerve fiber conduction velocities and group nerve fiber diameters following spinal cord injury

But to find out the changes in CNS organization following injury, we need to know that this classification scheme is also holding following CNS injury. Therefore, single-nerve fiber action potentials (APs) were recorded extracellularly from sacral nerve roots during surgery in nine paraplegic patients (Para 3 to Para 11) with spinal cord injuries for six months to six years. Again, conduction velocities of single fibers were calculated, and group conduction velocities were determined from peaks in the velocity distributions. The measured values are summarized in **Table 3**. It has been shown in an earlier paper for the same patients that the group conduction velocities did not change following spinal cord injury [1]. It was further shown that neither the group nerve fiber diameters did change following spinal cord injury [1].

Thus, the classification scheme of the human peripheral nervous system (Figures 2,3) can be used even in individuals with cord injuries. It is assumed that this classification scheme holds also in other CNS injuries, if the peripheral nerves are not directly injured. For a serious comparison of animal and human data (translational medicine), to repair the human nervous system, such detailed data are also needed to be known for animals.

Correlation between group nerve fiber conduction velocities and group nerve fiber diameters in the velocity-diameter plane [42, 54]

Peak values of group nerve fiber conduction velocities and group nerve fiber diameters are plotted in **Figure 46** into the velocity-diameter plane.

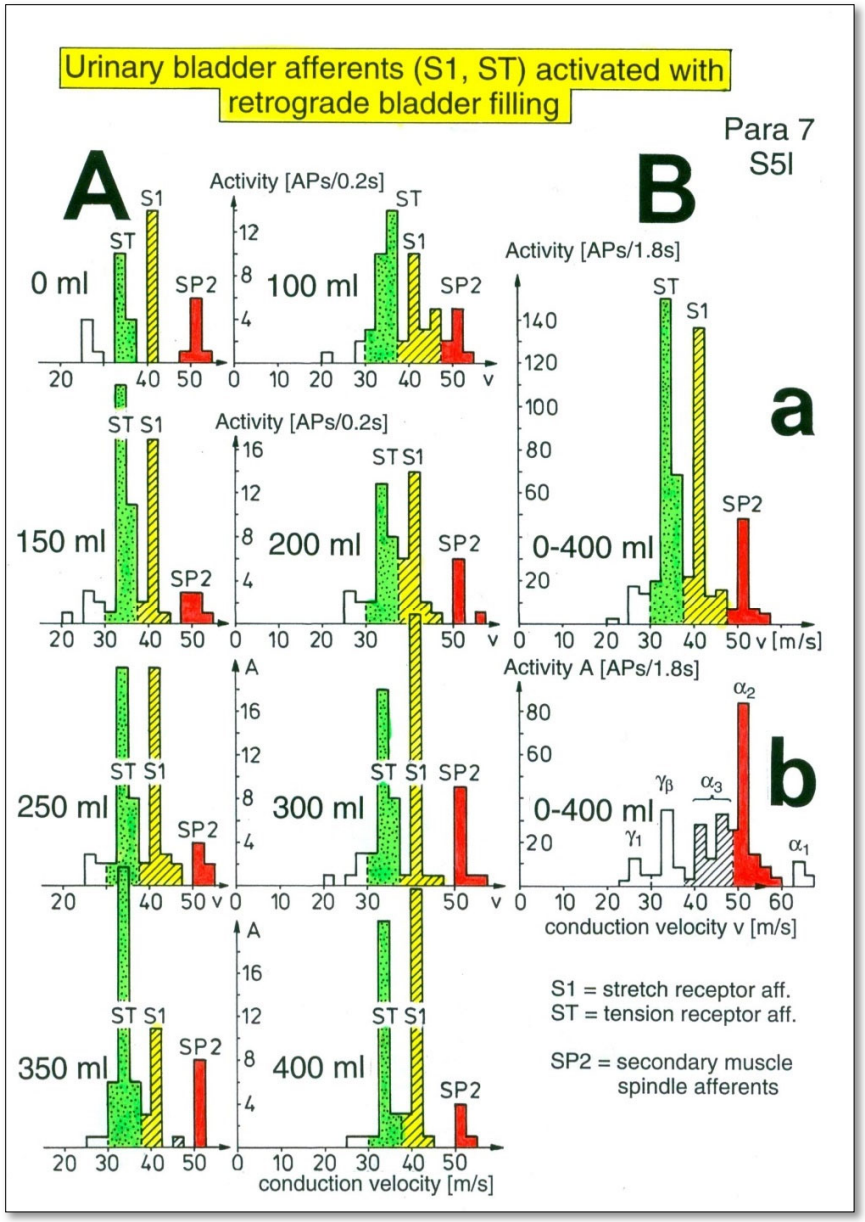

Figure 41. Conduction velocity distribution histograms for stretch (S1) and tension receptor afferents (ST) and secondary spindle afferents (SP2) for different retrograde filling stages of the urinary bladder (A). Summed histograms for afferents (a) and efferents (b) are plotted in B. α_1, α_2, γ_β, γ_1 represent velocity distributions of α_1, α_2, γ_β and γ_1-motoneurons. Para 7, left nerve root S5.

It seems that the γ-motoneurons have different velocity-diameter dependence than the α-motoneurons, and the γ_β-motoneurons seem to belong more to the α-motoneurons than to the γ-motoneurons **(Figure 46)**. The correlation curves of the skin touch afferents (T0 to T4) in the velocity-diameter plane **(Figure 45A)** indicate that the touch afferent fibers conduct slower than the α-motoneurons at a given fiber diameter **(Figure 45B)**. One possible reason for the reduced conduction velocity could be a thinner myelin sheath. But all α-motoneurons and all skin touch afferents lie mainly in the myelin sheath thickness range d = 1.8-2.3µm. Therefore, a different myelin sheath thickness may not be the main reason. There are probably differences in the axon membrane properties of skin touch afferents and α-motoneurons.

Natural firing patterns of motoneurons

The classification scheme for human peripheral nerve fibers would only be of limited help to analyze functions of the human CNS under physiologic and pathologic

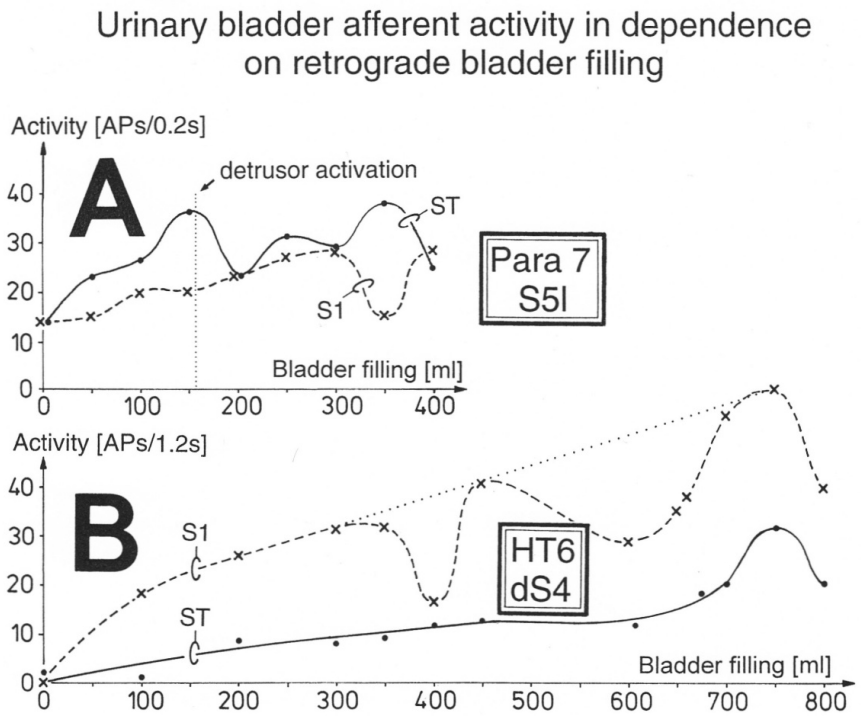

Figure 42. Activity increase of stretch (S1) and tension receptor afferents (ST) in response to retrograde bladder filling in paraplegic 7 (left root S5) and brain-dead human HT6 (dorsal root S4). APs = action potentials. The speed of filling was 130 ml/min in para 7 and 100 ml/min in HT6. Note, in Para 7 the S1 and ST afferents fired already when the bladder was empty, but not in HT6.

functions, if there would not be a reference base in neural network functioning/organization to which activities of single fibers can be related to. Such reference base is the coordinated oscillatory firing of motoneurons for high activation in general and that of α2-motoneurons in specific **(Figure 4).**

Premotor spinal oscillators

Typical firing patterns of motoneurons can be observed when motoneurons are activated with increasing strength of adequate afferent input. With low afferent input, the motoneurons fire occasionally. With increasing input, they fire intermittently in an oscillatory manner and then continuously oscillatory. This change from the occasional firing via the transiently oscillatory to the continuously oscillatory firing mode can nicely be demonstrated when filling retrogradely the urinary bladder and recording from a sphincter motoneuron, innervating the external urinary bladder sphincter **(Figure 47)**.

The characteristics of α_2-oscillators are in between those of the α_1 and the α_3-oscillators. They are self-organized by the adequate afferent input patterns from several kinds of receptors. The α_2-oscillator O1 **(Figure 47)**, innervating the external bladder sphincter, was organized/activated from receptors sensing bladder filling and emptying (stretch (S1), tension (ST) and mucosal (S2) afferents). The change from the occasional via the transient oscillatory to the continuous oscillatory firing mode to secure continence upon bladder filling and the increase of S1, S2 and ST receptor activity can nicely be seen in **Figure 47**. The α_2-oscillator O2, innervating the anal sphincter, was stimulated completely different to organize itself in neural networks, namely by the activity from secondary muscle spindle afferents (SP2) and skin and mucosal afferents from the anal reflex area. The stretch from the anal catheter stimulated the α_2-motoneuron O_2 to fire oscillatory to secure anal continence. Its firing was independent of the bladder filling.

The oscillatory firing of motoneurons was also demonstrated non-invasively by surface electromyography **(Figures 52, 53)**.

The demonstration that neurons of the CNS, in this case motoneurons, can fire both in an oscillatory manner and non-oscillatory manner is very important for the understanding of the functioning of the human CNS. To describe the functioning of the CNS merely by reflex pathways and loops or coupling of rigid oscillators (of cellular or network origin) is in contradiction to empirical human data, namely that premotor spinal oscillators self-

organize as was concluded from measurements of simultaneous natural impulse patterns of afferent and efferent nerve fibers.

For a better understanding of urinary bladder functioning, Figure 48 shows the probable location of the different receptors of the bladder and the anal canal.

These self-organized premotor spinal network oscillators, of which the motoneuron is most likely a part, are sub-neural networks which coordinate their functioning. When this coordinated communication becomes impaired due to insufficient inhibition, they synchronize their firing with the consequence of pathologic tremor, occurring for example in patients with Parkinson's disease.

The α_1-oscillators respond very dynamically, but have little oscillator network properties. Their firing is absolutely correlated to the firing of primary spindle afferents. The α_2-oscillators respond less dynamically, have strong oscillator properties and self-organize by the adequate afferent input patterns from several kinds of receptors including secondary muscle spindle and urinary bladder afferents. The behavior of α_3-motoneurons is more static and their input is polymodal. The dynamics of responding to inputs increases from α_3 to α_2 to α_1-oscillators in accordance with the dynamics of the 3 muscle fiber types the α-motoneurons innervate. The slow (S), medium fast (FR) (fast fatigue-resistant) and fast contracting muscle fibers (FF) (fast fatigable) have their own corresponding premotor networks in the spinal cord, namely that in which the α_1, α_2 and α_3-networks are integrated in **(Figure 4)**.

Surface Electromyography to record motor programs, oscillatory firing, and phase and frequency coordination among single-motor units

Recording of single-motor units

Another human electro-physiologic tool to measure natural impulse patterns of neurons is the surface electromyography (sEMG). With the same recording system used to record singe-nerve fiber APs, but just replacing the wire electrodes with EMG surface electrodes, single-motor unit firing and motor programs could be recorded non-invasively. The sEMG recording arrangement is shown in **Figure 49a**, c for recording motor programs from an infant.

When surface EMG is performed from a healthy person or child, coordinated motor programs can be recorded from the different muscles **(Figure 49)**. But the patterns of recruitment of motor units cannot be seen in such a motor program, because the number of activated motor units is so high that single-motor units cannot be followed up. However, when only a few motor units can be activated in a certain muscle, as for example in spinal cord injury, then the pattern of activation of motor units and the coordination between them can be observed **(Figure 52)**. If the CNS of a patient is functioning rather physiologically as a result of a long-lasting intensive coordination dynamics therapy, then an analysis of the generation of the motor program becomes possible based on single-motor unit firing. **Figure 50** shows the sEMG recording layout of such a patient from whom single-motor unit firing could be recorded.

Oscillatory firing of motoneurons and motor units

If we have two electrophysiologic methods to analyze CNS organization, then both methods should give same or similar results. In Figure 51 it is shown that the oscillatory firing of the three motoneuron types are the same for both electrophysiological methods. With the single-nerve fiber action potential recording method it can be recorded from single-motoneuron axons and afferent fibers. But the method is invasive. With the single-motor unit surface electromyography it can be recorded only from single-motor units, but the method is non-invasive. **Figure 51** compares the oscillatory firing of motoneurons and motor units.

Original records of oscillatory firing of the three kinds of motoneurons, shownin Figure 51, were taken with the single-nerve fiber action potential recording method from motoneuron axons and surface electromyography (sEMG) from single-motor units. α_1-Motoneurons innervate FF-type muscle fibers and fire rhythmically with impulse trains consisting of 1 action potential in the order of 10Hz **(Figure 4)**. α_2-Motoneurons innervate FR-type muscle fibers and fire rhythmically with impulse trains consisting of 2 to 5 action potentials in the range of 4 to 7 Hz. The amplitude of the extracellular action potential of the α_2-motoneurons (axon group diameter = 10.2µm, axon group conduction velocity = 50m/s) is on average smaller than that of the α_1-motoneurons (axon group diameter = 13.1µm, axon group conduction velocity = 65m/s), depending on the position of the axon in the nerve root with respect to the recording electrodes. FR-type motor unit potentials have much smaller amplitudes than the motor unit potentials of FF-type muscle fibers. The α_3-motoneurons (axon group diameter = 8.3µm, axon group conduction velocity = 37m/s) innervate S-type muscle fibers and fire oscillatory at a frequency of around 1 Hz with long impulse trains (up to 50 action potentials per impulse train). The motor unit firing of single S-type muscle fiber motor units could not be safely identified by sEMG so far because their amplitudes are still smaller than those of FR-type motor units and are thus difficult to identify. The impulse patterns of oscillatory firing motoneurons obtained with sEMG are similar or the same as those obtained with the single-nerve fiber action potential recording method. This confirms the accuracy of the single-nerve fiber action potential recording method.

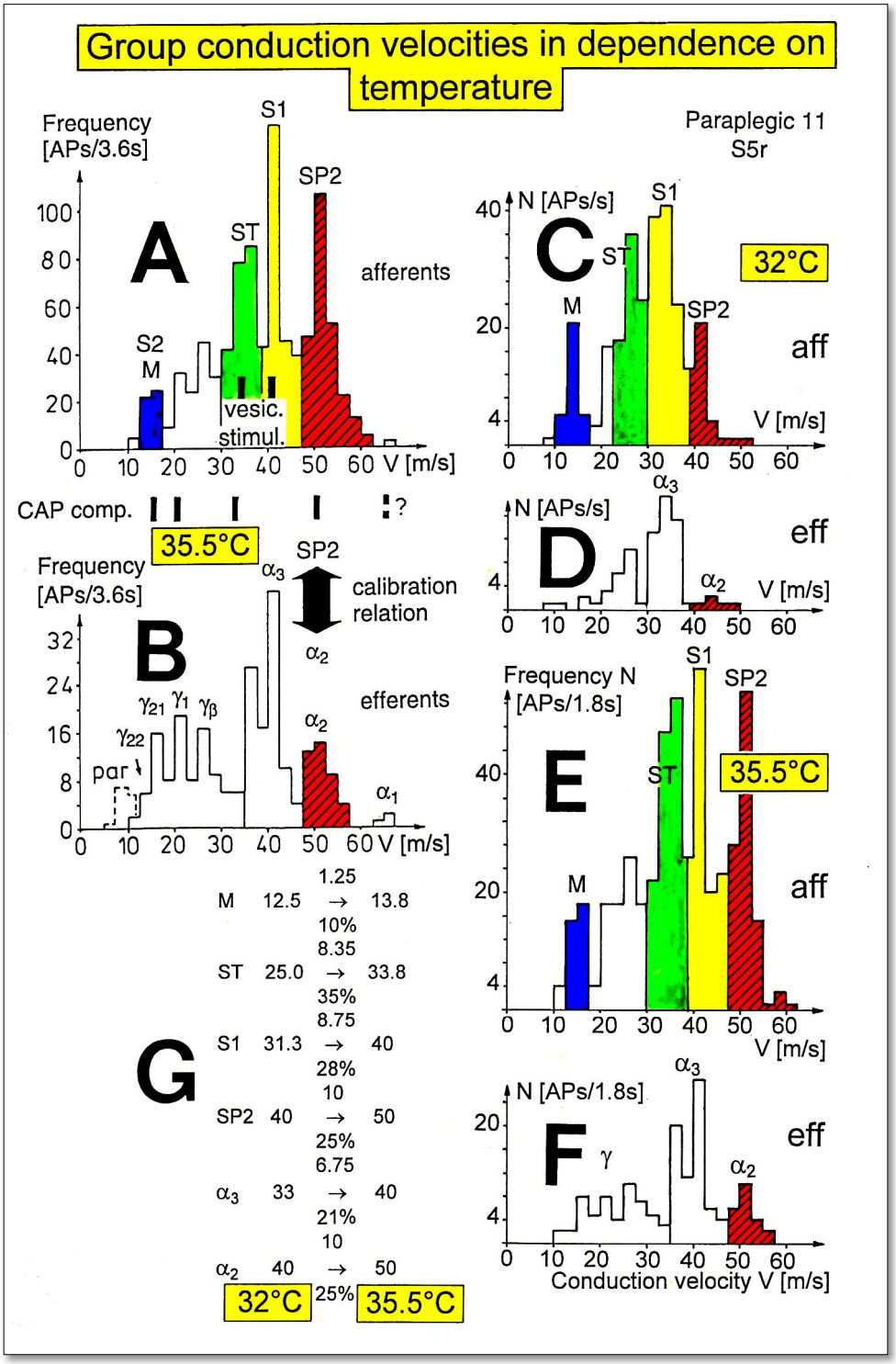

Figure 43. Conduction velocity distribution histograms with marked group distribution peaks in dependence on the nerve root temperature. Nerve fiber velocity borders for the different groups are given in A, B at 35.5°C. For symbols of the nerve fiber groups, see legend to Figure 3. In C, D and E, F, the velocity distributions are given for 32 and 35.5°C. In G, the velocity values are given for both temperatures for the different afferent and efferent nerve fiber groups along with the percentages of change. Note that the secondary muscle spindle afferents (SP2) and the α_2-motoneurons (FR) conduct with the same velocity (calibration relation) for both temperatures (temperature-independent calibration relation).

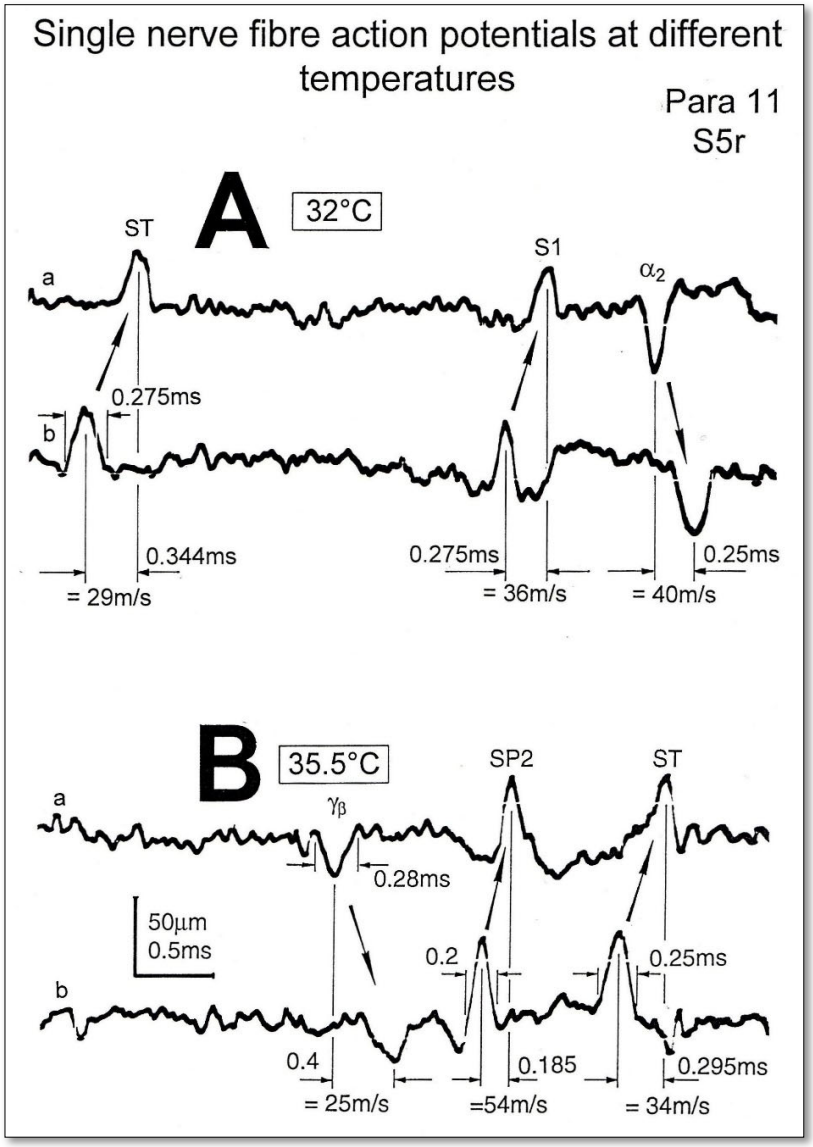

Figure 44. Original recording of an ST (tension) action potential at 32°C and 35°C.

Since sEMG is a non-invasive recording method, oscillatory firing can be recorded easily when using appropriate patients.

With the single-nerve fiber action potential recording method urinary bladder functions were successfully analyzed, whereas surface EMG was very helpful to analyze locomotion and movements.

With the single-motor unit sEMG, the coordinated firing between motor units can nicely be demonstrated and is shown in **Figures 52** and **53**.

Motor program generation, oscillatory firing and coordination among α_1-motor units (FF-type)

Figures 52 and **53** show, if only a few α_1-motor units can be activated in a muscle, how the CNS generates a motor program. By increasing the load in Newton's on the special CDT device, more muscle power is required to perform the movements and the motor unit firing rates increase. The motor units start to fire more rhythmically and with increasing frequency but coordinate their firing in order to avoid tremor.

In a patient with a spinal cord injury (injury level sub L2 following an accident), the left tibialis anterior muscle (third trace in **Figure 52**) was already strongly re-innervated after two years of treatment. The overlapping

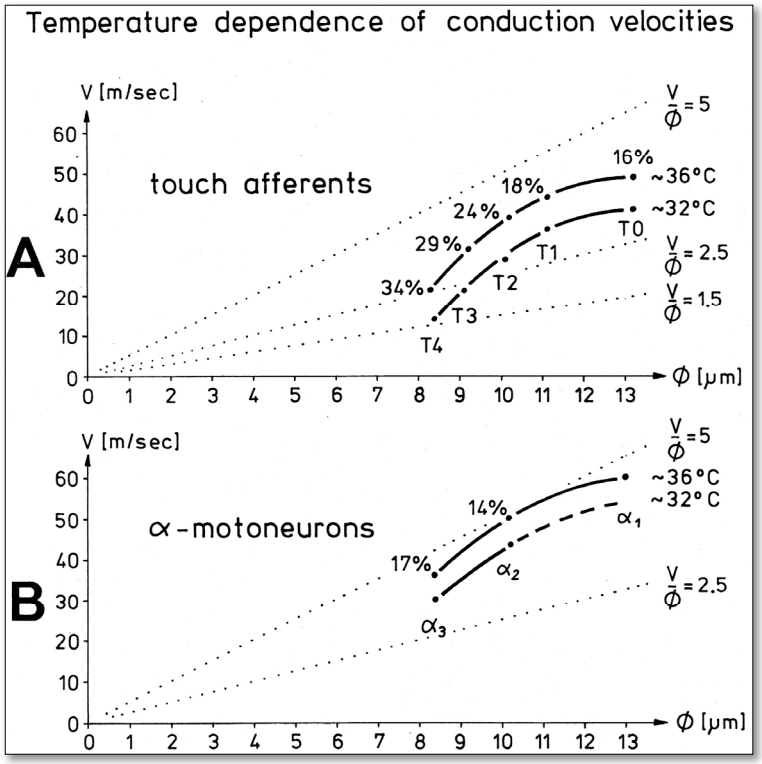

Figure 45. Temperature dependence of group conduction velocities (peak values) of skin afferents (A) and α_2 and α_3-motoneurons (B). 36°C-trace from HT3, 32°C-trace from HT6. Temperature values are only approximate. Percentages give the drop of conduction velocity values when changing from 36°C to 32°C.

of the motor unit potentials was so strong that single-motor unit firing could only be identified occasionally. In the right tibialis anterior muscle (top trace in **Figures 52, 53**) however, oscillatory and coordinated firing of mainly 3 singles α_1-motor units could be identified. **Figure 51H** shows the wave forms of the 3 different motor unit potentials (1, 2, and 3). Motor unit 1 had the lowest threshold and the largest amplitude. In the majority of cases, the motor units can be identified safely, though not always. It is especially difficult when the motor units fire simultaneously or nearly simultaneously. It will now be shown now how the firing frequencies and coordination between α_1-motor unit firings (FF-type) change for different movements and loads.

Firing frequency increases with increasing load

In Figure 52A, motor unit 1 fired oscillatory for a certain period of time to generate a motor program when the patient exercised at a load of 20N on the special CDT device **(Figure 50)**. The frequency fluctuated between 5 and 17Hz. Quite often, the frequency of this motor unit 1 was in the order of 10Hz for low load exercising at 20 or 50N **(Figure 52)**. Motor units 2 and 3 fired mostly only occasionally. In Figure 52F, motor unit 3 fired transiently oscillatory at the frequency of approximately 6Hz.

For exercising at higher loads, the firing frequencies of the motor units increased. At 100N, motor unit 1 reached 25Hz **(Figure 53A)**; the corresponding values at 150N and 200N being 37 Hz **(Figure 53B)** and 43 Hz **(Figure 53C)**. Also, motor units 2 and 3 increased their firing rates. They started to fire also rhythmically with increasing frequencies for increasing load. At 150N **(Figure 53B)**, motor unit 2 and 3 reached the frequency of 22Hz and 25Hz respectively. Exercising at 200N is a rather high load, even for a healthy person. The lowest frequencies measured at 200N were 9Hz and 10.5Hz for motor unit 2 **(Figure 53E)** and 3 **(Figure 53F)**, respectively. For some time, motor unit 1 stopped firing oscillatory **(Figure 53F)**.

Motor program development

In the left tibialis anterior muscle (Figures 52,53, third trace), motor unit activity was recorded when muscle power was needed, and none or nearly none was recorded when no muscle power was needed, in some similarity to a physiologic motor program in Figure 49d. In the right tibialis anterior muscle (top trace) the activation pattern was different. When the muscle had to be activated the motor units were more activated **(Figures 52A, 53B)** and when no muscle power was needed, less activity was recorded **(Figures 52B, G; 53E, F)**. The activity of the

Table 2. Peak conduction velocity values of conduction velocity distributions of single groups taken from conduction velocity distribution histograms and peak nerve fiber diameter values of fiber diameter distributions of single identified groups taken from nerve fiber diameter histograms from two cadavers (Cad), four brain dead human cadavers (HTs) and one patient (Pat). Values without brackets are afferents, values in round brackets from efferents. T0, Tl, T2, T3, T4 = touch stimulated afferents from skin and anal canal, P = skin pain afferents, M = touch afferents from the mucosa of the urinary bladder and the anal canal, S1, ST = stretch afferents of the bladder, probably measuring mural tension, S2 = flow receptor bladder afferents, stimulated by high pressure and fluid movements (may be identical with M), SP1, SP2 = primary and secondary spindle afferents. (α_1), (α_{11}), (α_2), (α_3) = extrafusal motoneurons, (α_{11}) - subgroup of (α_1). (γ_β)? (γ_1), (γ_2) = intrafusal motoneurons. (--), "-- " = no peak present, f = female, m = male, number behind "f" or "m " is age in years, numbers below "f" or "m" are the central temperature and the temperature of the fluid in the spinal canal in °C. v = ventral, d = dorsal, L = lumbal, S = sacral, Co = coccygeal, 19 = 9th intercostal nerve, musc = muscle branch, skin = skin branch, Ø = diameter.

case	root	peak conduction velocity [m/sec]											peak nerve fibre diameter [µm]										root
		P (γ_2)	M	S2	T4 (γ_1)	T3 (γ_β)	ST	T2 (α_3)	S1	T1	T0	SP2 (α_2) SP1 (α_1)	P (γ_2)	M (γ_1)	S2 (γ_β)	T4 (α_3)	T3	ST	T2 (α_2)	S1	T1	T0	SP2 (α_{11}) SP1 (α_1)	Ø [mm]
Cad f 47	dL4															8.2	9.1		10.3		11.1		12.2	13.3	
	vL4															(8.5)			(10.5)					(12.7)	
Cad3 m 64 I9	musc																						11.4	13.3	
	skin															8.2	9.1		10.3		11.1	13.2			
HT3 f 21 33,5/36°C	vS4				21	31		39 (37)		44	49	51 (51)				(8.5)			(10.1)		11.1		13 (12.1)		0.15
	L?	(15)			(20)							51 59 (50) (60)													0.1
HT4 f 56 32/32,5°C	dS5	4	7		7	14 (14)		21 (21)		26	29	(29)					9.4		10.3 (10.3)		11.3				0.25
HT5 f 58 38/32°C	dS3		6			14		19 (12)				(18)				8.2	9.3		10.1		11.2				0.4
HT6 f 37 33,5/33°C	dCo	5	--		6?	8		11 (--)		14	17	(--) (--)	7.1 or 7.6			8.5	9.1		10.1		11.2		--	(--)	0.12
	dS4	9 (10)	12	12	14 (14)	21 (20)	28	29 (30)	34	36	41	43 (43)	5.5-8.2 (6.2)	(6.7)	(7.2)	8.4	9.1		10.1		11.1		12-12.7	(13)	0.2
	dS3	efferents present															9.1		10.1		11.2		12.1	13.1	0.3
	vS3															(8.4)			(10.2)				(12.3)	(13.1)	
	vL5															(--)			(10.2)				(12.2)	(13.2)	
Pat 24 m 10 37/33°C?	dS?		5					20		25		30 43 (28.5) (40)													

motor units increased and decreased. For high load exercising, the motor units fired rhythmically with increasing and decreasing frequencies. During low load exercising, the motor units fired rhythmically with low frequencies or stopped firing in an oscillatory manner and fired only occasionally. The activity changes from motor unit firing to no motor unit firing during the motor program were in the right tibialis anterior muscle not as pronouncedas in the left tibialis anterior muscle. It was as if inhibition was missing. Inhibition is necessary to give motor unit firing patters their structure. As measured earlier with the single-nerve fiber action potential recording method, the high activity mode of α-motoneuron firing is the oscillatory firing **(Figure 47)**.

Phase and frequency coordination between the firing of the motor units

But how did the motor units coordinate their firing? As can be seen from **Figures 52 and 53**, the motor units did not synchronize their firing. In **Figure 52F**, motor unit 1 is firing in an oscillatory manner at around 10Hz and motor unit 3 shows a phase lag of 22ms with respect to motor unit 1 (the two right potentials). But when motor unit 2 fired additionally (on the left part of the trace), motor unit 3 changed its phase with respect to motor unit 1 so that all 3 motor units fired unequally to give rise to a smooth non-rhythmic muscle contraction. In **Figure 53D** (200N), motor unit 3 fired approximately at the same time as motor unit 1. The motor unit potentials partly added up, because of partial synchronized firing of the

Table 3. Group conduction velocities and group diameters (peak values of the distributions) obtained from the same sacral nerve roots. Para = paraplegic, centr. temp. = central temperature in the patient during surgery, f = female, m = male, age in years, temp measured = temperature measured close to the recording electrodes, real = approx. real temperature in the nerve roots. For designations of nerve fiber groups see legend to Table 2. Conduction velocity and fiber diameter values refer to afferents, those in round brackets to efferents. Edged brackets give conduction velocities of compound action potential components. Several peak diameters in the myelin sheath thickness class $0.25 \le d < 0.8$ µm are indicated and separated by "+"- signs. Percentual proportions of myelinated fibers in classes $0.25 \le d < 0.8$ µm to $1.8 \le d < 2.5$ µm. Arter. = Arteries. One to two APs for the root S5 in para 11 indicate that the α_1-motoneuron group in this root consisted of approx. two fibers only. In para 5, recording was performed from whole root S5, but the diameter distribution was taken only from the ventral root S5.

Case Centr. temp. [°C]	Sex/Age Lesion level/age of lesion	root temp measured /real	Group conduction velocity [m/s] (par)	M/S2 (γ_{22}) (γ_{21})	T4 (γ_1)	T3	ST (γ_β) [CAP-components]	T2	S1 (α_3)	T1	SP2 (α_2)	GO	SP1 (α_1)	Group diameter [µm] Peak diameters in myelin class $0.25 \le d < 0.8$ µm diameter range µm	T2 (α_2)	T1	SP2 (α_{11})	SP1 (α_{12})	Root Ø [mm]	Number of myel. fibres % in classes $0.25 \le d < 0.8$ µm/ $0.8 \le d < 1.3$ µm/ $1.3 \le d < 1.8$ µm/ $1.8 \le d < 2.5$ µm	Contribution in % to the cross section area from Arter.	Veins
Para 3 34.7°C	f 33 C6/3	S5l 28/31.5 vS4r 28/31.5			(16)				(31)		41 (41) 53 (52) [53]	51	58 (-) (59?)	2.5 + 4.0 1.8 - 5.5			12.1 -		0.33	2100 81/6/3/10	9	12
Para 4 35.7°C	f 26 TH4/6	vS3r 29/32.5			(16?)		(21?) [21]		33 (33)		36 (36) [36]		41 (41) [41]				- -					
Para 5 34.6°C	f 24 TH12/2	S5r(vS5) 26.5/30 dS4r 29/32.5	(5)		13 (14?)	20	(21) 35	25	(26) 41 (41)	33	35 (35) 50 (50)		40 (40) (65)	2.1 + 3.1 + 4.0 1.5 - 6.0 2.0 + 3.0 1.5 - 5.5	10.2 (10.2)	-	- 12.2	- 13.2	0.39 0.60	1300 52/21/12/15 5500 70/10/7/13	15 9	41 8
Para 7 35°C	f 37 TH5/2.5	S5l 29°/32.5		[15]	17 (25?) [26]	25	33 (33) [28]	36	41 (41)	44	50 (50)		60	3.1 2.0 - 5.5				12.8	0.48	2200 63/7/3/27	19	10
Para 8 35.2°C	f 20 TH6/1.5	S5l 28.5/32 S5r 27.9/31.5	[7]	[6] [14]	(8.5?) [8.5] (21)	[16]	[21] 26 (26) [26]		(35) [34] 33 (33)		41 (41) [41] 40 (40) [50?]		(49) (50)	3.0 + 4.0 + 5.0 1.5 - 6.0 3.0 + 4.0 1.5 - 5.5	(10.5)	11.8	12.0 (12.5)	(13.1)	0.49 0.50	2400 68/5/7/20 2500 67.5/7/7.5/18	21 23	6.5 23
Para 9 34.5°C	f 23 TH1/0.5	S5r 26/29.5 vS4r 25/28.5			(20?) (5)		(26?)		32 (32) (8)	36	42 (45) 16.5 (14) [16.7]		20 - [18.2]	3.3 2.0 - 5.5			12.1 -		0.77	8300 75/6/5/14	10	16
Para 10 34.3°C	m 30 TH12/0.5	S5r ? S5l 29.4/33 dS4r ?			14 (15)	21 [21]	28.5 [28.5]	26	(26) [26] 34 (34) -	28.5 31	33 (32) [30] 33 (33) - 41 (41) -		reflected ↓ [36] 50 (50) -	3.1 2.0 - 5.1		11.2?	12.2?	13.1 (13.1)	0.79	9500 69/9/6/16	2.5	4
Para 11 35.8°C	f 25 TH5/2	S5r 32.0/35.5 vS3r 32.0/35.5 vS4r dS4r dS2r	(9)	(13)	16 (16) [16] 21 (21) [21]	-	36 (26/30) [33] 36 (28) 35 (intravesical		41 (41) (41) (40) 41 stimulation)		51 (51) 50 (50)		1-2 APs (65) [65]	3.0 + 3.7 2.0 - 5.2 2.9 + 3.7? 2.0 - 6.0 3.0 2.0 - 5.0 3.1 1.8 - 4.6	-11.1 (10.4) (10.2) 10.1 10.1	11.1 11.1 11.1	12.1 12.1 (12.1) 12.1 12.1	(13.1) 13.1 13.0	0.34 0.31 0.46 1.6	907 70/5/4/21 898 77/4/1/18 4848 75/6/5/14 31600 59/3.5/3.5/34	29 6.5 1 1.4	12.5 20.5 5.5 4.7

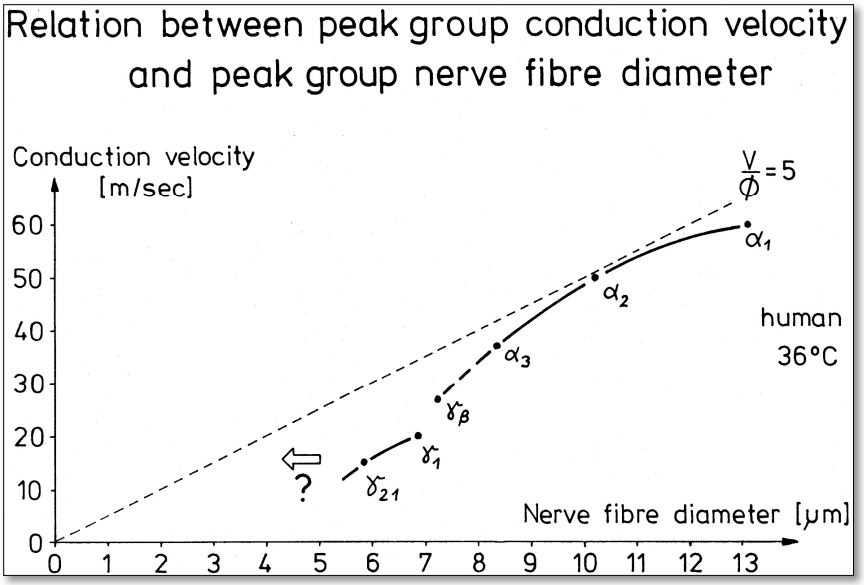

Figure 46. Relation between peak group conduction velocity and peak group nerve fiber diameter, 36°C, human.

corresponding motoneurons. The distributed firing of motor units was poor at that time interval. In Figure 53E, motor unit 2 fired approximately at the same time as motor unit 1. In Figure 53F, motor unit 3 fired in phase correlation to motor unit 1, but it was not synchronized. When motor unit 1 transiently stopped to fire in an oscillatory manner, motor unit 3 continued firing in an oscillatory manner. When motor unit 1 started to fire in an oscillatory fashion again, the same phase coordination built up to the firing of motor unit 3. For the high activation parts in Figure 53B, C, motor units 1, 2 and3, and some other unidentified units, fired very close to each other (but not in a synchronized manner) and the potentials overlapped, because the frequencies were very high to generate strong muscle power. For further surface EMG see [4,5].

In conclusion, it was shown that the classification scheme for human peripheral nerve fibers helped to better understand movement pattern, analyzed with surface electromyography.

DISCUSSION

Unchanged conduction velocities and nerve fiber diameters following CNS injuries

A classification scheme for the human peripheral nervous system has been developed by measuring conduction velocities and fiber diameters of single-nerve fibers in brain-dead humans and patients. This human neurophysiologic development is based on a new recording technique in man, the single-nerve fiber action potential (AP) recording from whole human sacral nerve roots and a further developed morphometry allowing for fiber diameters to be grouped into four ranges of myelin sheath thickness **(Figure 16)** [42,54]. Moreover, a new treatment has been developed, called coordination dynamics therapy, generated by human neurophysiologic research based on earlier, this, and following papers, which can repair urinary bladder and bowel functions [26], can partially repair motor and cognitive functions in humans with spinal cord [7,16-18] and brain injuries and can even inhibit cancer growth (see Introduction for references). The availability of single-nerve fiber AP recordings from dorsal roots, in which also dorsal root efferents are contained, in the lower sacral nerve roots [42,56], allowed to simultaneously measure conduction velocities and fiber diameters of single-afferent and efferent nerve fibers. Group conduction velocities and group nerve fiber diameters could be obtained from distribution histograms. The group conduction velocities and group nerve fiber diameters (peak values) obtained for paraplegics were found to be very similar to those estimated for brain-dead humans and patients with no spinal cord injury. Thus, the classification scheme of the human peripheral nervous system is preserved at least 0.5 to 6 years following spinal cord injuries and probably also other CNS injuries **(Figure 3)**. The subdivision of the α_1-motoneurons (FF) in α_{11}, α_{12} and α_{13}-motoneurons needs further clarification. The preservation of the classification scheme is not a trivial conclusion since changes occur in the peripheral and central nervous system following spinal cord injury. It has been shown in this paper that, at least for some patients, the tension receptor afferents of the bladder fired even when the urinary bladder was empty **(Figure 42)**. In following papers, it will be shown that functions of the spinal neuronal network change after injury, as judged by the impulse patterns of secondary muscle spindle afferents and premotor spinal oscillators.

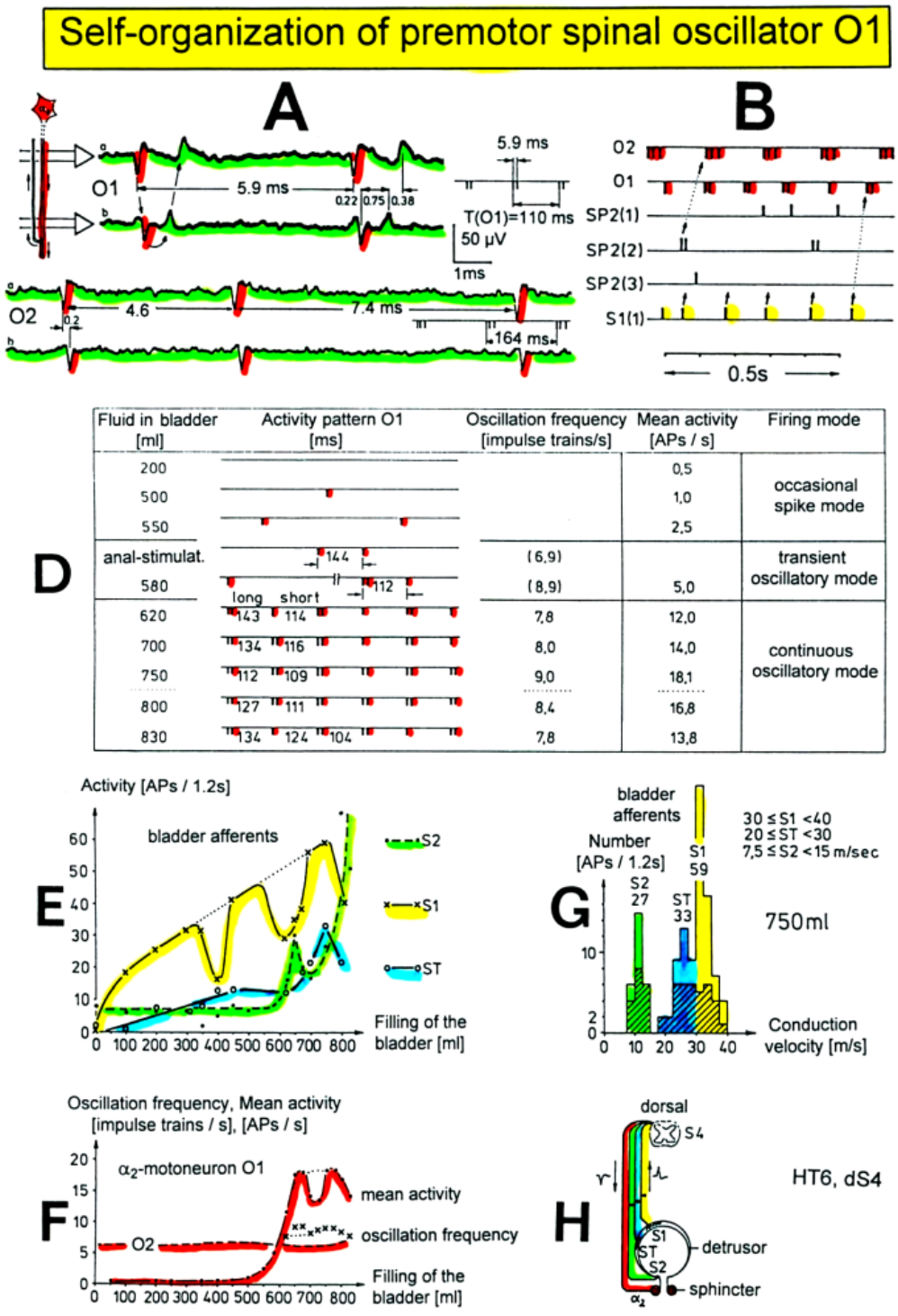

Figure 47. Self-organization of premotor spinal α_2-oscillator O1, which innervates the external urinary bladder sphincter (skeletal muscle). Brain-dead human HT6; recording from a dorsal S4 nerve root. --- A. Recordings from α_2-motoneurons O_1 and O_2, firing in the oscillatory mode with impulse trains of 2 (upper recording) and 3 (lower recording) action potentials (APs). The durations of the oscillation periods were 110 (O_1) and 164ms (O_2). The interspike intervals of the impulse trains were 5.9ms (O_1) and 4.6 and 7.4ms (O_2). Motoneuron O_1 conducted at 36 m/s; its recurrent fiber conducted at 21 m/s. Thelayout for measuring is shown schematically. The inserts show the oscillatory firing modes; they have not been drawn to scale. --- B. Impulse patterns of oscillatory firing α_2-motoneuron O_2 innervating the

external anal sphincter, in relation to the muscle spindle afferent activity SP2(1 to 3), activated by the stretch of the anal sphincter through an anal catheter, and impulse patterns of oscillatory firing α_2-motoneuron O1 innervating the external urethral sphincter, in relation to the stretch receptor afferent activity (S1(1)) of the urinary bladder, activated by 750 ml bladder filling. Phase relations between APs of SP2(2) and O_2 and between APs of S1(1) and O_1 are indicated by the small arrows. --- D. The firing in the occasional spike mode, the transient and the constant oscillatory firing mode of α_2-motoneuron O_1 in response to filling of the bladder. In the 'activity pattern' column changing durations of oscillation periods are given. The oscillation frequencies in the brackets give the frequencies at the moment of oscillation for the transient oscillatory firing mode. Downward deflections are schematized APs. Interspike intervals of the close APs ≈ 6.0ms (A). --- E. Activity levels of stretch (S1) and tension (ST) and flow receptor afferents (S2) (E) and of sphincter α_2-motoneuron O_1 (F) in response to retrograde filling of the bladder. The activity values of the S1, ST and S2 afferents are taken from histograms like the one in G. Filling of the bladder was stopped once between 600 and 650 ml. --- F. The small dotted lines represent mean activity (APs/s) and oscillation frequency (impulse trains/s) of α_2-motoneuron O_1 if bladder filling were not stopped in between. Note that the mean activity increases continuously with the filling of the bladder from 550 to 650 ml, even though motoneuron O_1 started to fire in the oscillatory mode from 620 ml on (D). Note further that the oscillatory firing motoneuron O_2 (frequency of firing with impulse trains is shown) is nearly not affected by the filling of the bladder and by the start of the oscillatory firing of motoneuron O_1. --- G. Conduction velocity frequency distribution histogram of stretch, tension and flow receptor afferent activity at 750 ml. The activities of afferents S1, ST and S2 are quantified by counting the afferent conduction velocities under the peaks (open plus hatched part), with the conduction velocity limits given in the insert. The counts (27, 33, 59) are given below the peak labeled S1, ST and S2 and plotted into E for the afferent activity at 750 ml. --- H. Schematic drawing of the anatomical arrangement of the afferents and the motoneuron O_1.

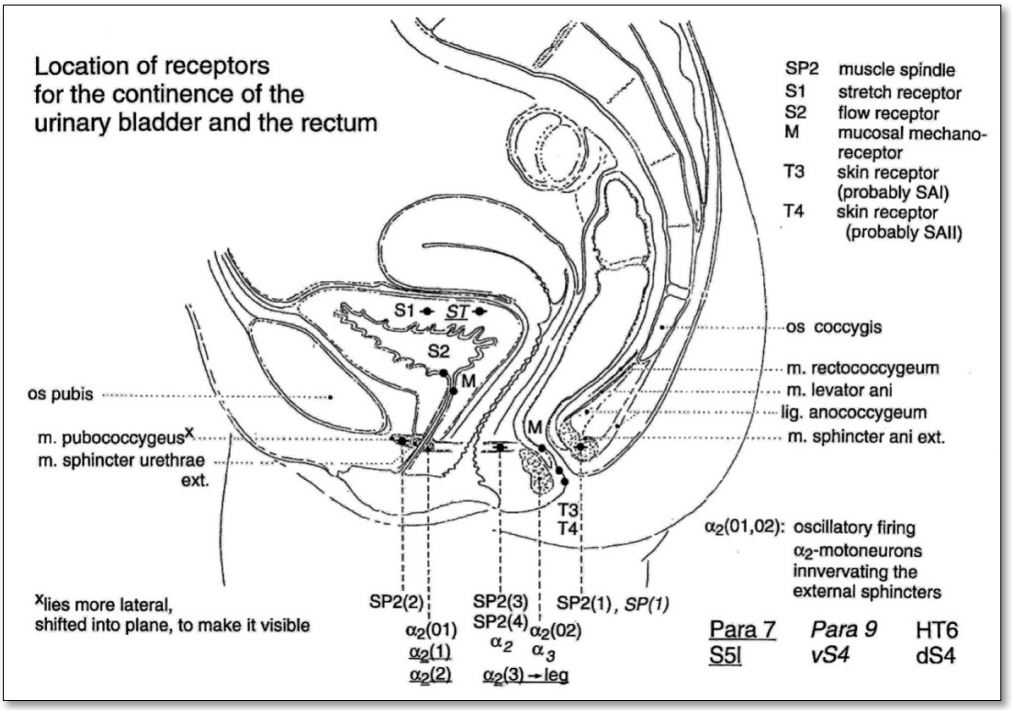

Figure 48. Location of receptors and muscles for the continence of the urinary bladder and rectum, from which was recorded in the brain-dead human HT6 (dS4 root), paraplegic 9 (vS4 root) and paraplegic 7 (nerve root S5).

Classification schemes

The classification schemes of Grundfest, Erlanger and Gasser and Lloyd and Hunt [38,65-74] do not apply to humans and are too inaccurate to be used for detailed analyses of human nervous system functions. The differentiation between α_1(FF), α_2(FR) and α_3(S)-motoneurons [75-78,42,54] is essential for the understanding of CNS functions, since the three α-motoneuron types are integrated in functionally different spinal circuitries and can be distinguished from each other by the different oscillation frequencies and impulse trains (high activity mode) [43,3], different recruitment in the occasional firing mode (low activity mode) [79, 80] and different motoneuron drive [3]. The existence of slow and fast systems in the CNS has already been suggested by Sherrington [81]. There have been no other authors dealing seriously with the measurements of urinary bladder afferents in humans [42,43]. Animal data [82-85]

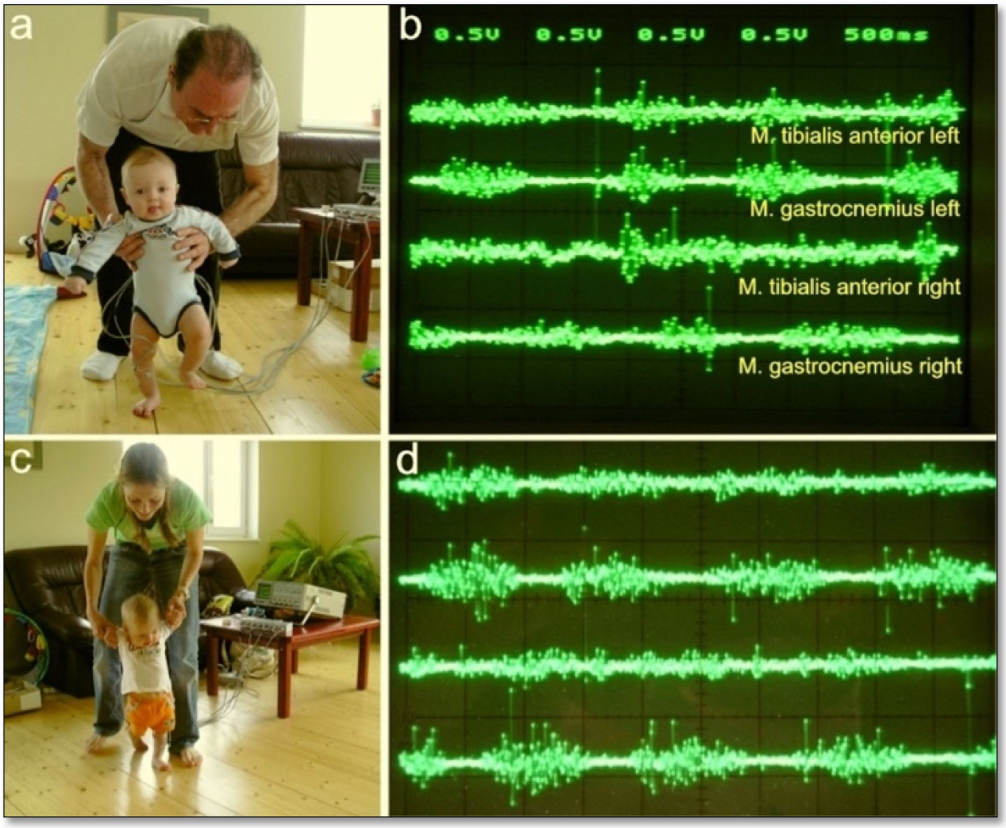

Figure 49. Surface EMG obtained from the healthy 5-months-old (a, b) and 8-months-old old "Jürgen" (c, d) during supported walking with the Author and the mother. a. Walking resembles automatic stepping, because of the strong lifting of the left knee. The toes of the right foot are plantar flexed, which is not physiologic. b. Surface EMG motor programs of left and right tibialis anterior and gastrocnemius muscles. Note that there is no antagonistic action between the tibialis anterior and gastrocnemius muscles. The right tibialis anterior muscle shows no motor program. c. The walking is more walking like and not so much anymore automatic stepping like. d. Better motor programs then 3 months earlier (b). Still there exists no antagonistic action between the tibialis anterior and gastrocnemius muscles. The activation of the right tibialis anterior muscle is a bit better than 3 months ago (b).

are not suitable for a direct comparison with human data, unless the classification schemes for animals are improved, which has been started [86,79,87] **(Figure 54)**. The differentiation between stretch and tension receptor afferents [42,43] will contribute to the understanding of pathologic micturition. Application of classification schemes to myenteric neurons has been attempted [88,89].

Temperature dependence of the conduction velocity

The conduction of APs in nerve fibers depends strongly on the temperature both in humans **(Figures 43-45)** and animals [73]. The increase of the conduction velocity of α_2-motoneurons and secondary muscle spindle afferents resulted here to approximately 2.8 m/s / °C. Other authors measured in humans a temperature dependence of 2.1 m/s /°C, but no differentiation between different groups was made [90].

In animals, a temperature dependence of 3.5%/°C was measured [38]; data for different groups were not given. In this paper, it was measured that in humans, the

temperature dependence of nerve fiber groups is different for the different groups. The effect of a strong temperature reduction is that the conduction velocity distribution peaks fuse, and it becomes difficult to identify the groups (peaks) **(Figure 43)**. In particular, the preganglionic parasympathetic motoneurons can be better differentiated from the static γ-motoneurons at a root temperature higher than 35°C. The temperature of the thin roots is not exactly measurable. Efforts should be spent to keep the temperature in the operational field close to the central temperature of the patient. In the future, conduction velocities obtained from the roots of the cauda equina have to be calibrated using conduction velocities obtained non-invasively from the same fibers of the leg. Such a comparison requires an analysis of CAPs with single-fiber APs [64]. Identification of nerve fiber groups

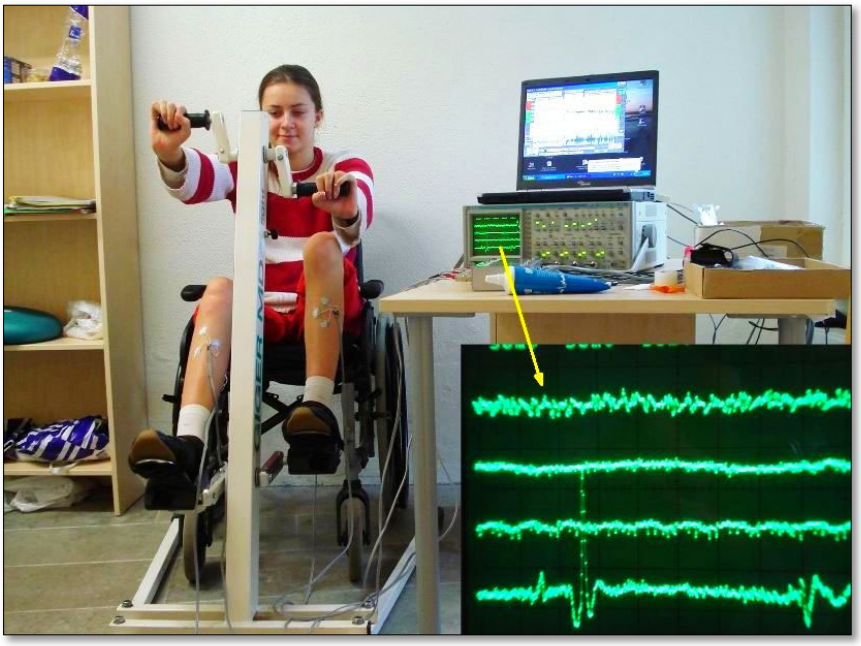

Figure 50. Layout for measuring coordination dynamics (arrhythmicity of turning) between arm and leg movements, displayed on the laptop. For the intermediate coordination's between pace and trot gait, the fluctuation of the network states is larger. The recording of sEMG activity (displayed on the oscilloscope) from the tibialis anterior and other muscles is also shown. The inset shows single motor unit action potentials on the lowest trace. The recordings are taken from a patient with a rather complete (95% injury) cervical spinal cord injury C5/6.

however does not depend on the knowledge of the exact conduction velocity: conduction velocity distribution histograms can be calibrated using the same velocity of conduction by α_2-motoneurons and secondary muscle spindle afferents (SP2), α_3-motoneurons and stretch receptor afferents of the bladder (S1), and approximately by α_1-motoneurons and primary spindle afferents (SP1). The SP2 fibers and the α_2-motoneurons showed the same temperature dependence of the conduction velocity; this calibration relation is therefore temperature independent in the temperature range 32 to 36°C.

Recording of APs from preganglionic parasympathetic motoneurons

In a first approximation, the action potential (AP) amplitude depends on the diameter of the axon and declines due to volume conductance if the axons are not positioned close to the recording electrodes. Thinner axons have smaller AP amplitudes than thicker ones [30]. But the area between the AP curve and the baseline is, in a first approximation, independent of the AP amplitude [64], because the AP duration increases for thinner, slower conducting fibers [38, 74, 30]. The preganglionic parasympathetic motoneurons with a peak group diameter of approx. 3.5 µm have very small AP amplitudes and very long duration **(Figure 35D)**, so that they are difficult to recognize in the noise and artefact level and are often overshadowed by large APs of thick fibers. Even though most likely, parasympathetic action can also be estimated from the impulse patterns of secondary muscle spindle afferents [87,2], sometimes it is very important to obtain also impulse patterns of single preganglionic parasympathetic motoneurons directly. Only in this way is it possible to analyze neuronal networks of the sacral micturition center. The asymmetrical distribution of preganglionic parasympathetic axons with a nerve fiber diameter of up to 6 µm will make it sometime possible to safely record parasympathetic APs and to extract natural impulse patterns of single fibers from the recordings, provided good recording conditions. Thin ventral S4 roots freed over long sections from other roots, with nearly no shunting blood vessels, are favorable for recording single-fiber APs in patients with no arachnoiditis.

Extension of the classification scheme to thinner fibers

As discussed above for the preganglionic parasympathetic motoneurons, the limit for recording single-fiber APs from undissected roots or fascicles are diameters between 3 and 4 µm. It was recorded therefore from myelinated fibers only. This does not mean that it is impossible to record from unmyelinated fibers. It should be possible to record extracellular APs from unmyelinated human axons thicker than 4 µm. To extend the classification scheme of the human peripheral nervous system to nerve fibers thinner than 3 to 4 µm, compound action potentials (CAPs) have to be analyzed with the single-fiber AP

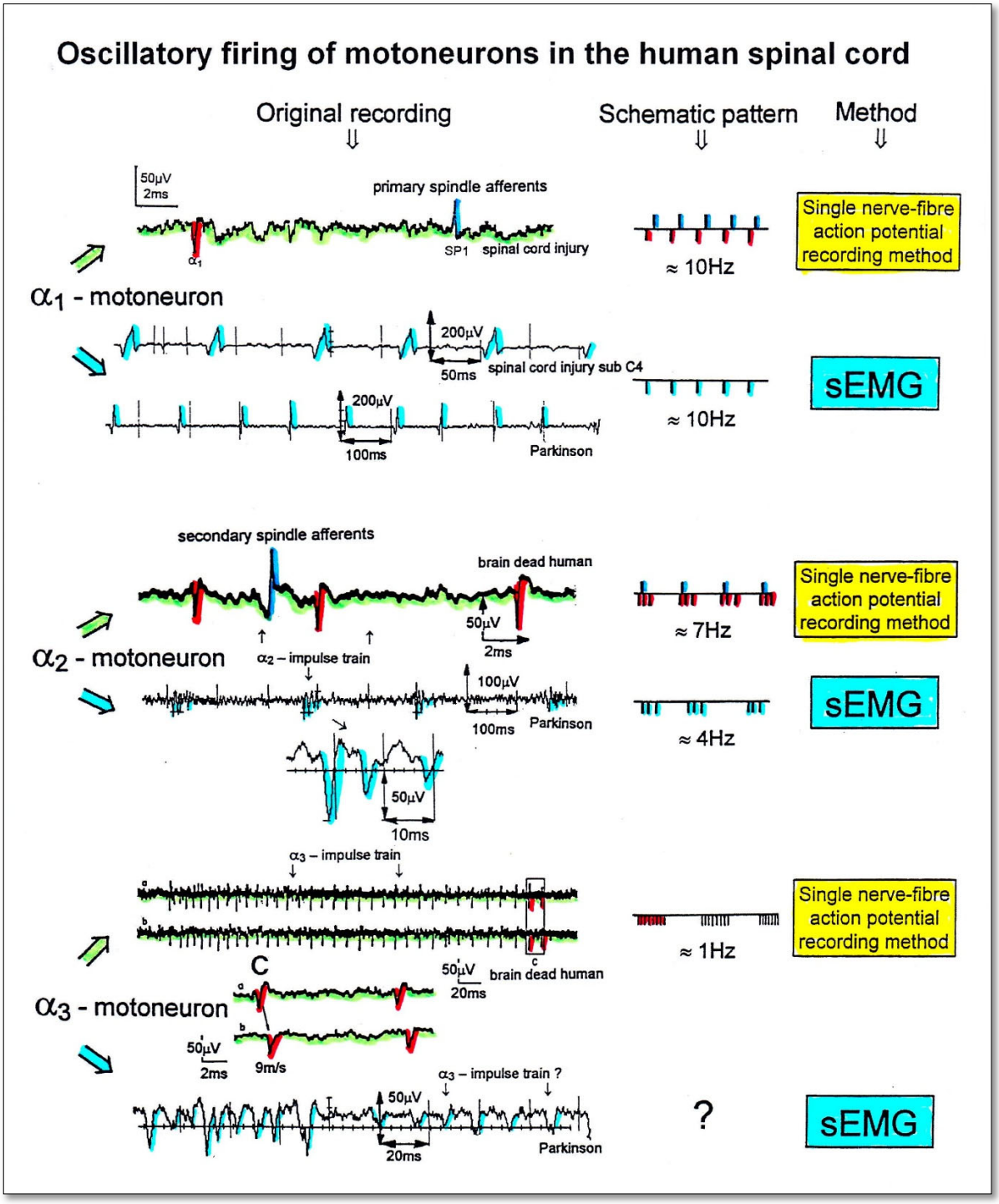

Figure 51. Oscillatory firing patterns of α_1, α_2, and α_3-motoneurons recorded from motoneuron axons with the single-nerve fiber action potential recording method (upper trace) and from FF, FR, and S-type motor units with the surface electromyography (lower trace). The left panel shows original recordings, the middle panel the schematic patterns and the recording method is indicated on the right side. The original recordings were taken from patients with spinal cord injury and Parkinson's disease and from brain-dead humans.

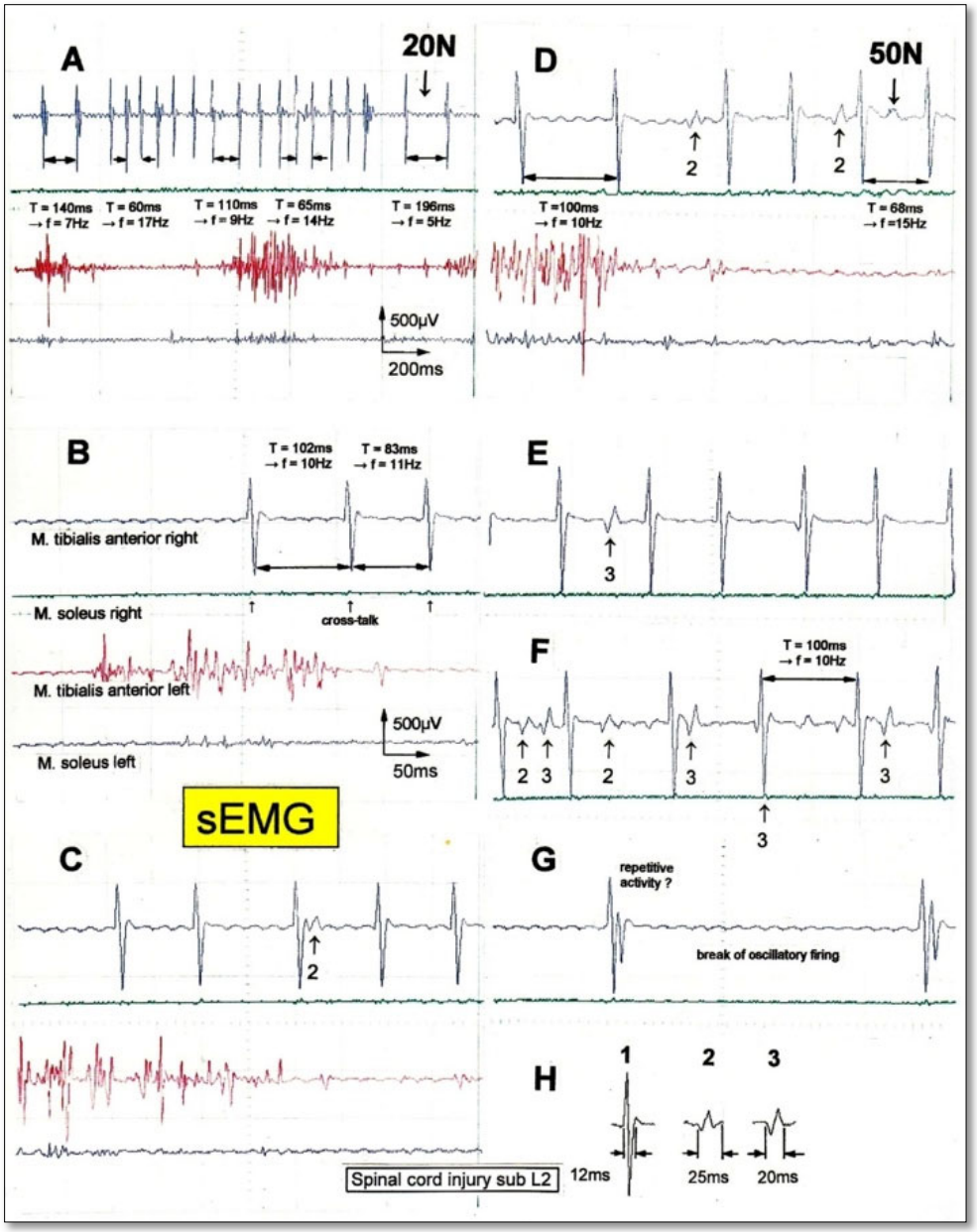

Figure 52. Non-synchronous partly coordinated firing of FF-type motor units of the right tibialis anterior muscle from a patient with spinal cord injury sub L2 suffered in an accident, measured by surface EMG. The firing was activated by exercising on the special coordination dynamics therapy device (Figure 50) at the loads of 20 and 50N. Oscillation periods (T [ms]) and oscillation frequencies (f [Hz]) of oscillatory firing motor unit 1 are partly indicated. The waveforms of 3 motor units are identified in the right tibialis anterior muscle (top trace) and are shown in 'H'. Motor units 2 and 3 are marked in 'A' through 'G'; the identification of large amplitude motor unit 1 is obvious. The left tibialis anterior muscle (third trace) shows already a motor program; little activity in the soleus muscles for this low-load activation.

recording method to identify the nerve fiber group composition, as has been started [64]. This seems possible since the radial decline of the AP amplitude due to volume conductance is reasonably small for very thin roots or fascicles. The area between the AP curve and the baseline is, in a first approximation, the same for all nerve fibers, so that CAPs can be analyzed with the simultaneously recorded single-fiber APs [64]. In this way, it seems possible to measure the conduction velocities of thin nerve fiber groups, in which the single-fiber APs cannot be recorded anymore, using conduction velocities of CAPs **(Figure 40C)**.

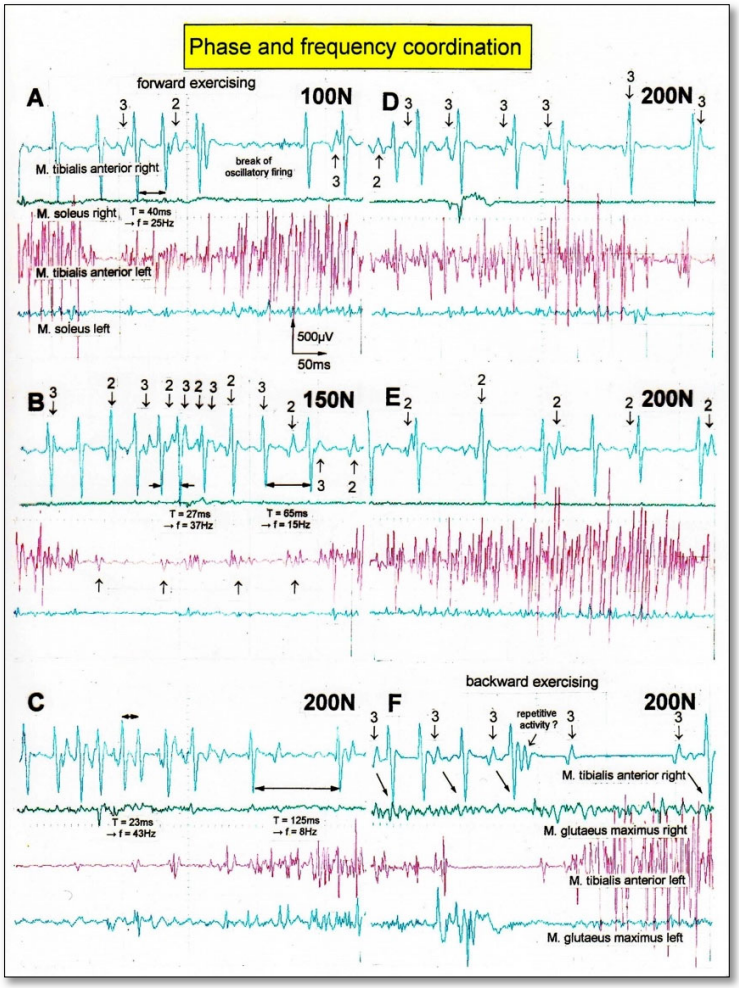

Figure 53. Phase and frequency coordination between oscillatory firing motor units (FF-type) during the generation of a motor program when the patient exercised on the special coordination dynamics therapy device at loads increasing from 100 to 200N. Oscillation periods (T) and oscillation frequencies (f [Hz]) of oscillatory firing motor unit 1 are partly indicated. A,B,D,E. same recording situation as in Figure 52. C,F. soleus electrodes shifted to gluteus muscles to check early re-innervation upon therapy. The waveforms of the 3 identified FF-type motor unit potentials '1', '2', and '3' are the same as in Figure 52; motor units '2' and '3' are partly marked. In 'F', some coordination's between motor unit '3' and '1' are marked.

The identification of further peak group nerve fiber diameters is more difficult. Firstly, there are afferent nerve fiber groups with strongly overlapping diameter distributions, and afferent fibers cannot be distinguished from efferent fibers. For a further identification of nerve fiber group diameters, peripheral nerves of known group composition have to be analyzed morphometrically, and this work has already been started [39, 40, 57, 58]. A comparison of nerve fiber diameters of fibers of the spinal canal with those at more distance from the medulla in the periphery is possible if there is no branching of fibers because the tapering of nerve fibers is small (0.2% per 13cm [59]).

Identification of muscle spindle afferents and α, β, and γ-motoneurons in animal and human (Translational medicine)

Muscle spindle afferents

Most receptors in the periphery, e.g., skin receptors, are defined by the receptor properties alone. However, muscle spindle afferent activity also depends on the γ (and probably β) -motoneuron drive of the CNS and, depending on the site of location, sometimes on the drive of sympathetic or parasympathetic efferents. The receptor properties are therefore not uniquely determined by the peripheral receptor properties alone. A false efferent innervation during the development may further be compensated for by a different neuronal network organization in the CNS. With respect to neuronal

network functions, it has been argued that the network connections may be even more important than its buildings blocks, namely the different nerve cells [92].

In animal research, primary and secondary muscle spindle afferents [93, 94] have been distinguished from each other by their responses to a ramp stretch. Primaries respond stronger to stretch and show an instantaneous frequency rise. The secondaries show only an initial burst and frequency changes as if they were smoothened by a condenser [95]. The conduction velocities of the primary and secondary spindle afferents are clearly different. If spindle afferents from several muscles are pooled, the conduction velocity ranges start overlapping, and if velocities are pooled from different animals, the velocities from primaries and secondaries even overlap more strongly.

In the recordings from the human lower sacral nerve roots, most spindle afferents were secondaries, because they conducted in the secondary range, they were projecting poly-synaptically onto α_2 and α_3-motoneurons (Figure 25F, G), innervated fast fatigue resistant (FR) and slow muscle fibers (S) **(Figure 4)**, and they drove premotor spinal oscillators with phase relations of the broad peak type [96]. It cannot be excluded that the primaries in continence muscles have different properties. Probably, a few primaries do innervate the spindles of the pelvic floor and the musculus flexor hallucis brevis (via S4 (!) and more rostral roots). The secondary muscle spindle afferents conduct with a group conduction velocity of 50 m/s at 36 °C (group nerve fiber diameter 12.1 µm) and the primaries with a group conduction velocity of 60 m/s (group fiber diameter = 13.2 µm), as identified by the group conduction velocities (Figure 3) and the conduction velocities of components of compound action potentials **(Figures 37 and 38)** [64]. Since the conduction velocity ranges of primaries and secondaries overlap, further criteria are needed for a safe identification and will be given below. In one measurement, a primary spindle afferent fiber could safely functionally be identified by its monosynaptic drive on an oscillatory firing α_1-motoneuron innervating fast fatigable muscle fibers (FF) **(Figure 4)** [97].

Identification of dynamic and static γ-motoneurons and α-motoneurons

Since nerve fibers taper only very little, the conduction velocities also vary only little if there is no branching and change of membrane properties along the fibers. The characterization of nerve fiber groups by a group conduction velocity and a group nerve fiber diameter can therefore be used to identify nerve fiber groups and neuron types.

In animal research, it has been found that the velocity ranges of static and dynamic γ-motoneurons overlap [98, 99].

In human research, measurements indicate that there are different peaks of γ-motoneurons according to the diameter and velocity distributions, even though the distributions strongly overlap. A better splitting of the different γ-peaks and preganglionic parasympathetic fiber peaks in conduction velocity distributions can be achieved if the velocities are plotted on a log-scale **(Figure 36)**. For further comparisons of human and animal velocities and fiber diameter distributions, the different measuring conditions have to be considered.

In the human cauda equina, where a nice alignment of nerve fibers was expected **(Figure 15)**, still quite a lot of variability was encountered. In peripheral nerves, more changes in the regrouping of nerve fibers and branching have to be expected. In CNS research, there is much discussion whether the branching of the reticular-spinal pathways already occurs in the reticular formation [100,101] or during their course in the spinal cord [102,103]. Further, if nerves are bathed in paraffin oil, as was frequently done in animal research, the conduction velocity will change at the bathed site [104]. It has to be measured how large the change in the conduction velocity is, if parts of the nerve fibers are bathed in paraffin oil for temperature regulation. It may well be, therefore, that variabilities in the conduction velocity measurements in animal experiments were due to the fact that a sufficient number of values (more than 100) are not measured simultaneously to obtain representative distributions and due to other reasons, so that group conduction velocities of the static and dynamic γ-motoneurons overlapped more strongly than in reality. Simultaneous velocity distribution measurements in animals, as in the human case, indicate that there is not so much overlap in the velocity distributions of static and dynamic γ-motoneurons **(Figure 54A)** in comparison to a human velocity distribution **(Figure 54B)**. A velocity plot on a logarithmic scale would enable a further separation of the peaks.

In man, on the other hand, α and γ-motoneuron groups were identified by the group conduction velocities and partly by group nerve fiber diameters and by the measured impulse patterns conducted along the fibers. Even though the conduction velocities were measured over small distances (10mm), the relative group conduction velocities were very reliable, because the conduction velocities of all nerve fiber groups were measured simultaneously and were calibrated by the calibration relation that secondary muscle spindle afferents conduct with the same velocity as the α_2-motoneurons, and this calibration relation is temperature independent, even though the conduction velocities

themselves are strongly temperature dependent **(Figure 43)**. Sufficient characterization of nerve fiber types is a principal problem when nerve fibers have to be safely identified for the understanding of neuronal network self-organization or the clarification of peripheral receptor properties of muscle spindles.

Since group conduction velocity distributions overlap, γ (and α) -motoneurons have to be identified additionally by their functions namely by their natural impulse patterns.

In measurements in man, the groups of α and γ-motoneurons were identified by the speed and the dynamics to respond to natural stimulations such as touch, pinprick and catheter pulling, and the conduction velocity [87]. The characteristics of the static (γ_2) and the dynamic (γ_1) γ-motoneurons are not the same as in animal research. In humans, the γ-motoneurons were therefore characterized by the central nervous system properties, namely by the cell soma and in what neuronal networks the motoneuron cells are integrated, whereas in animal research, they were characterized by the periphery, namely how do primary muscle spindle afferents respond to repetitive 75 Hz stimulation (not always 75 Hz) of the static and dynamic γ-motoneurons in parallel with a ramp stretch. To fulfil the needs of the human research and the clinical demands, a multiple group characterization of γ-motoneurons is needed, which can be used in animal research and in the clinical setting. For α-motoneurons, this has partly been achieved. α_2-Motoneurons, for example, fire for continuous high activation at a frequency of about 6.7 Hz, have a group conduction

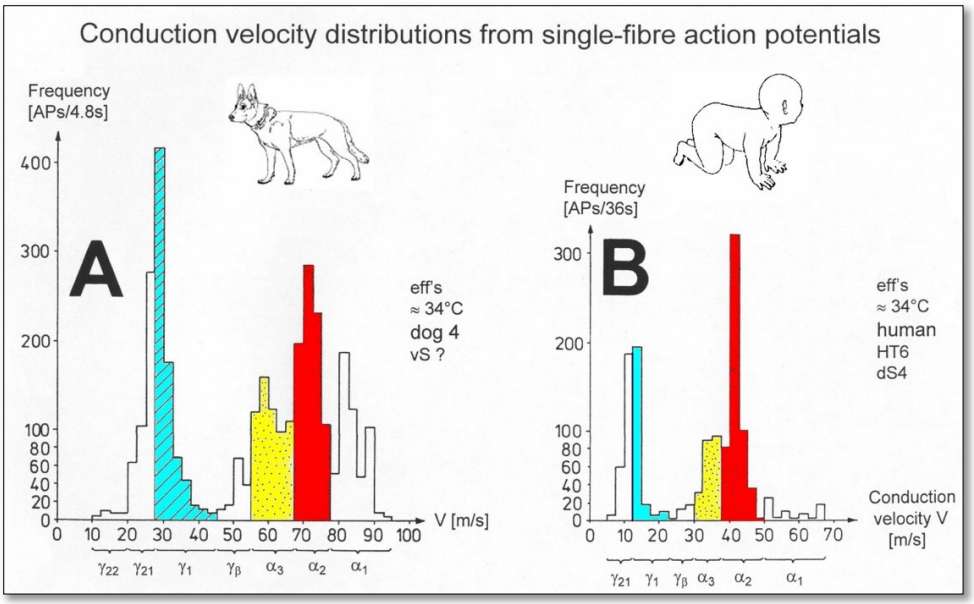

Figure 54. Conduction velocity distribution histograms of efferent action potentials from a dog (A) and a human (HT6; dS4) (B) of lower sacral nerve roots. The distribution peaks are labelled according to the respective groups they represent. Motoneuron velocity ranges are indicated. In A, 24 sweeps of 0.2s, and in B, 30 sweeps (stimulated and non-stimulated) of 1.2s duration were used. Note that dog α and γ-motoneurons conducted faster than the ones of humans, recorded with the same equipment at the same temperature by the Author.

velocity of 50 m/s, a group nerve fiber diameter of 10.2 μm and innervate FR-type muscle fibers, which are fast oxidative glycolytic fibers **(Figure 4)**. For dynamic and static γ-motoneurons, such a multiple characterization is not known in humans. In human measurements, three conduction velocity peaks of γ-motoneurons (γ_1, γ_{21}, γ_{22}) seem to exist. The γ_1-motoneurons respond faster to stimulation than the γ_2-motoneurons [87]. It has to be shown whether the human γ_1-motoneurons (identified centrally) actually correspond to the dynamic γ-motoneurons as identified in animal research (identified in the periphery) and whether the γ_2-motoneurons correspond to the static γ-motoneurons. The notion will be helpful that there is no tapering of nerve fibers. First electrophysiologic measurements from single human muscle spindles in the periphery indicate that the human muscle spindles may function similarly as do cat spindles, even though the human muscle spindles seem to be more complex [93], and human muscle spindles may be quite different in different parts of the body.

Differences between human and animal research

The simultaneous recording of the natural impulse traffic from a set of afferent and efferent fibers in a few seconds

is a powerful tool in human neurophysiology, because all data are obtained under the same condition from the CNS and the receptors in the periphery. This was demonstrated above by the considerations with the conduction elocities and will also hold for the impulse patterns. May be the recording of single-nerve fiber action potentials can also be used in certain animal settings.

The identification of the nerve fibers of different neurons by the conduction velocity and the natural firing pattern has the advantage that we can also judge the natural organization of the CNS under physiologic conditions and following injury, malformation or degeneration and repair the networks by movement-based learning.

Further, in clinics and in research, the electromyography is used which cannot be used in standard lab animals because of the hair. The quality of recording can be very high and phase and frequency coordination among motor units nicely be seen **(Figures 52 and 53)**.

In the next section, some out-of-date treatments in spinal cord injury will be discussed, which are used again and again with propaganda in the mass media. It will further be shown that animal experiments are removed from human reality.

Out-of-date treatment in spinal cord injury

A few comparisons will show that animal experiments are far away from human reality and normally cannot contribute to translational medicine or human disease research. A part of the research budget has to go to real qualified medical research and reviewer for medical research must have also published about human patients.

Electrical stimulation is a non-causal therapy and may be dangerous for patients

Nervous system functions can be repaired by movement-based learning. Natural physiologic impulse patterns, induced through physiologic movements, enter the CNS for repair by learning. The rather pathologic neural network organization are going to be changed in this way to become more physiologic again. If there is massive physiologic input the repair through learning is larger than as if there is only minor physiologic input.

Electrical stimulation, on the other hand, of skin and muscles generates completely unphysiological impulse patterns which the CNS does not understand. This unphysiological input may worsen the pathology of neural network organization. A repair of the urinary bladder and sexual functions may become impaired. Seeing muscles contracting is fascinating for a patient with a spinal cord injury, but it is not healthy. Physiologic input from the skin is shown in Figure 31. Physiologic muscle patterns are shown in **Figures 52** and **53**. It is impossible to stimulate electrically all three muscle fiber kinds physiologically at the same time. Their physiologic patterns are given in **Figure 4**. Each kind of muscle fiber type has its own activation pattern. If in a patient a muscle is strongly overstimulated, the muscle may even stop working and if it is the last breathing muscle in rostral spinal cord injury (diaphragm innervated by phrenic nerves) than the electrostimulation is life treating. A healthy athlete can tolerate a lot of pathologic stimulation, a CNS-injured patient cannot. In patients with Parkinson's disease, massive electrostimulation to the brain may even render the neural network that pathologic, that the tremor stops. – Electrical stimulation of the human body is the opposite to a natural healthy repair by movement-based learning, in which the patient is only getting and not losing functions. There may be exceptions that a transient electrostimulation is clinically justified.

Electrical anterior root stimulator for urinary bladder control according to Brindley

The electrical bladder stimulator according to Brindley [35] is a thoughtful stimulator, but is still out-of-date because the treatment is invasive, destructive and non-causal. Nerve roots have to be cut. The electrical sacral anterior root stimulation, according to Brindley, is discussed here mainly because of scientific reasons. The treatment involves the de-afferentation of the bladder to increase bladder storage volume. The electrical stimulation of the motoneuron and preganglionic parasympathetic axons afterwards in the motor roots of the cauda equina is performed to empty the urinary bladder. A precise electrodiagnosis during surgery is crucial for the cutting of the bladder afferents and the saving of the motoneurons for later stimulation and is performed by nerve root stimulation and bladder pressure measurements. The recording of single-nerve fiber APs and compound APs brings about an improvement of the intraoperative diagnosis. A more selective cutting of afferents and a partial saving of afferents transmitting sexual sensations would improve the treatment. The hope is that the dorsal S2 root contains many afferents conducting sexual sensitivity and only few conducting bladder fullness. The detailed representation of the urinary bladder and sexual organs in the sacral roots is still unclear. The representation varies among patients [105]. Further, little is known which fibers conduct sexual feeling. The touch 4 (T4) (may be SAII) skin afferents ("Streichel receptor afferents") [106] probably contribute to it. A case is known in which a lady with a partial spinal cord injury was operated for urinary bladder control by electrical anterior root stimulation. The dorsal S2, S3 and S4 roots and the whole S5 root were cut. The sexual sensitivity was partly preserved. Some sexual organ afferents may therefore also run through the plexus hypogastricus **(Figures 19, 57)** or the dorsal S1 root. Ventral root afferents are probably too few to account for the preservation of sexual feeling. Morphometric analyses may help to clarify the nerve fiber group composition of

nerves innervating pelvic organs [107] since the tapering of nerve fibers is very small. This new intraoperative electrodiagnosis may be of importance for refined surgical treatments.

Some history of spinal cord repair: Nerve anastomosis, stem cell therapy, regeneration

Pharmacological intervention is of importance following spinal cord injury in humans, since disorders of the spinal cord can be of such strength that even joints may dislocate. If, on the other hand, paraplegics don't want to reduce their life expectation times by the side effects of drugs and want to regain a higher quality of life especially in severe cervical spinal cord injury, other treatments have to be found and are found [7,26]. Also, drugs may hinder the reorganization and regeneration of the spinal cord. The geographical landscape of neuro-attractive gradients during endogenous stem cell therapy, induced by coordination dynamics therapy, may be disturbed with the consequence that the homing of cells and connections become impaired.

Spontaneous healing of the human spinal cord following injury has not been observed so far. Since neurogenesis is very limited in the adult, the CNS seems to recruit other nerve cells to take functions over. The substitution of a function from other parts of the CNS is only possible if the necessary connections exist or can be built anew and if there is enough plasticity in the human CNS for relearning functions. In spinal cord injuries, nerve cells and tracts are destroyed. Injuries of the tracts are worse since the caudal spinal cord is disconnected from supraspinal control. Tract cells regenerate only over small distances, are impeded by scar tissue formation and form inappropriate synapses (for references, see [87]). The normal surgical strategy to cut unhealthy tissue away and substitute nervous tissue (embryonic) is not feasible. Firstly, only few spinal cord injuries are complete. A resection of the damaged spinal cord parts would destroy still existing tract fibers. Secondly, by cutting the damaged spinal cord, e.g., in the lumbar range, the caudal spinal cord will be disconnected from the blood supply and also die, because 70% of blood is supplied via the largest feeder artery (Adamkiewicz = A. spinalis magna **(Figure 15)**) and is distributed via the longitudinal trunks [108]. Replacement of damaged spinal cord tissue by embryonic nervous tissue in animals is of interest for the study of the mechanism of regeneration but had no consequences so far for the reconstruction of functions in humans.

The injection of different kinds of stem cells had also so far, no consequences for the repair of the injured spinal cord in human. Worldwide performed stem cell therapies were doubtful because of missing scientific publications and necessary diagnostics, doubtful theory (stem cells were not integrated in the existing neural networks) and missing knowledge on the functioning of the human CNS under physiologic and pathologic conditions.

The therapeutic potential of neural stem cells has recently been reviewed [109]. A qualified study by the author on stem cell therapy and coordination dynamics therapy on a patient with a thoracic complete spinal cord injury showed that this combined treatment was not successful [110,111]. For discussions of stem cell therapies and literature, see Refs. [18,111]. Stem cell therapies are still in the experimental stage. Chapter VI of [4] is offering information why exogenous stem cell therapy does not work (new cells cannot be integrated into the existing adult networks).

Since the damaged spinal cord part cannot be removed, neurosurgeons used to bypass it by performing a nerve anastomosis from the lower intercostal nerves rostral to the level of injury to the cauda equina nerve roots caudal to the injury. Regeneration occurred, but no useful functions were obtained. In the most advanced operation [112], a regeneration of the urinary bladder could be obtained, but the detrusor and the sphincter contracted simultaneously (dyssynergia of the bladder). Dyssynergias of the bladder can be repaired by coordination dynamics therapy [26]. At the beginning of this research project to repair the human CNS, the Author also tried to improve such nerve anastomosis, so that the patients get useful functions reconstructed [39, 40, 57, 58]. The number of total nerve fibers, of afferents and efferents of the donor nerves has to be compared with the acceptor nerves. E.g., it is useless to try to reinnervate the lower human body on one side with one intercostal nerve, which contains 10,000 myelinated fibers, if 250,000 are needed. However, the number of myelinated fibers of one intercostal nerve is sufficient for a regeneration of the urinary bladder and the intercostal XII is sufficient long to reach caudal sacral nerve roots **(Figure 15A, B)** and is not needed for breathing. Mismatch and functional aspects have to be taken into consideration.

To make a separate function of the detrusor and the sphincter possible, the bladder has to be reinnervated by the two different motoneuron pools, present in the intercostal nerve distal to its branching into two skin nerves (nervus cutaneus lateralis), namely the pure muscle branch supplying the musculus obliquus externus abdominis and the mixed nerve running to the musculus rectus abdominis **(Figure 55)**. Specific bladder afferents can be reconstructed by using the skin afferents from the Head's zone (ramus cutaneus anterior of the intercostals T12 to S1). Numbers of myelinated nerve fibers in caudal sacral nerve roots are given in Figure 19. For further details of such a nerve anastomosis see [39,40,57,58,53]. The Author did not proceed further with this nerve anastomosis therapy, since firstly it is still a partial destructive operation, secondly the patients need more

than a functioning bladder, and thirdly, in cervical spinal cord injuries this anastomosis cannot be performed. Last not least, a reorganization without reconnections is more efficient in repair than a reorganization following an anastomosis. The reason to cite the Authors theoretical work on nerve anastomosis is to show on what level nerve anastomosis have to be performed. The human patient is no laboratory animal. Human trials have to be qualified. It is also not justified to perform therapies again and again, which have already been shown not to work 10 to 50 years ago.

It has been reported that in adult rats, axonal regeneration after partial cord transection is greatly increased by blocking a subset of inhibitory myelin-associated proteins with neutralizing antibodies [113]. It has then been discussed with respect to human applicability that it is "just" a question of making it work [114]. In a recent review article on the repair of spinal cord injury in the same journal, 12 years later [115], it is still "just" a question of making it work. Human research was not included in the review. Now, further 13 years later, still this regeneration method does not work. The leading biologist retired in the meantime. A lot of research money was spent, but absolutely no progress reached the patient. It seems that many animal researchers seem to think that one can repair the human CNS without understanding it's functioning and knowing the problems of the patients apart from walking (pain, incontinence, sexual problems, spasticity, bowel problems, and stones in kidneys or gall bladder, joint problems). The enhanced regeneration of corticospinal tracts of the treated rats has been demonstrated by an enhancement of regenerating axons in

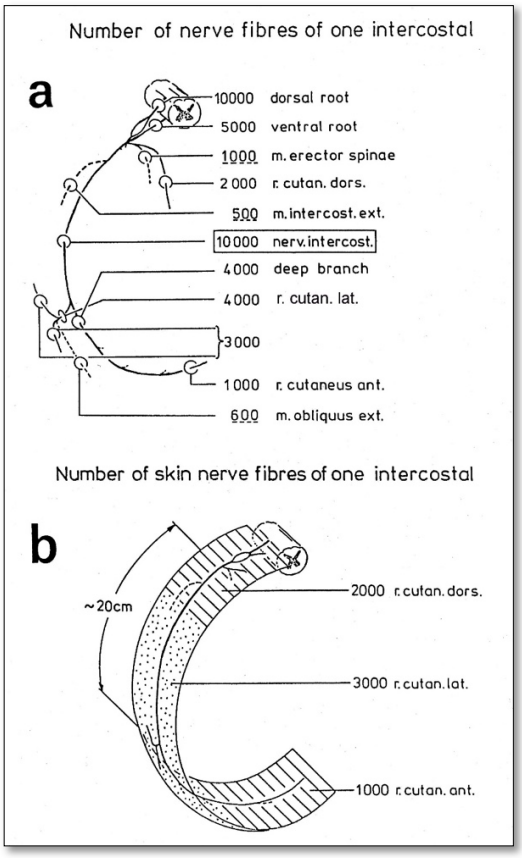

Figure 55. a. Summarized approximate numbers of myelinated nerve fibers of an average intercostal nerve (Th8-Th12) and its branches. Dashed nerve branches indicate pure muscle branches. Dashed underlined numbers indicate numbers of nerve fibers leading to muscles (about 50% motor). The nerve fibers of the rami communicantes have not been counted. b. Summarized numbers of myelinated nerve fibers of the three skin branches of the spinal nerve. Lined or dotted areas indicate approximate area of innervation. Dashed branches indicate muscle branches.

the not injured cord part and by the improved running. It has not been proven electrophysiological that the new corticospinal tract fibers and the formed synapses were functioning. Also, in rat regeneration, it has to be measured scientifically. The Author was able to do it [116]. It has also been reported that late-growing axons are able to take an aberrant route [117]. Still, the improved running of the treated rats is difficult to understand. Approximately 75 years ago, Sperry transposed the nerve supplies of flexor and extensor

muscles in rats [118] and monkeys [119]: the monkey relearned the task after some time; the rat did not. Surprisingly few trials were required for poliomyelitis patients to use transposed tendons successfully [120].

When cutting in experimental rats only 50% of the spinal cord, the repair results have no consequences for the regeneration of the human spinal cord, because firstly the rat has a higher capacity for regeneration and secondly it has been shown in a human patient with a 50% injured spinal cord (according to magnetic resonance imaging) that movement and bladder functions could be repaired by a mainly functional reorganization induced by coordination dynamics therapy [18]. Further, with respect to the nerve anastomosis from the lower intercostal nerves to the cauda equina nerve roots, nerve fibers of the intercostal nerves reinnervated the urinary bladder, but useful functions were not obtained [112]. Something like 25 years was not sufficient time to "just" to make a nerve anastomosis work.

In the human nervous system, the regenerative capacity is poor, but the learning-induced plasticity seems to be extremely high. A near-total functional recovery was achieved in a patient with an incomplete spinal cord injury after three years of coordination dynamics therapy [18]. In severe cervical spinal cord injury with a 95% injured spinal cord (according to magnetic resonance imaging), a partial repair was possible when coordination dynamics therapy (CDT) was administered [7.17,26,28]. Even a transient regeneration of the spinal cord was achieved in a 9.5-years-old girl through CDT (Figures 1, 5, 6, 7C, 59 (Nefeli)) [7]. The training and learning-induced plasticity, including learning transfer [28], of the human CNS has by far been underestimated.

Repair physiology: Human electrophysiology to analyze nervous system functioning and to develop treatment

With the new electrophysiological method, the single-nerve fiber action potential recording method, it is possible to analyze the functioning of the human CNS and probably also that of certain animals **(Figure 54)**, if the animal classification schemes are upgraded. The updated human classification scheme allows an identification of the nerve cells from which was recorded. This classification scheme is therefore a fundamental basis for human neurophysiology and repair physiology.

Figure 56 visualizes the importance of recording the communication between the CNS and the internal organs, besides motor functions, at the single-neuron level under rather natural conditions. When in spinal cord injury this communication becomes impaired, dysfunction of internal organs may occur and have to be counteracted by therapy besides repairing somatic functions. When the 13-year-old Nefeli **(Figures 1, 5 and 6)** stopped coordination dynamics therapy for 4 months, she got a stone in the galley bladder, because her injury was around the level of Th10/11. One can expect from Figure 56 that some problems of the internal organs can occur because of the loss of nerve cells in the spinal cord and loss of connections at the injury site and to the internal organs. In another 13-year-old girl, with an incomplete SCI, extending from the thoracic segments Th1/2 rostrally till to the medulla oblongata with an impairment of the nucleus of the vagus nerve, got stones in the kidneys and a big stone in the urinary bladder, indicating that, most likely, also the vagus nerve/nucleus was damaged, because the vagus nerve regulates the secretion of the kidneys **(Figure 56)** [121]. The stones appeared bevor coordination dynamics therapy was started. In spinal cord injury there are therefore more impairments of functions of the internal organs than just the impairment of the peristalsis of the bowel.

Figure 57 shows that in the complexity of neural networks of the human body there is a unique location, the sacral nerve roots, where one can measure and analyze CNS functioning at the single-neuron level. With this obtained knowledge, CNS functions can partly be repaired through CDT in different diseases.

The difference of this updated classification scheme for human peripheral nerve fibers to the earlier one of 25 years ago [1] is firstly that the classification and identification is backed by more basic data of the human nervous system and secondly that it became a basis for CNS repair physiology. With a developed movement-based learning therapy (CDT), the clinical application is fully reached. The injured, malformed or degenerating human nervous system can partly be repaired. And this statement is not just to raise false hope as in animal research.

The spinal cord injury patient Nefeli re-learned to walk **(Figure 1)** [7]. But still she is having problems with walking and scoliosis. Because the spinal cord injury is not just at Th10/11 **(Figure 58A)**, but extends also partly rostrally **(Figure 58B)**. This over several segments extending injury probably gave rise to a very severe scoliosis, which was operated. Further, Nefeli has to train at least one hour every day to keep the level. If she trains more and if CDT is further enhanced in its efficiency, more repair is possible. Training sometimes together with other patients or healthy persons is helpful **(Figure 58C)** for motivation and social life.

The motivation for training and the social life also holds for the cerebral palsy girl Sophie. To motivate her to train partly at limits, Sophie has to train sometime with other patients **(Figure 58C)** and most importantly with her relations **(Figure 59)**. In Figure 59 Sophie is training for motivation together with the mother, the grandfather and the grandmother. The father and the healthy brother are

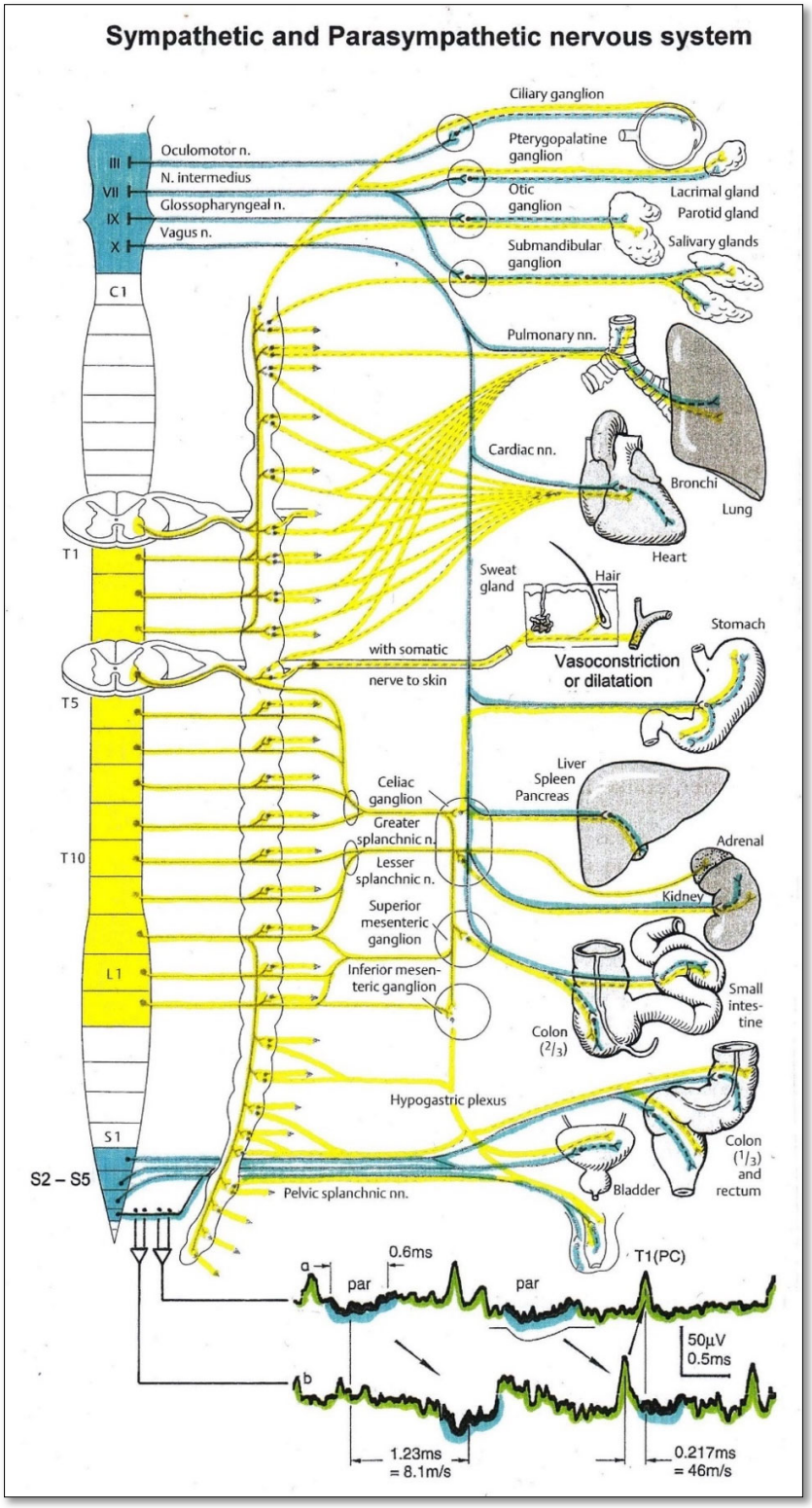

Figure 56. Schematic diagram of the sympathetic and parasympathetic nervous system. Yellow = sympathetic, blue = parasympathetic (it may be that the sacral parasympathetic division is also sympathetic). The recording of single-nerve fiber action potentials from preganglionic neurons (par) and a skin afferent fiber from a S5 sacral root is inserted.

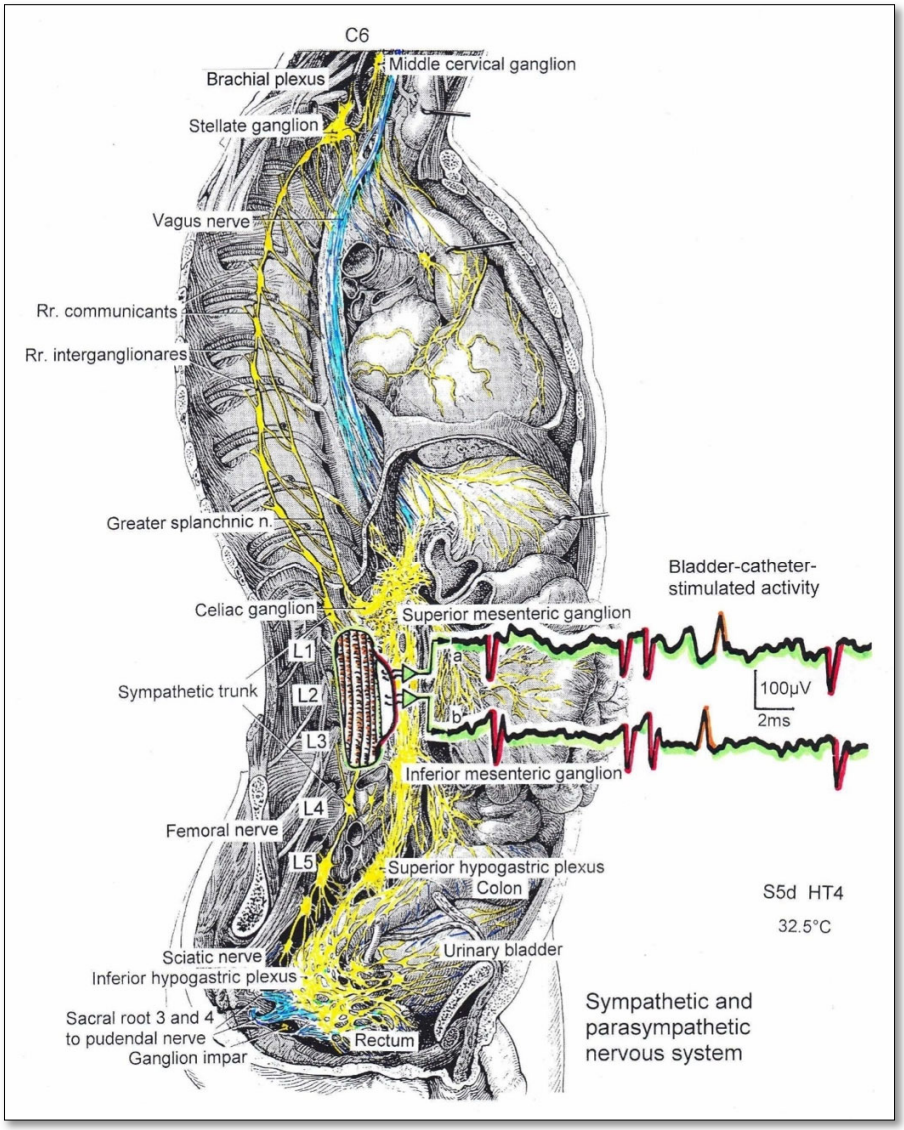

Figure 57. The picture illustrates the complexity of the autonomic nervous system. Connections of the different plexuses bypass the spinal cord and offer the structure for a functional repair of vegetative (and may be of somatic) functions like urinary bladder control, cardio-vascular performance and breathing. The recording of single-nerve fiber action potentials from human nerve roots, on the other hand, shows that in this complexity of human nervous system structures it is possible to record single-nerve fiber activity from several single identified neurons under rather natural conditions. Yellow = sympathetic, blue = parasympathetic.

having a rest and are not in the picture. Such stimulating surrounding is very important for further brain repair to improve motor and higher mental functions.

Based on the MRI of Sophie **(Figure 59**, insert), the radiologist diagnosed an atrophy of the cerebellum and pons. But probably there was more pathologic organization of Sophies brain because the higher mental functions were very low at the beginning of therapy and she was not fully continent, which cannot be seen in the MRI. The very intelligent patient Dr. Cwienk suffered with 55 a brain injury of the frontal and temporal lobe and lost 80% of the cerebellum **(Figure 9)**. With the injuries he lost intelligence. But with 21 years of CDT, his memory is with 80 still very good and his intelligence high to have qualified discussions with the Author. Such intelligent patients can explain what they feel, think and what has changed with their brain functioning following injury. Sophie, in comparison, has more impairment of the intelligence. More repair in the deepness of complexity of CNS organization is necessary to get her intelligence further higher.

Figure 58. A, B. MRI of the spinal cord injury of the 13.5-years-old Nefeli. Because of the scoliosis it is difficult to get the spinal cord into plane. The injury seems to extent also more rostrally (B) and is not only sited to the Th10/11 levels. C. Nefeli trains together with the 10.5-years-old Sophie on special CDT devices.

Figure 59. Sophie during group therapy on special CDT devices with her relations to become motivated to train at limits. The inset shows Sophies MRI.

The group training in Figure 59 is mainly to motivate Sophie to train at limits. But the grandfather is also training to live longer with a better quality of life [123]. The mother is training to reduce her trigeminus neuralgia and the grandmother wants to improve some finger functions and optimize the functioning of her artificial hip joints. The healthy brother, not in the picture, improved successfully by therapy eye functions, not to wear spectacles.

COVID-19 TREATMENT FROM HUMAN RESEARCH POINT OF VIEW

From basic human neurophysiology to Covid-19 treatment

One could ask what a qualified human classification scheme has to do with a treatment of virus infections? With the single-nerve fiber action potential recording method it was possible to measure impulse traffic at the neuron level, and for identification of nerve fibers a classification was built. It thus became possible to

understand some neural network organizations at the neuron level under physiologic and pathologic conditions and relate them to macroscopic functions. Out of the difference between physiologic and pathologic functioning, a repair method, the CDT, was developed with which it became possible to repair the human CNS or improve its functioning in the healthy case. Since the nervous system controls nearly all body functions **(Figures 56 and 57)**, these functions can be improved in the physiologic case and repaired in the pathologic case. With respect to treat infections, including Covid-19 infections, the immune system, cardio-vascular performance, blood pressure, diabetes and lung functions can be improved by movement-based learning. Through improving lung functions, the first protection shield of the body can be enhanced and thus a virus invasion stopped or reduced. This means that by exercising on the special CDT device, the body's defenses are improved. The strategy is in accordance with the ancient wisdom of Hippocrates that "natural forces are the true healers of disease".

The three strategies against Covid-19 virus infections

The pulmonologist Santiago Ewig stated that for basic medical treatment minimized effort has to be tried to achieve a maximized number of patients with a maximized health condition. He found regulations such as those for Covid-19 exorbitant. We have to learn to live with the virus as with the deaths in traffic and other diseases. This statement sounds logic from the medical point of view.

Whereas the virologist Alexander Kekule stated that there is for the time being no vaccine against the Covid-19 infection and also no treatment. This statement is wrong. Coordination dynamics therapy (CDT) is a causal therapy; it exists and is available. Mainstream medicine does not want to accept that movement-based learning is as important as surgery and pharmacotherapy. The human body needs to breathe, to eat and to move.

There are three strategies against the Covid-19 virus. The first one is to avoid an infection. Covid-19 regulations are sufficient effective in this first step. The second strategy is to improve the immune system of the lungs, especially the pulmonary surfactant, to stop low intensity invasion of viruses at the lung epithelia. This can be achieved by keeping the lungs in a healthy condition or even to train the lungs to function better. The third strategy, when the lungs are in a poor self-defence condition or too many viruses attacked it, viruses succeed to get through the epithelia and attack the body. Then the trained or not trained immune system has to manage to fight successfully against the virus infection.

The first strategy to avoid an infection concerns mainly the airborne infections. An infection by touching an infected substance can partly be avoided by wearing gloves and by having handles or hand rails made of metal, best of brass, to make them bacteriostatic [124]. The airborne infection can be separated into a low intensity concentration of Covid-19 viruses in the air and a droplet infection when speaking with another person. The droplet airborne infection is very dangerous because the virus infection concentration is high, when inhaling the droplets. Even a healthy and trained lung cannot fully stop the virus invasion. Being in a pub, where there is an infected person, there are viruses generally in the air and you may get a droplet infection when speaking with the infected person. When the air is polluted and has no negative ionization, the infection risk is higher.

Case report of a virus infection treatment of an 80-year-old patient with a severe cerebrum and cerebellum injury

The now 80-year-old patient Dr. Cwienk **(Figures 60, 9C)** suffered a severe cerebellum injury 25 years ago (80% lost tissue; Figure 9B) and a frontal **(Figure 9A)** and parietal lobe cerebrum injury. Following 21 years of CDT, he performed at the time of the infection 12 to 15 hours CDT per week, consisting of exercising on a special CDT device and walking on treadmill **(Figure 60)**. He lived in an old house with oven heating (mainly horizontal radiation heating) in a nice area of Graz (Austria) with little air pollution. During exercising, he had the door open to get fresh air in. It can be expected that his lungs were in a rather healthy condition. He was not vaccinated against the flu.

After being all January 2020 at home, he used a streetcar two times on February 1st 2020 and got infected. He was not wearing a breathing mask for protection because they were not available at that time in Austria. In the following night, he got high fever up to 40°C, as was diagnosed later on in the hospital. As the patient reported himself, he could nearly not move anymore when infected, but his cognitive functions were still working fine. His wife rang up the family doctor and he ordered an emergency car because of the possibility of a stroke. In the nearby university hospital, it was found out that he had no stroke but he had a flu virus infection. Drugs (Tamiflu) were administered. Since there were no free beds in the university hospital, he had the choice to be transported to another hospital or to go home with his wife. He decided for going home and obtained the Tamiflu medication for home. After being a week in bed with no training, he became able to get up again and started again with his regular CDT. A week later he was fully healthy again and had his full power back.

Flu versus covid-19 virus infection

In the streetcar, Dr. Cwienk was infected by a flu virus and not by a covid-19 virus. In mass media, it was not

Figure 60. The 80-year-old Dr. Cwienk with severe brain and cerebellum injury during exercising on the special CDT device and walking on treadmill. With 12 to 15 hours exercising per week, he can keep the level of health.

reported about infections and deaths through flu viruses or other bacteria, to have an idea through a comparison of the different infection and fatality rates how dangerous the Covid-19 virus really is. The society was therefore manipulated through selected information to accept impairments of basic human rights and an attack of democracy.

Why did the wife of Dr. Cwienk misjudge the disease? When a CNS-injured patient gets an infection, as for example the flu, the viruses or bacteria attack also the CNS and certain repaired functions become impaired again. There is too little safety in the repaired functions. Here an example. When a patient with a cervical spinal cord injury and repaired urinary bladder functions got a flu, he became incontinent. When the flu was over, he was continent again. Therefore, when a CNS-injured patient gets an infection, the disease can be misjudged at a first glance.

The patient decided to stay at home and get the care by his wife, because he thought that he is safer at home. He knew that the air he breathed in should have a negative ionization and no pollution. He was also afraid to get an additional infection in the hospital. In Switzerland, the infection rate in a hospital is 25%. Every fourth patient gets a hospital infection. And of course, the care situation is better at home, administered by the wife.

Exercises against virus infection and cancer recurrence

When the Author got a lung infection from a child, who caught it in a kinder garden, he trained during the infection, whereas Dr. Cwienk did not. The Author had no fever. It seems therefore that in the case of the Author (78 years old), the pulmonary epithelia worked well and protected the body sufficiently not to let the virus into the body to give rise to an infection and fever, whereas in the case of Dr. Cwienk the virus succeeded to penetrate the pulmonary epithelia and invade the body. At the time of infection, the Author was performing at least 25 hours therapy per week and was breathing healthy air. He was performing his own CDT, was exercising additionally with the patient Nefeli **(Figure 62A)** and walked an hour every day to the training place and back. It seems therefore that the more the subject trains the better the lung epithelia can protect against infection. The protection against disease through exercising is similar in cancer. The more the patient exercises during or after cancer treatment, the less is the probability of cancer recurrence [125].

Breathing healthy air to use the infection protection of the lungs against viruses and bacteria

In a healthy surrounding **(Figure 61A)**, the air is not polluted or polluted only little and has a negative ionization. When breathing this healthy air and exercising in it to be fit, the lungs are in a healthy condition and the pulmonary epithelia can defend the body against infection. The pulmonary surfactant with a pH of 5 destroys viruses and bacteria to a certain extent. The macrophages can easily move about and engulf particulates, viruses and bacteria **(Figure 61C)**. Especially exercising on a special CDT device and hiking or jogging in the forest helps the body to stay healthy and young.

A person has a chronological age, a medical age and a mind age. To realize yourself in the surrounding, you have to exercise your body and train your brain: "To a healthy body belongs a healthy brain and to a healthy brain belongs a healthy body". With increasing chronological age, you have to exercise your body and your neural networks of the brain to keep the medical and the mental age as low as possible, to live longer with a better quality of life. Walking and jogging improves the stability of neural network organization and exercising on a special CDT device improves the variability. There is a fine balance between variability and stability.

When living in a city with polluted air **(Figure 61B)** and a wrong heating system in the place you live, your health becomes impaired and the medical age will increase. The best heating system is through warmness radiation. This can be achieved through the Hypokausten technique. Most living and working places and hospitals have climatization systems or heating system where the breathing air is used for heating. The circulating air changes its ionization and transports dust, dirt, viruses and bacteria around. When breathing in such air, you inhale dust, dirt, viruses and bacteria and the surfactant changes its pH value in direction of 6 **(Figure 61D)**. The surfactant gets more rigid and cracky. Through these cracks viruses and bacteria can penetrate the epitheliamore easily and the immune cells cannot easily move about any more in the surfactant and engulf or attack viruses and bacteria. The pulmonary surfactant, the first protective shield against infection, becomes impaired. Viruses and bacteria can invade the body. You get infected. If you are young and healthy and have a trained immune system, the body will stop the infection, especially if vaccines are administered. When you are old and have a high medical age caused by several other diseases which impair immune system functions, you may die, or if you are religious, you rise to heaven **(Figure 61G)**.

If you are older and have a poor health condition (other diseases, the medical age is high), your survival depends additionally on the treatment quality in the hospital. The hardworking of nurses and young physicians is not sufficient if the treatment is non-optimal. The kind of administered treatment, the hospital infection risks and the air breathed in are also important. Most hospitals have an air conditioning system in which viruses and bacteria are breaded and the ionization of the air is changed as well. In Switzerland the infection rate is 25%. Being close to other infected patients will dramatically increase the additional infection risk. If the patient is ventilated, the survival depends also on the quality of the ventilated air (ionization, viruses). The conditions of the hospitals in Italy and New York were far from optimal and as a result many patients died there.

From the point of view of this human research project, the treatment was wrong. The patients should not just lie in bed like dead. They have to be urged to move. They would need Coordination Dynamics Therapy for an improved survival. The exercising on a special CDT device will activate the nervous system rather integratively and coordinatedly and will improve lung functioning. When patients are too weak from infections and other diseases, their exercising has to be supported, as the Author is doing it with the cancer and spinal cord injury patient Nefeliin Figure 62A. Through such exercising the lung functions improve, if ventilated or not. The ciliated epithelia increase their activity and transport more particles, viruses and bacteria out of the lungs **(Figure 62B)**. Exercising in the lying position will enhance the transport of infected mucus to the pharynx, because the gravity is not counteracting the action of the cilia **(Figure 62C)**. Through additional rotating movements, all parts of the lung epithelia are reached. The exercising on the special CDT devices improves the self-healing systems of the body. Leaving infected patients just lying in bed is no real treatment.

This lying-in-bed caring shows similarity to the care of permanent coma patients. Due to very severe brain injury, they lie in bed and cannot move. Real treatment means that movement therapy has to be administered to them. Some of them will even recover from the coma [12]. By just lying in bed, they will die with one of the next lung infections.

When the Author introduced CDT to residents of an old people's home, an old lady said to the Author: "Why should I train, I got to 90 without any such training". In Finland when the Author exercised close to a home for the old aged, a lady said: "I should also exercise on such a device, but I am too lazy". Finish women are developed and strong. This means that not only the society has to look for the older ones, but the aged also have to contribute to stay alive and should exercise to improve lung and other body functions **(Figure 61F)**. The 82-year-old wife of Dr. Cwienk stated: "I also want to have the right to die and hopefully I will die together with my husband".

CDT and Dementia

The brain-injured patient Dr. Cwienk exercised regularly 12 to 15 hours per week. He himself reported that if he stops training for longer than two days, his brain functioning is getting worse. But through his regularly performed CDT it seemed, as judged by the Author, that his brain functions still improved a bit with respect to cognitive functions following 21 years of CDT. For sure the short-term memory was not getting worse, even though the speech was still impaired, because also the language area was impaired on one side due to the injury.

Since his cognitive functions seemed to improve a bit further, CDT performed for 12 to 15 hours per week can probably counteract dementia, if it is started in an early stage of dementia. The only real problem is that too many patients do not have the mental discipline to exercise regularly. Even a friend of the Author, being formerly a chief neurologist and having seen the progress of brain-injured patients through CDT could not generate the power to exercise, even though his father got dementia and his wife was performing fitness training regularly.

The Covid-19 pandemic is partly self-made

To handle and treat virus infections like Covid-19, there are three to four possibilities. First, to try to avoid an infection of the whole society. But too much money is wasted to stop the pandemic. Furthermore, there will be a lack of money later on to treat patients with other diseases sufficiently. Moreover, the lung functions have to be improved especially in older patients with other diseases. The exercising in the lying position on the special CDT device will improve lung functions **(Figure 62A)**. Other diseases of infected patients are no problem because CDT can most likely also improve those other diseases through CDT simultaneous (see Introduction). Third, if the virus succeeded to get into the body, drugs or vaccines are needed, as in the case of Dr. Cwienk. Still, the patient should exercise or should be exercised in the lying position to better ventilate the lungs and to support the ciliated function of the pulmonary epithelia to get as much infected mucus and other liquids out of the lung as possible **(Figure 62B, C)**. Suction is insufficient, because it reaches only the thick bronchia. Fourth, as long as there is no vaccine available, the patients have to be exercised on a special CDT device to get some treatment. Very little power is needed in that treatment position to achieve plenty of coordinated movements for improving lung functions.

However, what happened with the mainstream medicine world-wide, a terrible lot of money has been spent to avoid infections and waiting for a vaccine to be developed. Mainstream medicine does not tolerate looking for other treatments, at least as long as no vaccine is available. It is well known that exercising helps in many diseases (Introduction). Mainstream medicine is just waiting for the miracle vaccine. This is the so called "tunnel view" of patients with severe brain injury. They are concentrating on one thing and are unable to see a bit right and left. And when other problems are coming, they get upset, nervous or even hysteric. Here an example. It was intended that the cerebral palsy girl Sophie **(Figure 7)** can go in the evening to her beloved grandmother. When it turned out for some reason that she could not go to the grandmother, she got nearly hysterical in the morning during therapy. It became impossible to continue the therapy. After a few hours she recovered.

Probably many thousands of patients did not need to die if CDT would have been administered to them. Mainstream medicine is narrow-minded by just waiting for a vaccine. If a vaccine becomes available, still some patients would die as in flu infections. The effect of a vaccination on flu-virus infected patients is minimal. Further, the covid-19 virus will also change through mutation. A vaccine will not solve all the problems. Other treatments will also have to be tried.

Extra corporal membrane oxygenation (ECMO) and movement-based health improvement

If Covid-19 infected patients are in the hospital, they should be exercised in the lying position as in Figure 62A to improve lung functions and the cardio-vascular performance. Many patients die on cardiac problems and a thrombosis, especially in the lung. In the final stage of living, even extra corporal oxygenation is used, which is a tremendous effort with nearly no effect. But physicians are not trying health improvement through movements? CDT improves the cardio-vascular performance and lung functions.

In high (rostral) cervical spinal cord injury, the patients cannot move any more. Not to get pressure ulcers and other problems, the patients are turned (rotated) in the bed day and night, which is quite an effort for nurses to turn the patients also at night. There are even beds which move a bit to move the patient and to stimulate the functions of the body a bit. To include movements into treatment seems to be foreign for physicians working with Codid-19 infected patients.

Deficits in medicine caused impairment of basic human rights and an attack on democracy

Even though more research is published in general, the quality of research went down. Every journal has its readership as well as its reviewers. Formally qualified journals related to medicine did not develop further and publish research which bypasses the interest of human patients. Medical (human) research is only rudimentarily organized. The deficits of the old journals, if existing, opened the research market for open access journals, which is in principle a good development, especially in the field of medicine. But often the level is too low and money is more of interest than the progress in research (Bells list of predatory publishers). Furthermore, the researcher has to pay for the publication. The consequence is an impairment of the freedom of research. Only those can publish easily who have the money for it.

Interdisciplinary research has been demanded for decades, but has yet not been organized. Reviewers who could judge qualified interdisciplinary research are rare. The discipline electrophysiology for research and diagnostic has been given up. Many physicians are not even able to perform electromyography anymore **(Figures 49-53)**. For

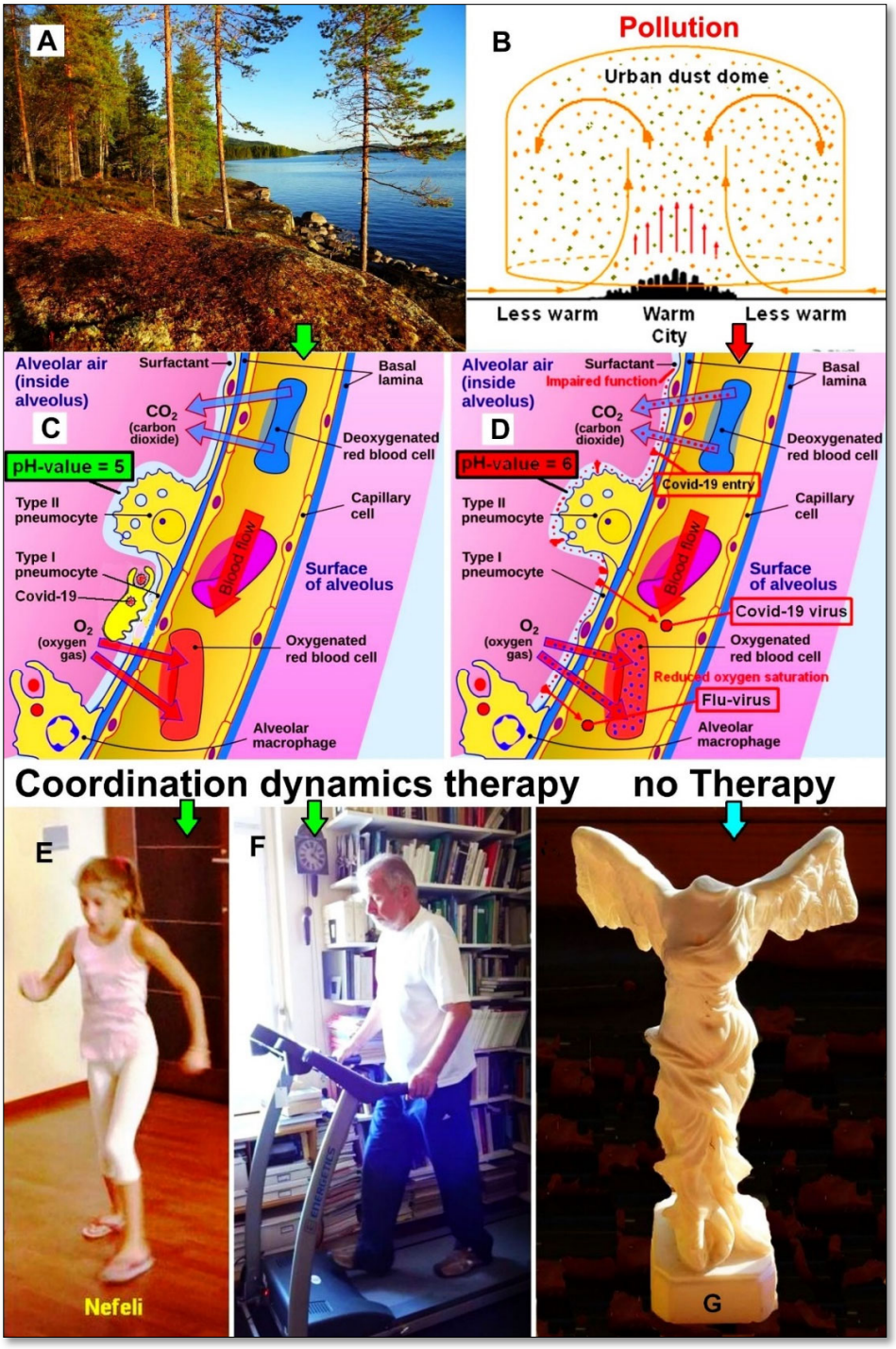

Figure 61. Physiologic and pathologic pulmonary epithelial functions to impede virus and bacterial infections. When living in a healthy surrounding (A) and exercising (E, F), the lung epithelia is in a healthy condition (C) and can partially protect against infections to a certain extent; the surfactant has a pH of 5 and is liquid so that macrophages can move about and engulf viruses, bacteria and particulates. The lung protection shield against infections is working. When living in a polluted surrounding with wrong air ionization (B), the surfactant gets a wrong pH value (pH value = 6) and becomes more rigid so that macrophages cannot move easily about and attack and engulf viruses and bacteria (D). Viruses can also invade the body through cracks. The pulmonary surfactant cannot protect any more against infections. Viruses and bacteria get into the body. Critical patients may die (G).

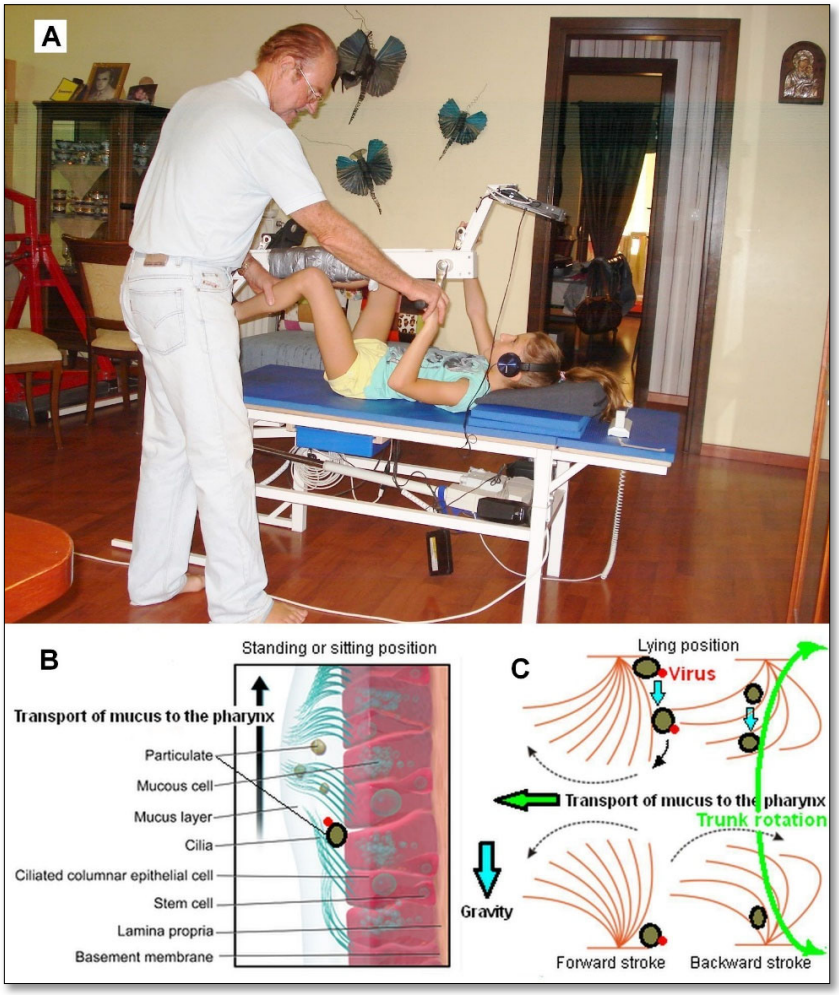

Figure 62. Improvement of lung functioning through Coordination Dynamics Therapy (CDT). A. Through exercising on the special CDT device, the CNS is activated for better functioning in the short-term memory and activates in turn the lungs for optimal breathing. B. Through the coordinated exercising, the ciliated epithelia will transport infected mucus, particulates and other liquids to the pharynx to cough up. C. Especially in the lying position, when the gravity is not working against the transport, the cilia are working efficiently. Through additional trunk rotation of the patient also big and heavy particles from the feet of the cilia can be transported to the pharynx.

treating patients with urinary bladder problems, for example, urodynamics is a powerful diagnostic. Bladder pressure is monitored when filling and emptying the bladder and simultaneously the electromyographic activity of the pelvic floor is recorded to measure Synergia or Dyssynergia of the bladder. Nowadays, often this urodynamic is not performed professionally anymore because of lack of the skills to perform electromyography. In this paper the power of electrophysiologyis demonstrated which lead to the repair of diseases, as for example brain injury.

The deficits in mainstream medicine induced a world-wide crisis through not accepting movement treatment and underestimating the pandemic in this way. The biased selection of information in mass media through not comparing Covid-19 with other infections lead to a restriction of basic human rights based on an out-of-date mainstream medicine which does not want to use new qualified research to save the lives of patients. And because it is unpleasant, no money can be earned and specific basic medical knowledge is missing.

The present Covid-19 treatment and evaluation systems for Switzerland were criticized by the physician DDr. Paul Robert Vogt [126].

ACKNOWLEDGEMENT

This research project was judged as unqualified and ethically not justified by the 'Deutsche Forschungsgemeinschaft' (DFG), the 'Swiss National Fond' and other institutions. Also, the 'Max Planck

Institution' refused support. Even the support of the German president Richard v. Weizsäcker did not help. No real funding could be obtained for 35 years. When the Author gave a presentation some 20 years ago in the Nobel institution of neuroscience (Prof. Grillner (pattern generators)), he was not allowed to discuss with assistances this human research project. It was intended there to design a rat experiment, what the Author had already performed on human. Most likely, all the reviewers of the negative decisions had less qualifications than the Author (Schalow G, Dr.med.habil., Dr.rer.nat., Dipl.Ing.).

REFERENCES

1. Schalow G, Zäch GA, Warzock R (1995) Classification of human peripheral nerve fibre groups by conduction velocity and nerve fibre diameter is preserved following spinal cord lesion. J Auton Nerv Syst 52: 125-150.
2. Schalow G (2009) The classification and identification of human somatic and parasympathetic nerve fibres including urinary bladder afferents and efferents is preserved following spinal cord injury. Electromyogr Clin Neurophysiol 49: 263-286.
3. Schalow G, Bersch U, Göcking K, Zäch GA (1995) Detrusor-sphincteric dyssynergia in paraplegia compared with the synergia in a brain-dead human by using the single-fibre action potential recording method. J Auton Nerv Syst 52: 151-180.
4. Schalow G, Bersch U, Michel D, Koch HG (1995) Detrusor-sphincteric dyssynergia in humans with spinal cord lesions may be caused by a loss of stable phase relations between and within oscillatory firing neuronal networks of the sacral micturition centre. J Auton Nerv Syst 52: 181-202.
5. Schalow G (2013) Human Neurophysiology: Development and Repair of the Human Central Nervous System. Nova Science Publishers, Inc, Hauppauge NY, USA 734 pp.
6. Schalow G (2015) Repair of the Human Brain and Spinal Cord. Nova Science Publishers, Inc, Hauppauge NY, USA 525 pp.
7. Schalow G (2015) Neural network learning in human. Nova Science Publishers, Inc, Hauppauge NY, USA 324 pp.
8. Schalow G (2019) Regeneration of the human spinal cord via coordination dynamics therapy. e-Book (open access). Peertechz Publications Inc.
9. Schalow G (2018) Paediatric acquired brain injury repair in 5 patients through Coordination Dynamics Therapy. Clin Med Rep 1: 1-19.
10. Schalow G (1998) Koordinationsdynamik-Training. Wiedererlernen des Rennens und der Kontinenz bei ZNS-Verletzung (Teil 2). Physiotherapy1989.
11. Schalow G (2006) Cerebellar injury improvement achieved by coordination dynamics therapy. Electromyogr. Clin Neurophysiol 46: 433-439.
12. Schalow G (2019) Brain repair and general health improvement through human neurophysiology and repair physiology. Clin Med Rep 2: 1-68.
13. Schalow G (2019) Permanent coma patient re-learned to speak via coordination dynamics therapy. Arch Clin Med Case Rep 3: 33-50.
14. Schalow G (2002) Stroke recovery induced by coordination dynamic therapy and quantified by the coordination dynamic recording method. Electromyogr Clin Neurophysiol 42: 85-104.
15. Schalow G (2002) Improvement after traumatic brain injury achieved by coordination dynamic therapy. Electromyogr. Clin Neurophysiol 42: 195-203.
16. Schalow G, Jaigma P (2006) Improvement in severe traumatic brain injury induced by coordination dynamics therapy in comparison to physiologic CNS development. Electromyogr Clin Neurophysiol 46: 195-209.
17. Schalow G (2002) Recovery from spinal cord injury achieved by 3 months of coordination dynamic therapy. Electromyogr Clin Neurophysiol 42: 367-376.
18. Schalow G (2003) Partial cure of spinal cord injury achieved by 6 to 13 months of coordination dynamic therapy. Electromyogr Clin Neurophysiol 43: 281-292.
19. Schalow G, Jaigma P, Belle VK (2009) Near-total functional recovery achieved in partial spinal cord injury (50% injury) after 3 years of coordination dynamics therapy. Electromyogr Clin Neurophysiol 49: 67-91.
20. Schalow G, Jaigma P (2005) Cerebral palsy improvement achieved by coordination dynamics therapy. Electromyogr Clin Neurophysio 45: 433-445.
21. Schalow G (2006) Hypoxic brain injury improvement induced by coordination dynamics therapy in comparison to CNS development. Electromyogr Clin Neurophysiol 46: 171-183.
22. Schalow G, Pääsuke M, Ereline J, Gapeyeva H (2004) Improvement in Parkinson's disease patients achieved by coordination dynamics therapy. Electromyogr Clin Neurophysiol 44: 67-73.

23. Schalow G, Pääsuke M, Jaigma P (2005) Integrative re-organization mechanism for reducing tremor in Parkinson's disease patients. Electromyogr Clin Neurophysiol 45: 407-415.
24. Schalow G, Nyffeler T (2001) Koordinationsdynamik-Therapie: Myelomeningozele (Spina bifida). Physiotherapie.
25. Schalow G, Nyffeler T (2000) Koordinatiosdynamik-Therapie: Skoliose. Physiotherapy.
26. Schalow G (2010) Cure of urinary bladder functions in severe (95%) motoric complete cervical spinal cord injury in human. Electromyogr Clin Neurophysiol 50: 155-179.
27. Schalow G (2017) Breast cancer growth inhibition via Coordination Dynamics Therapy. In: "Horizons in Cancer Research. 68. Editor: Hiroto S. Watanabe. Nova Science Publishers, Inc, Hauppauge NY, USA 125-151.
28. Schalow G (2010) Scientific basis for learning transfer from movements to urinary bladder functions for bladder repair in patients with spinal cord injury. Electromyogr Clin Neurophysiol 50: 339-395.
29. Schalow G, Lang G (1987) Recording of Single Unit Potentials in Human Spinal Nerve Roots: a New Diagnostic Tool. Acta Neurochir 86: 25-29.
30. Schalow G, Lang G (1989) Elektrodiagnosis of human dorsal sacral nerve roots by recording afferent and efferent extracellular action potentials. Neurosurg Rev 12: 223-232.
31. Schalow G, Zäch GA (1999) Koordinationsdynamik-Therapie als Lernprozess, Teil I. Physiotherap. 8: 4-12.
32. Schalow G (2006) Symmetry diagnosis and treatment in coordination dynamics therapy. Electromyogr Clin Neurophysiol 46: 421-431.
33. Johannson RS (1978) Tactile sensibility in the human hand: Receptive field characteristics of mechanoreceptive units in the glabrous skin area. J Physiol 281: 101-123.
34. Vallbo AB, Hagbarth K-E, Torebjörk HE, Wallin BG (1979) Somatosensory propioceptive, and sympathetic activity in human peripheral nerves. Physiol Rev 59: 919-957.
35. Brindley GS, Polkey CE, Rushton DN, Cardozzo L (1986) Sacral anterior root stimulation for bladder control in paraplegia: the first 50 cases. J Neurol Neurosurg Psychiatr 49: 1104-1114.
36. Schalow G (1985) The problem of Cauda equina nerve root identification. Zbl Neurochirurgie 46: 322-330.
37. Schalow G (1987) Single unit potential amplitude in relation to the conduction velocity in frog and human. Zent bl Neurochir 48: 109-113.
38. Paintal AS (1966) The influence of diameter of medullated nerve fibres of cats on the rising and falling phases of the spike and its recovery. J Physiol 184: 791-811.
39. Schalow G, Aho A, Lang G (1992) Microanatomy and number of nerves fibres of the lower intercostal nerves with respect to a nerve anastomosis. Donor nerve analysis. I (IV). Electromyogr Clin Neurophysiol 32: 171-185.
40. Schalow G (1992) Number of fibres and fibre diameter distributions of nerves innervating the urinary bladder in humans - Acceptor nerve analysis. II (IV). Electromyogr Clin Neurophysiol 32: 187-196.
41. Schalow G (1989) Efferent and afferent fibres in human sacral ventral nerve roots: Basic research and clinical implications. Electromyogr Clin Neurophysiol 29: 33-53.
42. Schalow G (1991) Conduction velocities and nerve fibre diameters of touch, pain, urinary bladder and anal canal afferents and □ and □-motoneurons in human dorsal sacral nerve roots. Electromyogr Clin Neurophysiol 31: 265-296.
43. Schalow G (1991) Oscillatory firing of single human sphincteric □2 and □3-motoneurons reflexly activated for the continence of urinary bladder and rectum. Restoration of bladder function in paraplegia. Electromyogr Clin Neurophysiol 31: 323-355.
44. Gossard JP, Brownstone RM, Barajon I, Hultborn H (1994) Transmission in a locomotor-related group Ib pathway from hindlimb extensor muscles in the cat. Exp Brain Res 98: 213-228.
45. Lawson J (1974) Pelvic anatomy, I. Pelvic floor muscles. Ann R Coll Surg Engl 54: 244-252.
46. Percy JP, Swash M, Neill ME, Parks AG (1980) Electrophysiological study of motor nerve supply of pelvic floor. Lancet 3:16-17.
47. Garry RC, Garven HSD (1957) The ganglia, afferent nerve-endings and musculature of the urethra in the cat. J Physiol 139: 1P-2P.
48. Kugelberg E, Hagbarth KE (1958) Spinal mechanisms of the abdominal and erector spinae skin reflexes. Brain 81: 290-304.

49. Schalow G, Aho A, Lang G (1987) Nerve fibre counts for an intercostal nerve to cauda equina nerve root anastomosis. Zent bl Chir 112: 457-461.
50. Nadelhaft I, Ropollo J, Morgan C, Groat WCD (1983) Parasympathetic preganglionic neurons and visceral primary afferents in monkey sacral spinal cord revealed following application of horseradish peroxydase to pelvic nerve. J Compar Neurol 216: 36-52.
51. Bors E, Porter RW (1970) Neurosurgical consideration in bladder dysfunction. Urol Int 25: 114-133.
52. Gosling JA, Dixon JS, Humpherson JR (1983). Functional anatomy of the urinary tract. Churchill Livingston distributed, Gower Medical Publishing, London, pp: 5-18.
53. Evans JP (1936) Observation on the nerves of supply to the bladder and urethra of the cat, with a study of their action potentials. J Physiol 86: 396-413.
54. Schalow G, Barth H (1992) Group conduction velocities and nerve fibre diameters of and -motoneurons from lower sacral nerve roots of the dog and humans. Gen Physiol Biophys 11: 85-99.
55. Schalow G (1992) Recruitment within the groups of 1, 2 and 3-motoneurons in dogs and humans following bladder and anal catheter pulling. Gen. Physiol. Biophys 11: 101-121.
56. Schalow G (1992) Ventral root afferent and dorsal root efferent fibres in dog and human lower sacral nerve roots. Gen Physiol Biophys 11: 123-131.
57. Schalow G, Barth H (1992) Single-fibre action potential recording from the nerve to the musculus obliquus externus abdominis following pin-prick in humans. III (IV) Electromyogr Clin Neurophysiol 32: 197-205.
58. Schalow G (1992) Impulse pattern, innervation density and two-point discrimination of skin and mucosal afferents in humans. Consideration for a sensory reinnervation of urinary bladder and anal canal in spinal cord lesion. IV (IV) Electromyogr Clin Neurophysiol 32: 259-285.
59. Schalow G (2005) Tapering of human nerve fibres. Gen Physiol Biophys 24: 427-448.
60. Espinosa-Medina I (2016) The sacral autonomic outflow is sympathetic. Science (6314) 354: 893-897.
61. Carlstedt T (1977) Observation on the morphology at the transition between the peripheral and the central nervous system in the cat. I. Preparative procedure useful for electron microscopy of the lumbosacral dorsal rootlets. Acta Physiol Scand (Suppl.) 446: 5.
62. Huxley AF, Stämpfli R (1949) Evidence for saltatoric conduction in peripheral myelinated nerve fibres. J Physiol 108: 315-339.
63. Rasminski M, Kearney RE, Aguayo AJ, Bray GM (1978) Conduction of nerve impulses in spinal nerve roots and peripheral nerves of dystrophic mice. Brain Research 143: 71-85.
64. Schalow G, Zäch GA (1994) Nerve compound action potentials analysed with the simultaneously measured single fibre action potentials. Electromyogr Clin Neurophysiol 34: 451-465.
65. Arbuthnott ER, Boyd IA, Kalu KU (1980) Ultrastructural dimensions of myelinated peripheral nerve fibre in the cat and their relation to conduction velocity. J Physiol 308: 125-157.
66. Boyd IA, Davey MR (1968) Composition of peripheral nerves. Livingston, Edinburgh.
67. Boyd IA, Kalu KU (1979) Scaling factor relating conduction velocity and diameter for myelinated afferent nerve fibres in cat hindlimb. J Physiol 289: 277-297.
68. Erlanger J, Gasser HS (1937) Electrical signs of nervous activity. Philadelphia, University of Pennsylvania Press.
69. Gasser HS, Grundfest H (1939) Axon diameter in relation to the spike dimension and the conduction velocity in mammalian A fibres. Am J Physiol 127: 393-414.
70. Hunt CC (1954) Relation of function to diameter in afferent fibres of muscle nerve. J Gen Physiol 38: 117-131.
71. Hursh JB (1939) Conduction velocity and diameter of nerve fibres. Am J Physiol 127: 131-139.
72. Lloyd DPC (1943) Neuron patterns controlling transmission of ipsilateral hind limb reflexes in cat. J Neurophysiol 6: 293-315.
73. Paintal AS (1965) Effect of temperature on conduction in single vagal and saphenus myelinated nerve fibres of the cat. J Physiol 180: 20-49.
74. Paintal AS (1973) Conduction in mammalian nerve fibres. In: J.E. Desmedt (Ed.). New Developments in Electromyogr Clin Neurophysiol 2: 19-41.
75. Burke RE, Levine DN, Tsairis P, Zajak III FE (1973) Physiological types and histochemical profiles in motor units of the cat gastrocnemius. J Physiol 234: 723-748.
76. Fleshman JW, Munson JB, Sypert GW, Friedman WA (1981) Rheobase, input resistance, and motor

unit type in medial gastrocnemius motoneurons in the cat. J Neurophysiol 41: 1326-1338.

77. Gustafson B,Pinter MJ (1984) Relations among passive properties of lumbar □-motoneurons of the cat. J Physiol 356: 401-431.

78. Kernell D, Zwagstra B (1981) Input resistance, axon conduction velocity and cell size among hindlimb motoneurons of the cat. Brain Research 204: 311-326.

79. Schalow G, Wattig B (1993). Recruitment of □ and □-motoneurons in rats, dogs and humans. Electromyogr Clin Neurophysiol 33: 387-400.

80. Schalow G (1993) Recruitment of motoneurons in the occasional firing mode in paraplegics. Electromyogr Clin Neurophysiol 33: 401-408.

81. Sherrington CS (1913) Nervous rhythm arising from rivalry of antagonistic reflexes: Reflex stepping as outcome of double reciprocal innervation. Proc R Soc Lond (Biol.) 86: 233-261.

82. Garry RC, Garven HSD (1957) The ganglia, afferent endings and musculature of the urethra in the cat. J Physiol 139: 1P-2P.

83. Garry RC, Roberts TDM, Todd JK (1957) Reflex responses of the external urethral sphincter of the cat to filling of the bladder. J Physiol 139: 13P-14P.

84. Garry RC, Roberts TDM, Todd JK (1959) Reflexes involving the external urethral sphincter in the cat. J Physiol 149: 653-665.

85. Iggo A (1955) Tension receptors in the stomach and the urinary bladder. J Physiol 128: 593-607.

86. Burke RE, Levine DN, Tsairis P, Zajak III FE (1973) Physiological types and histochemical profiles in motor units of the cat gastrocnemius. J Physiol 234: 723-748.

87. Schalow G (1993) Action potential patterns of intrafusal □ and parasympathetic motoneurons, secondary muscle spindle afferents and an oscillatory firing □2-motoneuron, and the phase relations among them in humans. Electromyogr Clin Neurophysiol 33: 477-503.

88. Bornstein JC, Furness JB, Kunze WAA (1994) Electrophysiological characterization of myenteric neurons - How do classification schemes relate (Review). J Auton Nerv Syst 48: 1-15.

89. Wood JD (1994) Application of classification schemes to the enteric nervous system (Review). J Auton Nerv Syst 48: 17-29.

90. Buchthal F, Rosenfalck A (1966) Evoked potentials and conduction velocity in human sensory nerves. Brain Res 3: 1-122.

91. Gath I, Stahlberg E (1977) On the volume conduction in human skeletal muscle: In situ measurements. Electroencephalo Clin Neurophysiol 43: 106-110.

92. Kelso JAS (1995) Dynamic Patterns. The Self-Organization of Brain and Behavior. MIT Press, Cambridge.

93. Gladden MH (1985) Efferent control of human muscle spindles. In: Boyd, I.A. and Gladden MH (Eds.) The Muscle Spindle, Stockton Press, New York 243-254.

94. Gladden MH (1992) Muscle receptors in mammals. Adv Comp Environ Physiol 10: 281-302.

95. Boyd IA (1980) The isolated muscle spindle. Trends Neurosci 3: 258-265.

96. Schalow GM, Zäch GA (1996) Mono and polysynaptic drive of oscillatory firing □1 (FF) and □2-motoneurons (FR) in a patient with spinal cord lesion. Gen Physiol Biophys 15: 57-74.

97. Schalow G, Bersch U, Zäch GA, Warzock R (1996) Classification, oscillatory and alternating oscillatory firing of □1 (FF) and □2-motoneurons (FR) in patients with spinal cord lesion. Gen Physiol Biophys 15: 5-56.

98. Boyd IA, Gladden MH, McWilliam PN, Ward J (1977) Control of dynamic and static nuclear bag fibres and nuclear chain fibres by gamma and beta axons in isolated cat muscle spindles. J Physiol 265: 133-162.

99. Taylor A, Durbaba R, Rogers JF (1992) The classification of afferents from muscle spindles of the jaw-closing muscles of the cat. J Physiol 456: 609-828.

100. Scheibel ME, Scheibel AB (1958) Structural substrates for integrative patterns in the brain stem reticular core. In Jaspers, H.H. et al. (Eds.), Formation of the Brain Stem Reticular Core, Little and Brown, Boston, pp: 31-55.

101. Waltzer R, Martin GF (1984) Collateralization of reticulospinal axons from the nucleus reticularis gigantocellularis to the cerebellum and diencephalon. A double-labelling study in the rat. Brain Res 293: 153-158.

102. Martin GF, Cabana T, Humbertson AO Jr (1981) Evidence for collateral innervation of the cervical and lumbar enlargements of the spinal cord by single reticular and raphe neurons. Studies using fluorescent

markers in double-labelling experiments on the North American opossum. Neurosci Lett 24: 1-6.

103. Peacock MJ and Wolstencroft JH (1976) Projections of reticular neurons to dorsal regions of the spinal cord in the cat. Neurosci Lett 2: 7-11.

104. Hodgkin AL (1948) The local electric changes associated with repetitive action in a non-medullated axon. J Physiol 107: 165-181.

105. Arbib MA (1995) The Handbook of Brain Theory and Neural Networks, MIT Press, Cambridge.

106. Deliagina TG, Feldman AG (1981) Activity of Renshaw cells during fictive scratch in the cat. Exp Brain Res 42: 108-115.

107. Corda M, Euler C, Lennerstrand G (1966) Reflex and cerebellar influences on α and on "rhythmic" and "tonic" γ activity in the intercostal muscle. J Physiol 184: 898-923.

108. Schalow G (1990) Feeder arteries, longitudinal arterial trunks and arterial anastomosis of the lower human spinal cord. Zbl Neurochir 51: 181-184.

109. Martino G, Pluchino S (2006) The therapeutic potential of neural stem cells. Nat Rev Neurosci 7: 395-406.

110. Schalow G, Vaher I, Jaigma P (2008) Overreaching in coordination dynamics therapy in an athlete with a spinal cord injury. Electromyogr Clin Neurophysiol 48: 83-95.

111. Schalow G (2008) Stem cell therapy and Coordination dynamics therapy improve Spinal cord injury. Electromyogr Clin Neurophysiol 48: 233-253.

112. Carlsson CA, Sundin T (1980) Reconstruction of afferent and efferent nervous pathways to the urinary bladder in two paraplegic patients. Spine 5: 37-41.

113. Schnell L, Schwab ME (1993) Sprouting and regeneration of lesioned corticospinal tract fibres in the adult rat spinal cord. Eur J Neurosci 5: 1156-1176.

114. Björklund A (1994) A question of making it work, spinal cord repair. Nature 367: 112-113.

115. Bradbury EJ, McMahon SB (2006). Spinal cord repair strategies: Why do they work? Nat Rev Neurosci 7: 644-653.

116. Wattig B, Schalow G, Heydenreich F, Warzok R, Cervos-Navarro J (1992) Nucleotides enhance nerve fibre regeneration after peripheral nerve crush damage - Electrophysiologic and morphometric investigation. Drug Res 42 (II) 9: 1075-1078.

117. Bregman BS (1987) Development of serotonin immunoreactivity in the rat spinal cord and its plasticity after neonatal spinal cord lesion. Brain Res Dev Brain Res 34: 245-263.

118. Sperry RW (1945) The problem of central nervous reorganosation after nerve regeneration and muscle transposition. Quart Rev Biol 20: 311-369.

119. Sperry RW (1947) Effect of crossing nerves to antagonistic limb muscles in the monkey. Arch Neurol Psychiatr Chicago 58: 452-473.

120. Weiss P, Brown PF (1941) Electromyographic study on recoordination of leg movements in poliomyolitis patients with transposed tendons. Proceedings of the Society for Exper. Biology Med 48: 384-387.

121. Schalow G (2019) Brain repair and general health improvement through human neurophysiology and repair physiology. Clin Med Rep 2: 1-68.

122. Schalow G (2020) Potential organ donor recovered from severe brain injury spontaneously and CNS functions improved through coordination dynamics therapy. Int J Med Clin Imaging 6: 95-108.

123. Schalow G (2020) To live longer with a better quality of life through coordination dynamics therapy especially in patients with severe brain injury and brain-cancer. Int J Med Clin Imaging 5: 118-155.

124. Schalow G (2020) Anaplastic Oligodendroglioma WHO III brain cancer-patient recovered following operation, radiation and chemotherapy through coordination dynamics therapy, which is also a Covid-19 treatment without ventilator. Int J Clin Imaging 5: 165-219.

125. Brown JC, Stone KW, Schmitz KH (2012) Cancer, physical activity, and exercise. Compr Physiol 2: 2775-2809.

126. Infosperber (2020) Available online at: https_www.infosperber.ch_data-attachements_Vogt